Aus dem Institut für Integrative Neuroanatomie
der Medizinischen Fakultät Charité – Universitätsmedizin Berlin

DISSERTATION

Characterization of inhibitory and projection specific neurons of the presubiculum

zur Erlangung des akademischen Grades
Doctor medicinae (Dr. med.)

vorgelegt der Medizinischen Fakultät
Charité – Universitätsmedizin Berlin

von

Roxanne Lofredi

Aus Frankfurt am Main

Datum der Promotion: 10.03.2017.....

TABLE OF CONTENTS

ABSTRACT (English)

Presubiculum (PrS) is a transitional cortical area of the parahippocampal formation in the temporal lobe, close to hippocampus and entorhinal cortex. PrS is involved in spatial navigation processing by encoding an animal's head direction (HD). The HD signal is most likely generated in lateral mammillary nucleus (LMN) and relayed in anterodorsal thalamus (ADN) before being processed in the PrS. PrS is thought to be crucial for updating the HD signal with visual landmark information as it receives direct projections of visual cortex and projects back to downstream ADN and LMN.

The aim of my work has been twofold. First, I examined the GABAergic neurons of the PrS. GABAergic interneurons are the source of inhibitory activity that is essential for local signal generation. I quantified the total number of presubicular interneurons in the GAD67-GFP transgenic mouse and investigated morphological properties and layer specific distribution of interneuron subtypes. The proportion of interneurons in the PrS was 11% of all neurons. To identify neurochemical subpopulations, I performed double immunolabeling with combinations of Parvalbumin (PV), Calretinin (CR), Calbindin (CB), Somatostatin (SOM), Vasointestinal Peptide (VIP) and Neuropeptide Y (NPY). Largest population of presubicular interneurons was PV+ (36%). CR, CB and SOM interneurons contributed evenly to the population (~18%), while there were less VIP+ interneurons (9%). Double labeling experiments revealed a small subpopulation of presubicular interneurons positive for PV and SOM, a co-expression pattern seen in the hippocampal formation but usually absent in neocortical regions. Indeed, the PrS displays a unique expression pattern of inhibitory cells, and their functional role within the presubicular microcircuit will have to be investigated in future studies.

The second part of my work focused on projection-specific neurons of the PrS targeting LMN and ADN. To reveal their morphological and electrophysiological identity, I injected retrogradely transported fluorescent beads into LMN or ADN which allowed assessing the laminar origin of projection neurons. While LMN projecting neurons were exclusively seen in layer IV, ADN projecting neurons were restricted to deep layers. Patch clamp recordings of bead-containing presubicular neurons indicated a relatively homogenous population of LMN projecting neurons, displaying an intrinsic bursting behavior which matches their presumed role of operating fast visual update. ADN projecting neurons were mostly regular spiking with otherwise heterogeneous intrinsic properties. Both populations had dendrites extending up to superficial layers, making them well suited to receiving visual input and updating subcortical HD-signal with landmark information. Future work should shed light on recruitment of neuronal subpopulations by specific afferent inputs for a better understanding of information processing in the PrS.

ABSTRACT (Deutsch)

Das Präsubiculum (PrS) zählt zu der parahippokampalen Formation (PHF) und liegt im Temporallappen zwischen Hippokampus und entorhinalem Kortex. Die PHF enthält spezialisierte Zelltypen, die räumliche Informationen verarbeiten und die neuronale Grundlage eines inneren Navigationssystems darstellen. Im PrS sind dies vor allem die so genannten „Head direction (HD) cells“, die als eine Art innerer Kompass eine Orientierung im Raum ermöglichen.

Das HD-Signal wird vermutlich im subkortikal liegenden lateralen Mammillarkörper (LMN) durch vestibuläre Aktivität generiert, anschließend im anterodorsalen Kern des Thalamus (ADN) umgeschaltet und in kortikalen Regionen mit visuellen Orientierungspunkten abgeglichen. Hierbei könnte das PrS eine entscheidende Rolle spielen, da es afferente Verbindungen mit dem visuellen Kortex sowie eine efferente Verbindung mit LMN und ADN unterhält.

In der vorliegenden Arbeit habe ich mich zunächst der weitestgehend unerforschten Population der Interneurone des PrS gewidmet. Mit Hilfe des transgenen GAD67-GFP Maus-Modells und immunohistochemischen Methoden, konnten die GABAergen Zellen dieser Region quantifiziert werden. 11% aller Neurone des PrS sind Interneurone. Durch Immunfärbungen für Parvalbumin (PV), Somatostatin (SOM), Vasointestinal Peptide (VIP), Calretinin (CR), Calbindin (CB) und Neuropeptide Y (NPY) konnten diese Interneurone weiter unterteilt werden. Die größte Interneuron- Subpopulation ist PV+ (36%). SOM, CR und CB findet man in etwa zu gleichen Teilen (18%) während VIP von einer kleineren Zellgruppe exprimiert wird (11%). Das PrS enthält zudem eine kleine Gruppe von Interneuronen, die sowohl positiv für PV als auch für SOM sind. Dieser Subtyp ist typisch für den benachbarten Hippokampus und wurde in neokortikalen Regionen bisher nicht beobachtet. Die vorliegenden Ergebnisse zeigen, dass das PrS eine einzigartige Interneuron-Population aufweist, deren funktionelle Bedeutung in zukünftigen Studien untersucht werden sollte.

Im zweiten Teil meiner Arbeit beschäftigte ich mich mit projektions-spezifischen Neuronen des PrS. Durch Injektion von retrograden Tracern konnten Neurone markiert werden, die zum LMN und dem ADN projizieren. LMN- projizierende Zellen befinden sich demnach in Lamina IV, wohingegen die Zellkörper der zum ADN projizierenden Neurone in Lamina V/VI liegen. Diese Projektionsneurone unterscheiden sich in ihren elektrophysiologischen Eigenschaften. In patch-clamp Ableitungen erwiesen sich die LMN-projizierende Neurone als „intrinsic bursting“ (IB) und die ADN-projizierende Zellen als „regular spiking“.

Besonders die zum LMN projizierenden IB- Neurone könnten ein schnelles visuelles Update des subkortikalen HD-Signals ermöglichen. Beide neuronalen Populationen zeigten aszendierende Dendriten, so dass sowohl LMN als auch ADN projizierende Neurone in den oberen Laminae von Afferenzen des visuellen Kortex kontaktiert werden könnten.

Ob visuelle oder auch andere Afferenzen selektiv neuronale Subpopulationen rekrutieren sollte Gegenstand weiterführender Untersuchungen sein, um abschließende Erkenntnisse über die Informationsverarbeitung innerhalb des PrS sowie des HD-Schaltkreises zu erhalten.

LIST OF ABBREVIATIONS

ADN	anterodorsal thalamus
ap	antero-posterior
AP	action potential
AV	anteroventral thalamus
BC	basket cells
CA	cornu ammonis
CB	calbindin
CBP	calcium binding protein
CCK	cholecystokinin
CGE	dorsocaudal ganglionic eminence
CR	calretinin
CV	coefficient of variation
Dapi	4’,6’-diamidino-2-phenylindole
DC	direct current
DG	dentate gyrus
dl	dorso-lateral
DTN	dorso-tegmental nucleus
DTX	dendrotoxin
EC	entorhinal cortex
EGTA	ethylene glycol tetraacetic acid
FRB	fast repetitive bursting
FS	fast spiking
GABA	γ amino-butyrique acid
GAD67	glutamic acid decarboxylase 67
GFP	green fluorescent protein
HD	head direction
HDC	head direction cell
HF	hippocampal formation
HPC	hippocampus
DTN	dorsal tegmental nucleus
IB	intrinsic bursting
LEA	lateral entorhinal cortex

LDN	laterodorsal thalamus
LMN	lateral mammillary nucleus
LTS	low-threshold spiking
MEC	medial entorhinal cortex
MGE	medial ganglionic eminence
NPY	neuropeptide Y
O-LM	stratum oriens- stratum lacunosum moleculare
PHF	parahippocampal formation
PHR	parahippocampal region
PaS	parasubiculum
PB	phosphate buffer
PBS	phosphate buffered saline
PER	perirhinal cortex
POA	preoptic area
POR	Postrhinal cortex
PoS	postsubiculum = dorsal part of PrS
PrS	presubiculum
PV	parvalbumin
RB	retrobeads
R_{in}	neuronal input resistance
RMP	resting membrane potential
RS	regular spiking
RSC	retrosplenial cortex
SOM	somatostatin
Sub	subiculum
TLE	temporal lobe epilepsy
TTX	tetrodotoxin
VIP	vasointestinal peptide
Vm	ventro-medial

LIST OF FIGURES

1. INTRODUCTION

1.1 Anatomy of the presubiculum

The presubiculum (PrS) is a curved, rather trapezoid cortical region within the temporal lobe. Its ventral part corresponds to Brodman's area 48, whereas the dorsal portion of PrS is referred to as Brodman's area 27[1]. The latter is still assigned as postsubiculum (PoS) [2–4] by some authors[4,5]. PrS is part of the hippocampal- parahippocampal formation that comprises the hippocampal formation (HF) and the parahippocampal region (PHR). The HF includes dentate gyrus (DG), the cornu ammonis fields CA 1-3 (hippocampus proper) and the subiculum. Subiculum (Sub), PrS and parasubiculum (PaS) form the so called "subicular complex". In contrast to hippocampal subiculum, PrS and PaS are part of the PHR, which furthermore comprises entorhinal, perirhinal and postrhinal cortices (Fig. 1).

As its name suggests, the PrS is adjacent to Sub along the proximal-distal axis. Over most of its longitudinal dorso-ventral extent, proximal side of the PrS borders the Sub. On its distal side, the PrS is juxtaposed with the PaS. Generally, the PrS is easy to distinguish from neighboring regions by the characteristics of its cytoarchitecture, as it belongs to periallocortex. Periallocortex is built of 3 layers and can be considered as a transitional cortex between older archicortex and six layered isocortex. It is organized in an outer and an inner lamina, separated by a cell-poor lamina dissecans[6] and can further be subdivided into 6 different layers [7]. Layer I, called molecular layer, is a relatively cell-free plexiform layer with some putative interneurons and glial cells. Layer II is easily identifiable in Nissl- or NeuN- stained sections, as a thin zone, densely packed with small pyramidal cells. It serves as a distinguishing landmark to neighboring regions and can be labeled by molecular marker Calbindin (CB) [8] (Fig. 1). In the dorsal part of the PrS, afferent fibres fragment Layer II into small clusters[9]. Layer III is larger and presents a looser cell arrangement than Layer II (Fig. 2C). Layers I, II and III form the superficial layers[10–12]. In horizontal sections, their thickness increases from the proximal end of the PrS, next to the Sub, to the distal one, next to PaS. Layer IV, a cell-sparse band of large pyramidal cells, corresponds to the aforementioned Lamina dissecans which visually separates superficial of deep layers. Layer IV had for a long time been described as "neuron free" until a recent study identified its neuronal population[12]. The deep layers (layers V/VI) both typically feature a columnar arrangement and it is unclear if they are functionally separated. The main cytoarchitectonic characteristic differentiating them from each other is that layer V contains one or two rows of large pyramidal cells, whereas layer VI harbors

a variety of generally smaller fusiform or pyramidal cells [6,13]. Deep layers are in continuity with those of the entorhinal cortex[6,14](Fig. 2A).

In contrast to the PrS, the adjacent Sub is organized more like a cloud[15], and the sudden emergence of a superficial cortical sheet and a six layered organization of the PrS allows a reliably separation of both structures. On the other side, PaS lacks the densely packed Layer II of the PrS. To determine borders between deep layers of pre- and parasubiculum, molecular marker Parvalbumin (PV) provides a useful criterion. Strong immunoreactivity for this protein in the PrS contrasts with low staining intensity in the PaS[8] (Fig. 1). At its dorsal extreme, the PrS borders retrosplenial cortex. The delimitation between the PrS and retrosplenial cortex is marked by the presence of the lamina dissecans in the PrS, in contrast to its absence in the retrosplenial cortex. The transition between PrS and retrosplenial cortex is further marked by the topography of afferent fibers targeting PrS. These are numerous in the dorsal part of the PrS and show an abrupt interruption at the border to the retrosplenial cortex.

The PrS is a highly interconnected brain area, and diverse anatomical tracing studies revealed its afferent and efferent projections (Fig. 3). It is known to receive strong input from thalamic nuclei[16] (antero-dorsal, latero-dorsal and anteroventral nucleus) and neighboring cortical areas (anterior cingulate, retrosplenial and entorhinal cortices[16,17]) to all layers, except for layer II. Indeed, most afferent fibers tend to avoid layer II, that receives mainly projections from the contralateral PrS[18] (Fig. 2B). Afferent projections from the Sub target preferentially deep layers of the PrS,[16,19] while primary visual cortex is sending direct projections exclusively to superficial layers I and III.[20] The main efferent projections of superficial layers are ipsi- and contralateral entorhinal cortices.[11,16,21] Deep layer neurons target multiple brain areas such as the visual cortex[20], thalamic nuclei (ADN, LDN, AV),[16,22,23] the retrosplenial cortex[16] and the ipsilateral medial entorhinal cortex (MEC). Recently, layer-specific projections from layer IV to LMN and from deep layers to ADN have been discovered[22]. While conducting the present study, I examined the intrinsic properties of these projection specific neuronal subpopulations of PrS that are proposed to play a major role in the visual control of the sense of orientation.

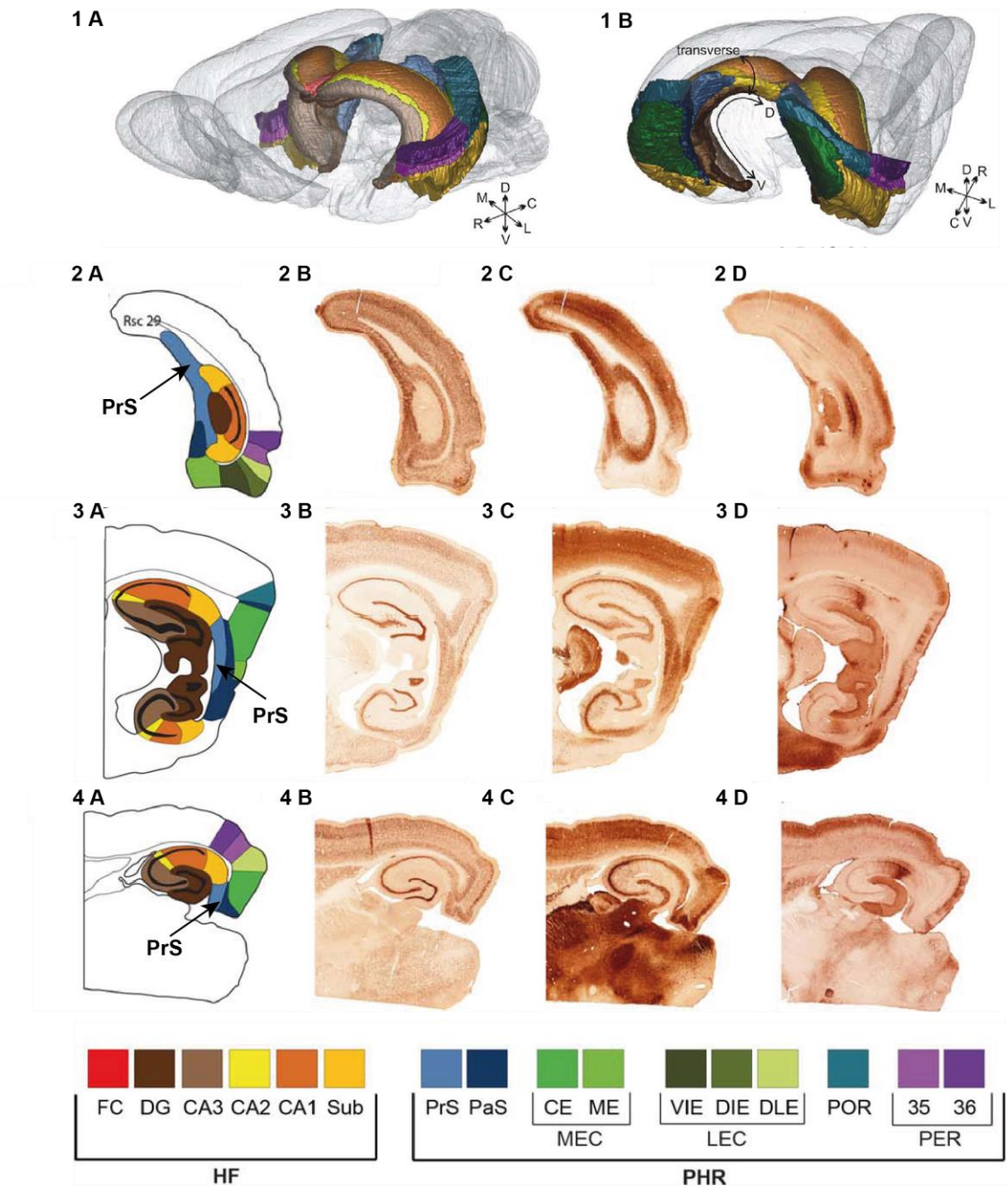

Figure 1 : **Views of the hippocampal region of the rat brain**

1A, 3D Oblique frontal view embedded in a transparent rat brain. **1B,** 3D Oblique occipital view. **2** Coronal sections, **3** Sagittal sections, **4** Horizontal sections. **A** Schematic color-coded delineation of divisions of the hippocampal region. Color code as presented in the lower panel. **B** NeuN-stained sections. **C** PV-stained sections. **D** CB-stained sections. Abbreviations: CA1–3, Cornu ammonis 1–3; CB, Calbindin; DG, Dentate Gyrus; EC, Entorhinal Cortex; FC, Fasciola Cinereum; HF, Hippocampal Formation; LEC, Lateral Entorhinal Cortex; MEC, Medial Entorhinal Cortex; PaS, Parasubiculum; PER, Perirhinal Cortex; PHR, Parahippocampal Region; POR, Postrhinal Cortex; PrS, Presubiculum; PV, Parvalbumin; Rsc, Retrosplenial Cortex, Sub, Subiculum; 35, Perirhinal Area 35; 36, Perirhinal Area 36. Adapted from Boccara et al. (2015).

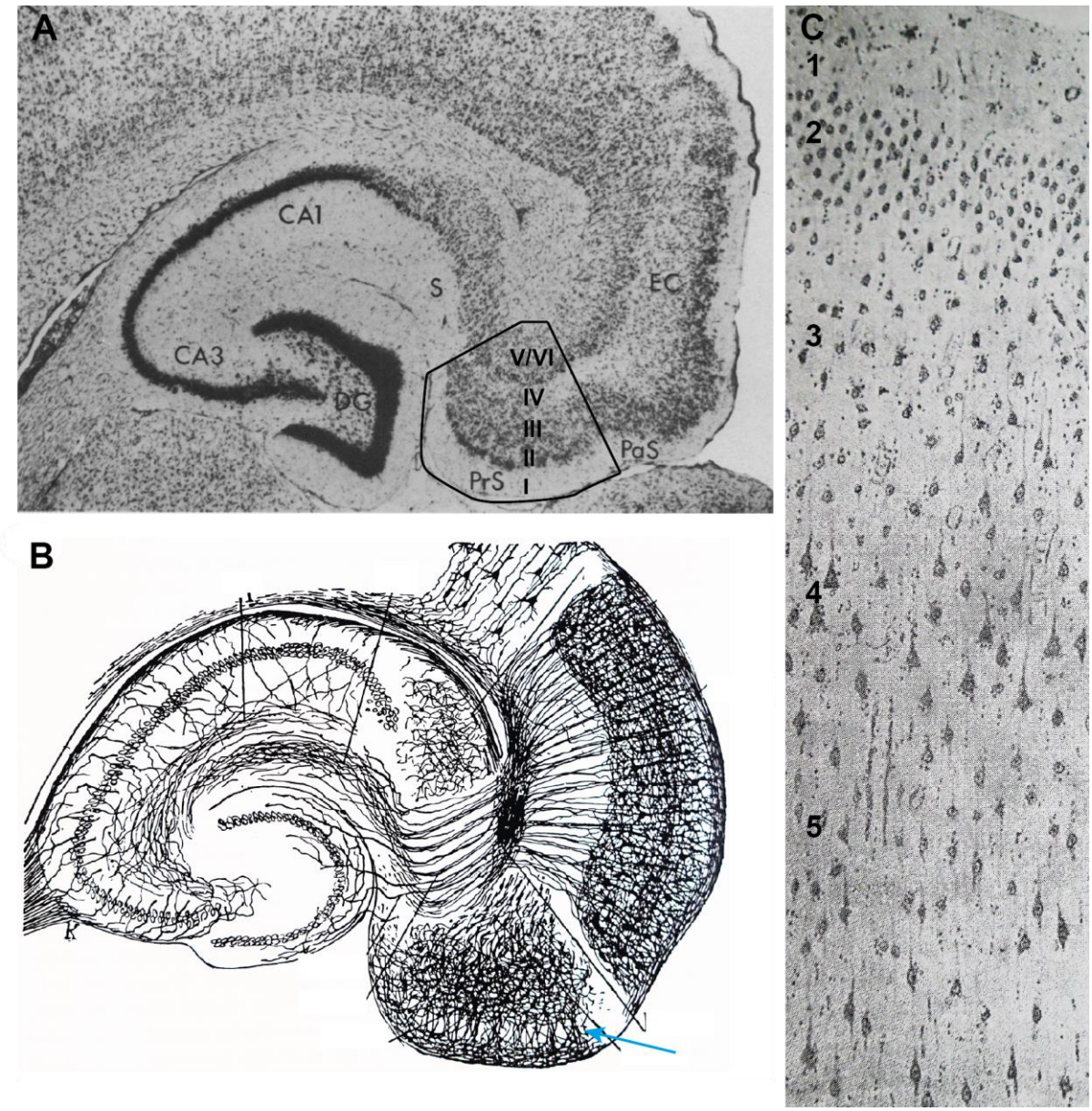

Figure 2 : **Layers and afferent fibres of the presubiculum**

A Rat tissue. Thionin-stained horizontal section through the hippocampal formation. Layer IV (Lamina dissecans) separates visibly superficial from deep layers. Within superficial layers, layer II is denser than layer III. Deep layers appear as continuation of those in subiculum and EC. Adapted from Amaral and Witter, 1989. **B** Drawing of a horizontal section, stained with the Golgi method. Adapted from Ramon y Cajal (1899). Note the dense "plexus" of afferent fibers in the PrS that partially avoids layer II (blue arrow). **C** Human tissue. Nissl method from Ramon y Cajal (1899), Nomenclature: 1, plexiform layer; 2, small pyramidal and fusiform cell layer; 3, deep plexiform layer; 4, large to medium size pyramidal cell layer; 5, fusiform and triangular cell layer. Abbreviations: EC, Entorhinal Cortex; DG, Dental gyrus; PaS, Parasubiculum; PrS, Presubiculum.

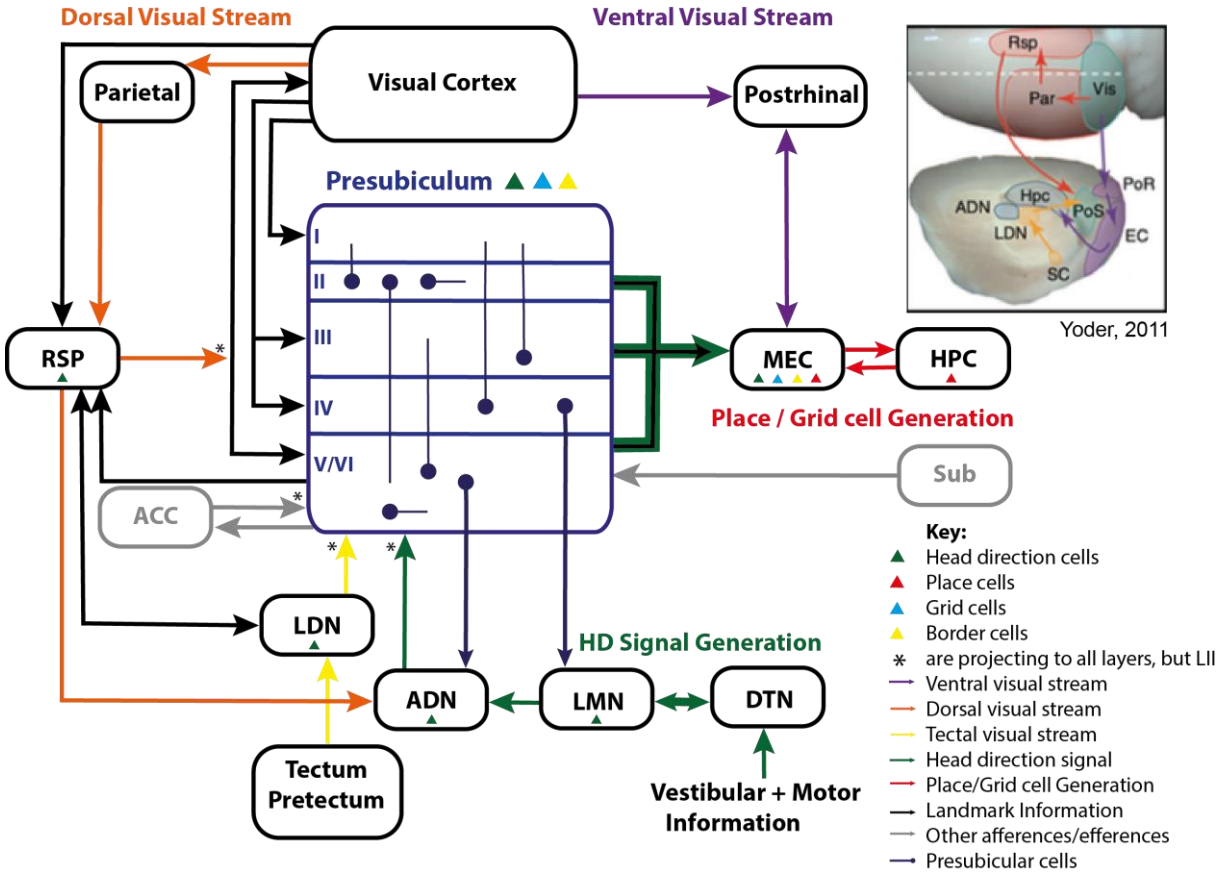

Figure 3: Functional connectivity of the presubiculum

Blue rectangle in the center: Presubiculum with its inter- and intralaminar projection patterns as well as layer specific afferences and efferences. Blue dots correspond to laminar location of cell bodies with blue lines indicating their intra- or interlaminar axonal projections. Presubiculum is shown in a working model of the landmark-processing circuit in rodents. The HD signal (green arrows) is generated within the reciprocal connections between LMN and DTN, based on information arriving from subcortical motor and vestibular systems. PrS receives landmark information from visual cortex, the dorsal (orange) and tectal (yellow) visual stream. These pathways also target RSP, which has reciprocal connections with PrS. The presubicular signal provides information to downstream areas of the head direction circuit, respectively ADN and LMN (Note the projection specific neurons in layer IV to LMN and deep layers to ADN). Integrated signal ascends back to PrS where it is projected probably with additional landmark information to the RSP and MEC, which have reciprocal connections with PrS. In MEC the HD signal is integrated into the grid cell signal and the place cell signal, generated in MEC and HPC (red arrows). Find the projection of the three major visual processing streams onto lateral and parasagittal views of the rat brain in the top-right (Adapted from Yoder, 2011). Abbreviations: ADN, Anterodorsal thalamus; ACC, Anterior cingulate cortex; DTN, Dorsal tegmental nucleus; HPC, Hippocampus; LDN, Lateral dorsal thalamus; LMN, Lateral mammillary nuclei; MEC, Medial Entorhinal Cortex; Parietal, Parietal cortex; Postrhinal, Postrhinal cortices; PrS, Presubiculum; RSP, Retrosplenial cortex; Sub, Subiculum.

1.2 Function of the presubiculum

As a highly interconnected structure within the temporal lobe, presubicular cortex is involved in various information processing circuits located in this brain area. In particular, presubicular function is thought to play a significant role for the sense of orientation[5,8,24–26]. Beside this, it is also known to serve as a pathway in the temporal lobe memory circuit by conveying hippocampal information onto the entorhinal cortex[27]. Combination of both may be required to create a memory of space-related information. Temporal lobe epilepsy (TLE) is a pathological condition due to presubicular impairment. It has been shown that presubicular projections onto seizure-sensitive cells in layer III of entorhinal cortex are implicated in the generation of epileptiform discharges during TLE in humans and animal models[28–30]. In the following, however, I will focus on regular functioning of the PrS and concentrate on its role within the spatial navigation circuit.

1.2.1 The sense of orientation

The sense of orientation is essential for mammals to find what they need for survival: food, water or a safe place to sleep. In our everyday life, our sense of orientation helps us to recognize our way to work or to remember the way to our favorite coffee place. Two main cognitive processes are necessary to create a neuronal representation of space, enabling us to remember and recognize our environment: Path integration and landmark navigation. Path integration uses internally generated information, referred to as idiothetic cues (vestibular, proprioceptive and motor input), to encode our position in space. Landmark navigation relies on external cues, especially on visual but also olfactory or auditory information. Processing of space-related information occurs in the hippocampal- parahippocampal area, in particular through the dense interconnection between hippocampus and entorhinal cortex, by functionally specific cell types that selectively encode spatial information (Fig. 4A).

First evidence for neurons coding spatial information were “place cells” in hippocampus[31], which fire only when an animal finds itself at a discrete location. Then, “head direction cells” were described in the PrS, constituting the major cell population in the presubicular cortex with about 50-60% [8,24,25]. Head direction cells (HD cells) rely principally on vestibular[32] and visual[33] input, by robustly increasing their firing rate when the animal’s head points in a specific direction (Fig. 4B-D). Since then, “grid cells” have been discovered in entorhinal cortex[34], para- and presubiculum[8,35]. Grid cells are activated at multiple locations, arranged in a hexagonal grid-like manner. The emergence of the grid cell signal in the entorhinal cortex is assumed to critically

depend on the activity of presubicular HD-cells [36]. Final and latest discovery are "border cells", located in the medial entorhinal cortex, subiculum[37], para- and presubiculum[8,35]. Border cells show increased activity when the animal is close to an environmental border. These four different subtypes of spatial neurons are thought to be directly or indirectly interconnected, this way encoding our internal representation of space.

1.2.2 The head direction signal

Among all cognitive processes that are needed for a complete representation of space, the PrS is mainly known to play a crucial role in the neuronal encoding of an animal's head direction which is processed by HD-cells. In the PrS, HD-cells are distributed throughout all presubicular layers,[8,24] but have been mainly observed in its dorsal portion[38]. Each HD-cell is activated by a specific head direction. If an animal heads in the preferred direction of one cell, its firing rate increases in accordance with a stable tuning curve (Fig. 4B). The tuning curve generally corresponds to a Gaussian distribution around this direction[39] and maximal firing rate is reached when the animal's head is directly turned towards the preferred direction. Maximal firing rate varies between cells, lying between 5 and 115 Hz[3]. As long as the preferred head position is maintained, the HD-cell shows persistent firing. Cellular mechanisms for the non-adapting HD-signal still remain unknown but may be supported by a tetrodotoxin (TTX) - insensitive sodium current with slow kinetics that was revealed in superficial presubicular neurons, presumably expressed at sites distant from the soma [40]. To generate the head direction signal *in vivo*, it has to be computed through a circuit of interconnected cortical and subcortical brain areas, all including head direction cells. Besides the PrS, the head direction circuit includes dorsal tegmental nucleus (DTN)[41], anterodorsal thalamic nucleus (ADN)[42], laterodorsal thalamic nucleus (LDN)[43], lateral mammillary nucleus (LMN) [44] as well as the retrosplenial (agranular and granular)[41] and the entorhinal cortex[36] (Fig. 3).

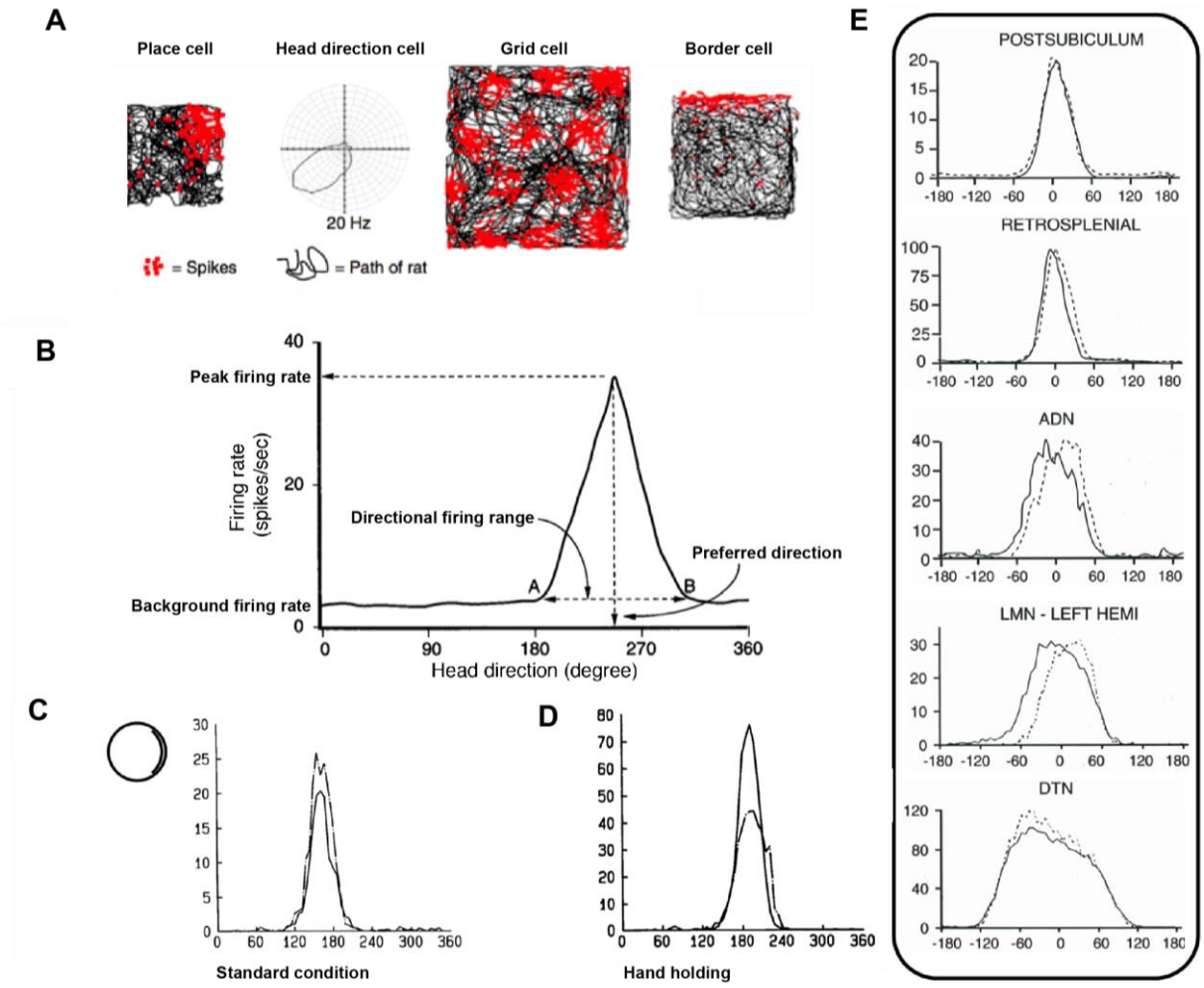

Figure 4 : Spatial neurons involved in navigational processing and tuning properties of HD-cells

A Cell types encoding space related information in hippocampal-parahippocampal areas. Cellular activity (spikes, red dots) is related to the animals position (path of rat, black lines). **B** Firing rate as a function of head direction in a presubicular HD-cell with specific tuning curve features (adapted from Taube, 1995): Background firing rate is close to zero. It increases within the directional firing range to reach the peak firing rate for the preferred direction. **C** Recording of a representative cell across two recording sessions, one (dashed line) recorded 15 days after the other (solid line) shows stability over time. In standard condition, a prominent cue card is disposed as a polarizing cue on one side of the open field wall. **D** Carrying the animal by hand and moving it around in the arena (dashed line) decreases peak firing rate compared to standard condition (solid line). Note the different preferred direction and peak firing rate for each cell. There are low- (B), medium- (C) and high- (D) peak firing rate cells. **E** Typical tuning curves of head direction cells in different areas of the head direction circuit. Solid lines represent tuning curves during clockwise, dashed lines during counterclockwise head turn. Note the larger tuning curves in subcortical ADN, LMN and DTN. (adapted from Taube and Wiener 2005).

Hierarchy of the HD-circuit was mainly established through lesion studies[45] that revealed a subcortical origin of the head direction signal. Subcortical nuclei DTN and LMN receive vestibular information about self-movement and interaction between both is thought to convert angular velocity information to the head direction signal[45,46]. Reciprocal connection between LMN and DTN was therefore identified as HDC generative circuit. From LMN, the HD-signal is projected onto ADN which appears to be a critical relay station as its lesion leads to a complete disruption of the head direction signal in upstream cortical areas like retrosplenial cortex, para- and presubiculum[16,22,38,47,48]. In the cortical part of the HD-circuit, the head direction signal is refined: the tuning curve of cortical head direction cells has a narrower range and a higher stability over time than its subcortical precedent (Fig. 4E). Increased precision may result from integration of sensory input such as visual information. The PrS is a major entry point for visual landmark information, receiving direct input from visual cortex[20] as well as previously relayed visual information from retrosplenial cortex and laterodorsal thalamus[26] (Fig. 3). As PrS sends descendent projections to LMN, ADN[26], LDN[49] and retrosplenial cortex[50] it may refine the local HD signal with visual information in these areas by exerting significant feedback control. Indeed, after lesion of the PrS, reduced influence of visual cues on preferred direction of HDC has been noticed in ADN and LMN[26,38]. The PrS seems therefore to be an important relay station, contributing to the transformation of the subcortical HD-signal that principally relies on egocentric information to an allocentric representation that is the cortical HD-signal by adding external visual information.

As in many sensory systems, the relationship between stimulus driven and internally generated origin of the head direction sense has not yet been settled. The head direction signal is assumed to be largely controlled by peripheral inputs, primarily the vestibular afferents[25,41]. In addition to the stimulus-driven HDC activity, computational models postulate internally generated (attractor) mechanisms to be at the origin of the head direction sense. They assume HD- cells with similar preferred directions to fire together within a temporally correlated group of HD- neurons (activity packet). The activity packet is believed to move on a virtual ring as the animal turns its head while neurons with greatly different preferred directions are suppressed by lateral inhibition[51,52]. That way, a sustained “hill” of excitation is formed, centered on the animal’s current HD (Fig. 5).

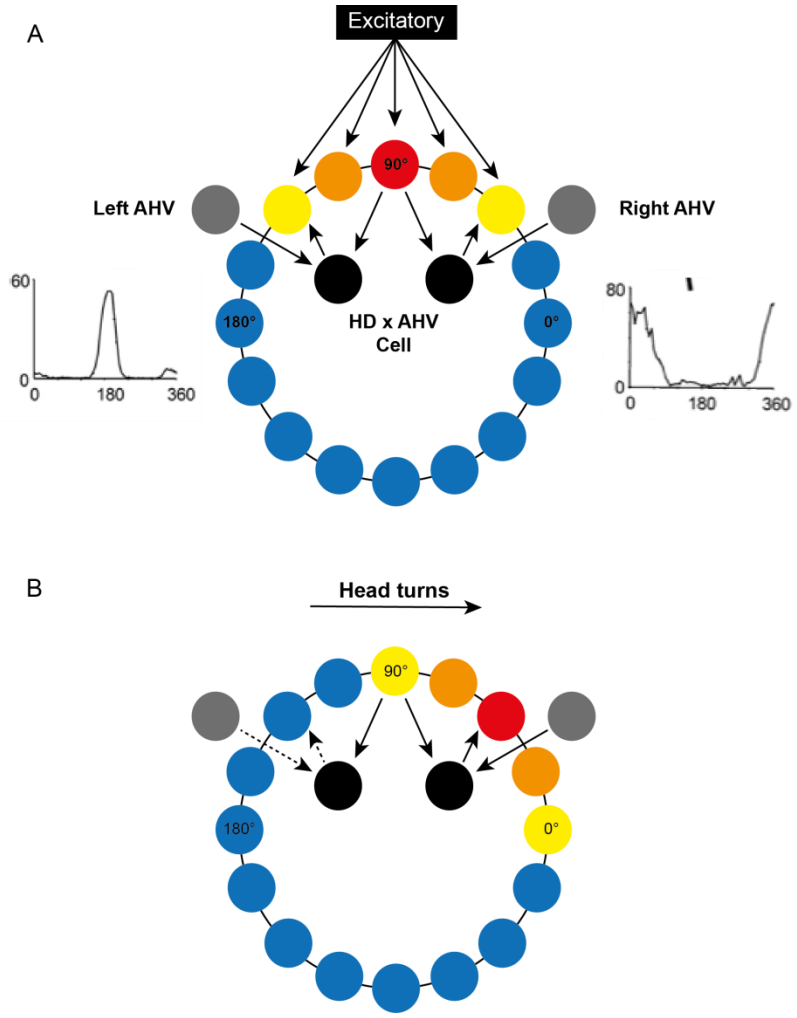

Figure 5: Attractor network model

A Visualization of a possible attractor model for HD sense generation. In general, HD cells are conceptually arranged in a ring with each cell's position (colored circle) corresponding to its preferred firing direction. Neighboring cells (similar preferred tuning directions) are connected by strong excitatory connections. The strength of this connection decreases with increasing distance between cells. Not shown are the inhibitory projections which limit net activity. This reciprocal connectivity results in a focused point of high activity (warm colors). Two additional signals lead to movement of the activity hill corresponding to an animal's head direction: changes of angular head velocity (gray circle) and conjunctive encoding of current HD x AHV (black circle). Cells that encode HDxAHV are either sensitive to rightward head turns and project to the right of the ring to which they receive input or the other way around. **B** Conjunctive HDxAHV cells drive the activity hill in the appropriate direction following a head turn. Hence, a right head turn would engage neurons specifically sensitive to clockwise turns (solid arrow). In turn, these neurons would activate proximal HD cells to the right of the hill. This way, activity focus is driven to the animal's current head direction. Adapted from Clark and Taube (2012); See also Peyrache et al. (2015).

A recent study by Peyrache et al. (2015)[5] compared double-site multi-unit recordings in ADN and PoS in waking and sleeping brain states. They found a preserved correlated activity of HD neurons in both regions across different brain states, a finding that provides experimental support for the postulated ring-attractor hypothesis. They further suggested the ADN-PoS-ADN excitatory loop to contribute to the internal self-organized mechanism. Such an internally generated origin of the HD-signal would imply ongoing HDC activity even after lesion of its major external input, the vestibular afferences. Although it had previously been demonstrated that lesions of the peripheral vestibular system completely abolished directional activity in the anterodorsal thalamus[38]. Therefore, HD activity results most likely from a combination of internal and external processes[52] but far more experimental data has to be provided to prove what origin the HD signal has and which structures contribute to its coding system.

1.3 Information processing in the presubiculum

All spatial and non-spatial information received by the PrS is processed at the microcircuit level in order to build a local signal, such as the HD- signal. While anatomical connectivity studies show possible informational pathways, the nervous signal is computed through a microcircuit consisting of neurons with specific characteristics that influence signal transmission. Specific cellular characteristics such as resting membrane potential, input resistance or time constant determine the excitability of neurons and their firing pattern. This explains the importance of knowing about neuronal intrinsic and integrative properties, their connectivity within the local circuit and the strength and dynamics at a given synapse to understand the complexity of computation in a microcircuit. Yet it is worth noting that intrinsic properties are flexible entities and can change under a number of conditions, for example by distinct network activity occurring during different brain states[53]. While long range connectivity of the PrS has been of interest in several studies[2,11,16,20,54], the local circuit of the PrS remains widely unknown. Morphological and electrophysiological results suggest that the PrS contains elements of horizontally and vertically organized structural modes (Fig. 3) which may result from the particular location between hippocampus and neocortex. In hippocampal archicortex, cells are packed in a single layer and neighboring cells have similar intrinsic properties[55]. In six-layered neocortex on the other hand, excitatory neurons are organized in vertical columns and horizontal layers differing in their characteristics [56].

In the PrS, evidence for vertical modularity are for instance the orientation of pyramidal cells dendrites towards the cortical surface and radially towards deep layers orientated axons of layer II/III neurons[12,57]. Also, interlaminar projections from superficial layers to deep layers have been revealed, a connectivity that is less frequently seen the other way around[10–12]. Despite these indications, a specific functional unit, such as the canonical cortical column, has never been demonstrated in the PrS but cannot be excluded either[2].

1.3.1 Excitatory microcircuit

Within every microcircuit there is excitatory and inhibitory activity. Excitatory neurons represent the largest population of cortical neurons, therefore they are called principal cells, and are distributed through all cortical layers and areas. They rely on chemical signal transmission using the neurotransmitter glutamate[58]. Morphologically, excitatory cells show either a pyramidal shaped or, when localized in cortical layer IV, a star-like (stellate) somata. Their dendritic arborization varies between layers, areas and species[59] but is generally composed of a basal dendrite, spreading horizontally, and an apical dendrite which is orientated vertically towards the pial surface. Moreover, dendrites of excitatory neurons are characterized by their spiny appearance, reflecting their multiple synaptic contacts. Principal cells are connected locally (within one layer and column) and/or with neurons of other brain areas through long-range projecting axons. Therefore, principal cells are part of the micro- but also build the macrocircuit. Regarding their firing properties, excitatory neurons can be grouped into three main categories: Regular spiking (RS), intrinsic bursting (IB) and fast repetitive bursting (FRB) neurons[58,60]. RS cells are the most common category of cortical pyramidal cells. Their regular firing frequency of action potentials (AP) increases with increasing current injection and decreases with its duration. The decrease of the AP frequency is called adaptation and its progression varies between RS cells. IB cells show typical clusters of high frequency firing (150-250 Hz) shortly after current injection, the so called “burst”, reappearing rhythmically (5-15 Hz). One burst is composed of 3-5 APs with decreasing amplitude, due to the inactivation of sodium channels. FRB neurons are characterized by a fast repetition (20-80 Hz) of high frequent bursts (200-600 Hz)[58]. Intrinsic firing patterns of neurons play substantial roles as they determine their response properties within the cortical circuit[61] and may thus be associated to a specific function. For example, bursting behavior is linked to a more efficient initiation of synchronized cortical activities[62].

For a long time characterization of excitatory neurons in the PrS had been done only to a certain degree [10,18]. First studies recorded some RS neurons in layers III and V[10] but didn't give a clear view of neuronal diversity in the PrS across all six layers. Recently, two studies established an extensive classification of principal cells in the rat PrS by using unsupervised clustering. The first one, by Simonnet and colleagues (2013), included cells of all layers and based its classification on electrophysiological and morphological criteria, such as dendritic length and form[12] whereas the second, by Abbasi and Kumar (2013), concentrated on electrophysiological properties of neurons in superficial layers. According to the study by Simonnet et al. (2013), principal neurons in the PrS can be classified into 3 major classes, generally conform to neurons of the periarchicortex like the entorhinal cortex and less resembling those of the neighboring subiculum. The first class contained regular-spiking principal cells, located in the superficial layers II and III. They appeared as little excitable neurons by their hyperpolarized resting membrane potential and high rheobase. Morphologically, they were small, pyramid-shaped neurons with axons projecting towards deep layers. Abbasi and Kumar distinguished 5 additional cell types in the upper layers, some of them expressed exclusively in layer II or III and some of which could be interneurons.

The second major cell class described by Simonnet et al. (Fig. 6) were IB cells in layer IV, a layer previously considered cell-free. These cells had a resting potential close to threshold and discharged in single or repeated bursts (weakly and more strongly bursting neurons). Their apical dendrites spread to layer I, where they might receive visual inputs as well as projections from entorhinal cortex [49]. Their axons ramified to all layers, except for layer I. Locally, bursting behavior of layer IV neurons could reliably excite postsynaptic targets, helping to define functional units for processing head direction. Presence of this distinct group of IB-cells clearly distinguishes the PrS from neighboring entorhinal cortex. In contrast, IB cells are present in the subiculum[55] where they are especially dense close to the PrS[19]. This may reflect a common origin of both regions. Also, subicular IB-cells are known to display a target specificity[19]. The question therefore emerged if presubicular IB cells could also constitute a projection-specific subpopulation, considering that they are localized in LIV which targets subcortical LMN (Fig.7).

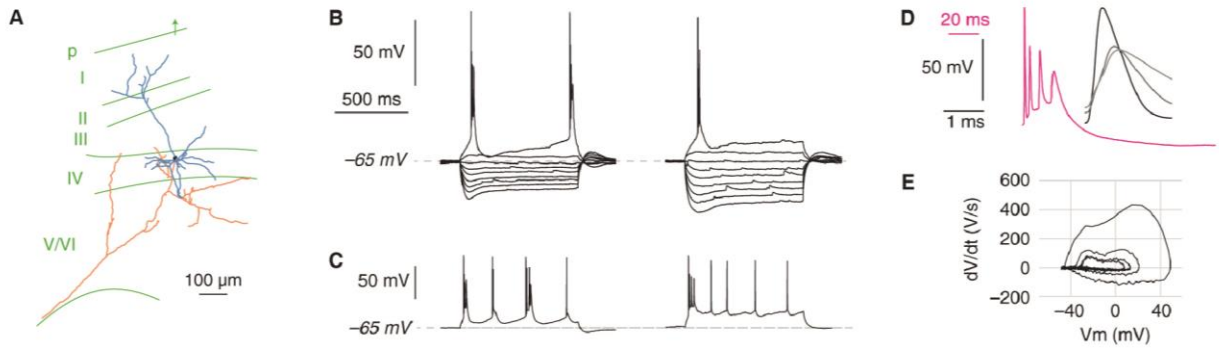

Figure 6 : **Intrinsic bursting neuron of Layer IV (Cluster 2 of presubicular principal cells)**

A Reconstruction of a biocytin-filled cell. Note apical dendrite projecting close to the pial surface. Axons are red, dendrites blue, layer limits and pial surface green. **B** Responses to 800 ms of current injection, starting at -100 mV and depolarizing with steps of Δ 25 pA. Note the pronounced sag. **C** Burst firing induced by +100 pA step current injection. **D** Two to four APs occur within a burst. **E** Phase plot of AP bursts. Vm, membrane potential. Adapted from Simonnet et al., 2013.

The third major class of presubicular principal cells was expressed in deep layers (V/ VI). Neurons of group 3 generally tended to be larger than cells of the superficial layers and seemed similar in form and physiology to neurons in corresponding layers of the entorhinal cortex[21]. They appeared as a very heterogeneous population of spiny neurons and could be divided into two subgroups. The first subgroup included RS neurons with diverse morphologies, whereas the second contained more excitable regularly spiking, pyramid-shaped cells. It is not known yet if the differences between these two neuronal populations are linked to target specificity of their long-range projections.

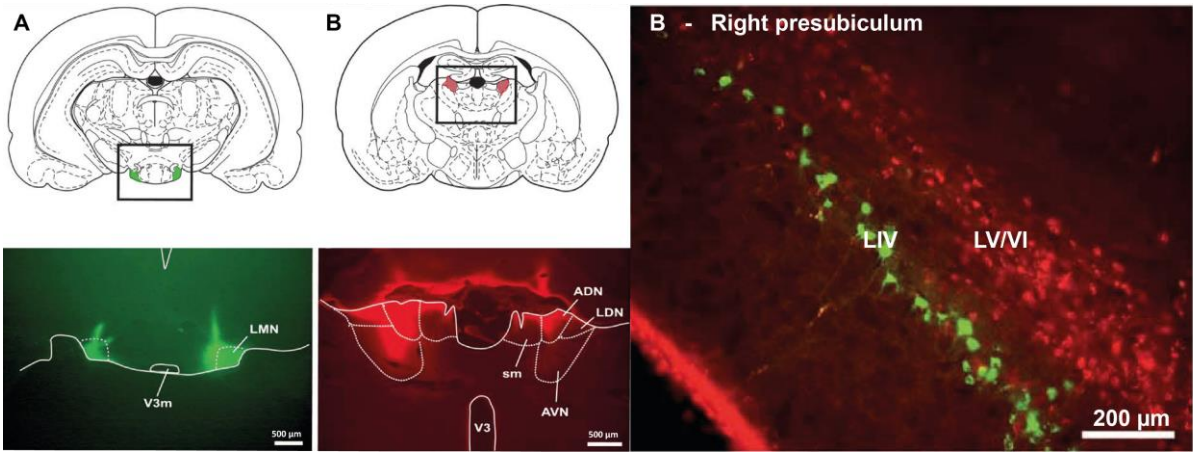

Figure 7 : Projection specific neurons in layer IV and deep layers (V/VI)

Injection of Cholera toxin fluorophore conjugates into LMN (**A**, Alexa Fluor 488) and ADN (**B**, Alexa Fluor 594). Dashed lines indicate areas corresponding to diagrams above. LMN and ADN correspond to shaded areas in rectangle in diagrams above. **C** Tracer was transported retrogradely in non-overlapping neuronal populations in the presubiculum. Somata of layer IV neurons show green labeling (green) as injected tracer in LMN. Somata of layer V-VI neurons show labeling following tracer injection (red) into the right ADN. ADN, Anterodorsal thalamus ; AVN, Anteroventral thalamus ; LMN, Lateral mammillary nucleus ; sm, stria medullaris ;V3, third ventricle; V3m, third ventricle, mammillary recess. Adapted from Yoder and Taube (2011).

1.3.2 Inhibitory microcircuit

Inhibitory activity is crucial to limit excitatory activity by controlling neuronal excitability or reducing the magnitude and duration of a single neurons activation. However, inhibition can do more than just counterbalance the excitatory network. Indeed, typical connectivity motifs of inhibitory cells such as feedback or feed-forward inhibition[63–66] contribute to the generation of oscillatory network patterns by defining when and where neurons discharge, thereby patterning the information flow in space and time of entire cortical networks. Within the presubicular microcircuit, inhibition could be important to define functional units and shape the head direction signal. While recent works shed light on the population of excitatory neurons in the PrS, presubicular inhibitory neurons (their properties, distribution and connectivity patterns) remain an unexplored cell population.

Inhibition is mediated by GABAergic interneurons, also called ‘non-principal cells’, non-pyramidal or short-axon neurons. Their names refer to the fact that their axons usually arborize locally, often displaying a laminar oragnization[67,68]. Interneurons constitute about 10-30% of the total neuronal population in cerebral cortex depending on area, species and cortical layers[67]. Although a relatively small neuronal population, highly diverse and distinctive interneuron-types can be recognized, suggesting specialization. This diversity had already been noticed by Ramon y

Cajal[69], who was therefore convinced that they could be the key to understanding the complexity of the mammalian brain. Ever since, classification of interneurons remains a matter of debate. Its importance derives from the assumption that subtypes may be associated to specific functions. Indeed, it has been demonstrated that the deterioration of specific interneuron subtypes is related to a vulnerability to pathological conditions like schizophrenia or autism[70–72]. To unify a sometimes conflicting terminology the "Petilla nomenclature" [68] is a widely accepted and useful reference for interneuron classification[67,73]. It is mainly based on the specific output characteristics of interneurons, as all axons of one interneuron generally target identical neuronal subdomains (axon, soma, perisomatic region or dendrites). The largest population of interneurons, about 50%, is soma-targeting and called basket cells[74], as their axon forms a basket-like structure around the innervated cell body. Other common types are chandelier cells[75], targeting the initial segment of principal cells, or dendrite-targeting cells. Beside the output characteristic, the Petilla nomenclature also includes molecular, morphological and electrophysiological properties of interneurons which often converge to non-overlapping well-defined subpopulations. The first electrophysiological property related to interneurons is their fast-spiking behavior [60]. About one third of all inhibitory cells are fast-spiking,[76] discharging up to 500 Hz, which is 2-3 times faster than pyramidal neurons. Beside this large group, interneurons show five other main discharging types that are classified as adapting, accelerating, irregular, intrinsic bursting or non-adapting non-fast spiking.

On a molecular level, inhibitory neurons express a subset of proteins that excitatory neurons generally don't. Moreover, every protein is expressed only by a subset of GABAergic cells and often linked to a specific connectivity pattern[77]. The most commonly used molecular markers are 4 neuropeptides (Vasointestinal Peptide [VIP], Somatostatin [SOM], Cholecytstokinin [CCK], Neuropeptide Y [NPY]) and 3 calcium-binding proteins (Parvalbumin [PV], Calretinin [CR], Calbindin [CB])[78]. Other, less frequently used molecules are for example the ionotropic serotonin receptor 5HT3a, Reelin, nitric oxide synthase or choline acetyltransferase. Marker proteins are mostly used as a convenient tool to label interneuron subtypes, and only few studies aimed to elucidate their presumable functional role have been conducted. Calcium binding proteins (CBP) are thought to have a neuroprotective capacity by buffering intracellular calcium[79] and it has been shown that PV expression in axonal terminals can affect GABA release dynamics[80]. Neuropeptides SOM and NPY are assumed to function as co-transmitters or modulators of interneurons with specific effects on neuronal excitability and synaptic transmission. They are also believed to play a role as endogenous anti-epileptic agents[81,82]. Neuropeptide VIP is presumed to have a vasoactive

effect[83]. Some interneurons co-express up to seven different molecular markers,[84] and patterns of co-expression differ between regions and species. In neocortex, typical patterns of co-localization are VIP and CR or SOM and CB, whereas hippocampus contains other molecular subpopulations, such as PV+/SOM+ interneurons[81,85–87]. Therefore, multiple labeling is of particular interest to define different interneuron classes.

In addition to the classification criteria of Petilla nomenclature, it has recently been suggested that the developmental origin of interneurons could further refine the classification system[88]. From a developmental point of view, interneurons arise either from medial ganglionic eminence (MGE), lateral and dorsocaudal ganglionic eminence (CGE) or preoptic area (POA)[88,89]. Interneurons expressing PV and SOM would arise from MGE, while VIP and CR expressing neurons would belong to the CGE group[90,91].

As already mentioned, interneuron cell types are usually defined by the combination of above named criteria: marker expression, morphology, connectivity pattern and intrinsic firing properties. The best known example would probably be the Parvalbumin positive, fast spiking basket cell[92] (Fig. 8). Another extensively studied interneuron type is the neocortical Martinotti cell, mainly localized in layers II-IV with ascending axonal arborization, extending up to layer I[93]. It is a SOM positive, dendrite targeting interneuron subtype, displaying an adaptive firing behavior. The hippocampal correspondent to the Martinotti cell is called O-LM cell[81,82], referring to its soma, which is primarily confined to stratum oriens (O) and its axon terminal fields in stratum lacunosum-moleculare (LM). Both, Martinotti and O-LM cells, are suggested to suppress calcium spikes and bursting in targeted dendrites[88]. PV+ and SOM+ interneurons constitute two major interneuron subtypes, appearing as distinct computational elements and often opposed in terms of function[94]. In addition to the concept of distinct interneuron classes, some authors note that a continuum of phenotypes may exist[95].

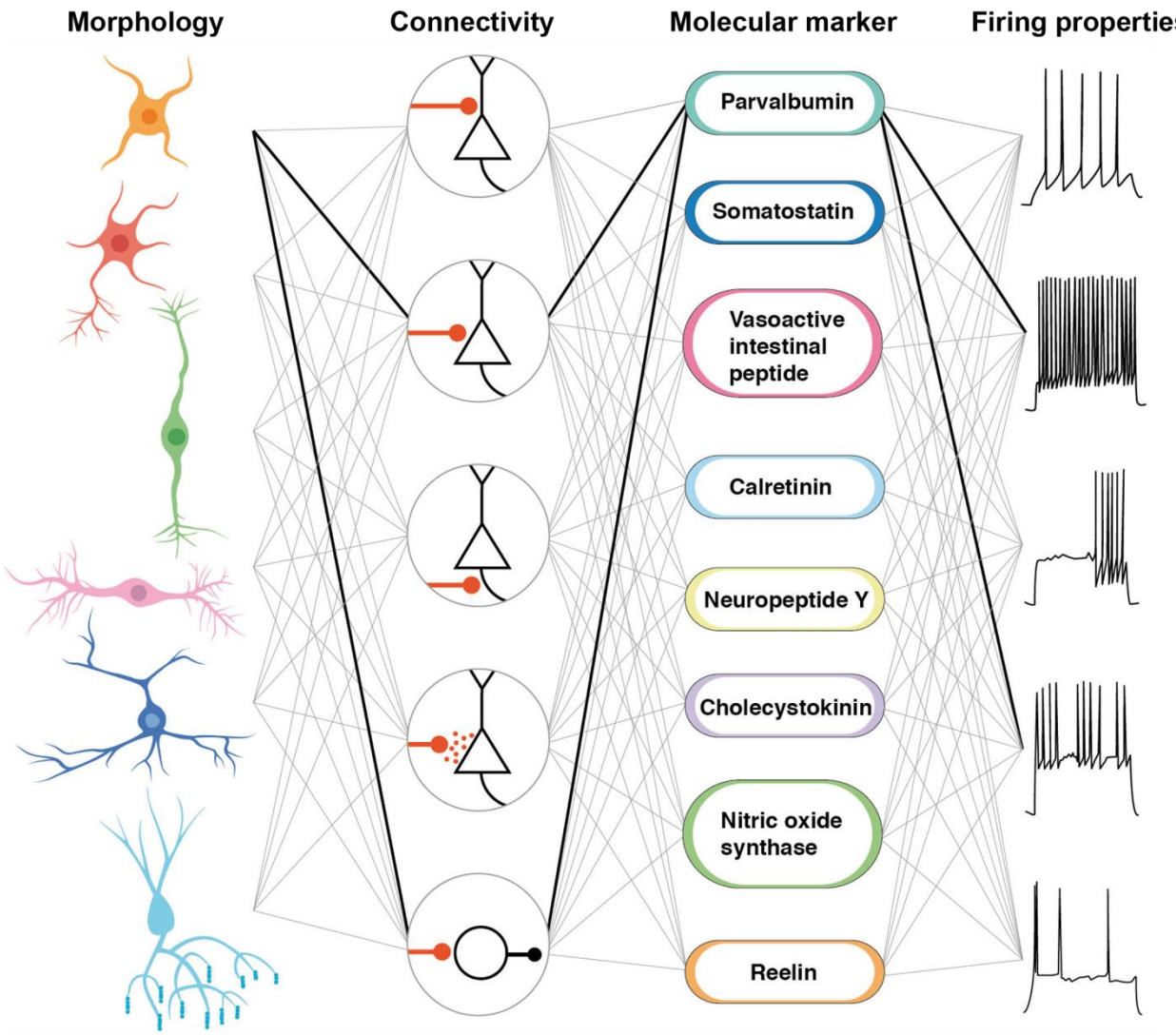

Figure 8: Dimensions of interneuron diversity

Multiple morphologies, connectivity patterns, marker expression and intrinsic firing properties have been reported for interneurons. Combination of all aspects gives rise to specific interneuron classes. Highlighted connections define fast-spiking cortical basket cells. Adapted from Kepecs and Fishell (2014).

1.4 Main questions of the present study

As presented in the introduction, many aspects of the structural organization and the functioning of the presubicular cortex still remain unknown. In this framework, the present study aimed to characterize and quantify the molecular and electrophysiological properties of specific neuronal populations in the PrS.

In a first step, I decided to concentrate on a general quantification of interneurons in the PrS, an unexplored cell population, by using a mouse model that expresses green fluorescent protein in inhibitory neurons (GAD67-GFP line). In addition to a general quantification of interneurons in the PrS, I performed double immunostaining with neurochemical markers in order to shed light on the distribution of molecular interneuron-subpopulations in this area. Distribution and marker expression of presubicular interneurons probably displays a specific pattern that may correlate with specific functional requirements, given the exceptional anatomical and functional position of the PrS. As described above, the PrS lies at the junction between cortical areas and the hippocampal formation, both displaying differences in their interneuron populations. It has thus been of interest to see whether interneurons of the PrS can clearly be assigned to the neocortical or hippocampal interneuron population, combine characteristics of both or show completely different characteristics.

In a second step, I focused on the characterization of projection specific neurons, testing if their target specificity predicted a distinctive output pattern. I therefore injected a retrograde tracer into LMN and AND, both receiving efferent projections of the PrS. Labeled presubicular neurons were then recorded *in vitro* and morphologically reconstructed after biocytin-filling. Previous studies had revealed layer specificity of presubicular projections to LMN and ADN, from dorsal part of presubicular layer IV and deep layers, respectively. Both subcortical regions, LMN as well as ADN, are suggested to play a fundamental role in the emergence of the HD-signal. Electrophysiological and morphological properties of projection neurons give a better insight into information integration within the HD circuit that allows the transformation of a signal primarily relying on egocentric information into an allocentric representation.

2. METHODS AND MATERIALS

2.1 Animals

For interneuron characterization, experiments were performed on 28- to 39-days-old male transgenic GAD67-GFP knock-in mice (n=9), provided by Yuchio Yanawaga[96]. In GAD67-GFP knock-in mice, GABAergic neurons are highlighted by green fluorescence from early development stages on. A cDNA encoding a green fluorescent protein (GFP) is inserted between the GABA synthesizing enzyme glutamic acid decarboxylase (GAD67) 5' flanking region and the GAD67 codon start. In GAD67-GFP mice, GFP is specifically expressed in GAD67+ and GABAergic interneurons, thereby enabling their selective targeting and characterization[96]. One should however note that homozygous GAD67 positivity is a knockout criterion.

For long range connectivity studies, wild type C57BL/6 (n=64) and GAD67-GFP knock-in mice (n=5) were used. At injection they were about 2 months old (m=51.04 +/- 12.65 days) and recordings were done 1-2 weeks after injection (Age at recording: m=71.2 +/- 17.82 days). GAD67-GFP knock-in mice were used to verify, whether supplementary source of information in order to check if GABAergic long-projection neurons were part of the labeled LMN/ADN projection neurons.

Care and use of the animals conformed to the European Communities Council Directive of 22 September 2010 (2010/63/EU) and French law (87/848). The study was approved by the local ethics committee Charles Darwin N°5 and the French Ministry for Research.

2.2 Immunohistochemistry

Animals were anesthetized with 100µl pentobarbital (i.p.), a letal dosis, respectively before being perfused intracardially with 20 ml of a mixture containing paraformaldehyde (4%) and 0.12 M Phosphate buffer (1l PB 0.24 M pH 7.4: H_2O with 33.76 g Na_2HPO_4, 7.72 g NaOH). The brain was then removed from the skull and submerged at 4°C for 24 h in the fixative previously used for perfusion. It was rinsed 3 times in Phosphate buffered saline (PBS), a solution containing (in mmol/l): 137 NaCl, 2.7 KCl, 10 Na_2HPO_4 and 1.8 KH_2PO_4 at pH 7.4. Afterwards, each brain was stored for at least 2 days at 4° C in 30% sucrose buffered in PB 0.12 M for cryoprotection.

Horizontal slices of 50 µm thickness were cut using a slicing vibratome (Microm HM650V). Sections containing the subicular complex, hippocampus and entorhinal cortex were retained. Slices were frozen and put on dry ice (Carboglace®) five times for membrane permeabilization, before being transferred in KPBS 0.02M (7% KH_2PO_4, 0.5M, 33% K_2HPO_4 0.5M, 96% H_2O, 9g NaCl, pH=7,4) diluted with 2% milk powder and 1% Triton X-100 (Saturation buffer) for saturation for 2h on an agitator (30 Hz). Sections were transferred into a 500 µl well containing the primary antibodies mixed with PBS and 1% Triton X-100. Also, the fluorescent stain 4',6-diamidino-2-phenylindole (Sigma), DAPI, that is a DNA-specific fluorescent probe, was always added to primary antibody solution in a 1:1000 dilution. After incubating overnight at 4°C, sections were rinsed 3 times in PB (first and second rinsing over 2 hours, last one overnight). In a final step, sections were incubated with secondary antibody solution overnight. The solution contained secondary antibodies, PBS and 1% Triton X-100. Secondary antibodies were conjugated to different fluorophores visible either in the Cy3 or Cy5 channel.

The following primary antibodies were used: Mouse Anti-PV (Sigma #P3088, 1:500), Goat Anti-PV (Swant, PVG-214, 1:500), Rabbit Anti-VIP (Abcam, 1:500), Mouse Anti-CR (Swant #6B3,1:1000), Rabbit Anti-NPY (Millipore #AB9608, 1:500), Rat Anti-Somatostatin (Chemicon #MAB357, 1:200), Mouse Anti-Calbindin (Swant #300, 1:1000) and Mouse Anti-NeuN (Millipore #MAB377, 1:500). All antibodies were tested for specificity, according to the data sheets provided by the suppliers. There was no detectable cross-reactivity between any of the molecules that were tested in experiments of colocalization. The secondary antibodies were: Donkey Anti-Mouse (Cy3 and Cy5, Jackson ImmunoResearch, 1:500), Donkey Anti-Rabbit (Cy5 and Cy3, Jackson, 1:5000), Donkey Anti-Goat (Life technologies A647 or A488, 1:500) and Donkey Anti-Rat (Cy 3, Millipore #AP189C, 1:500). Protocols slightly differed for SOM immunostaining with Rat Anti-SOM antibody, where the incubation time was increased to 48-72 hours with the primary antibody and to 24h with the secondary antibody. These long incubation times were also applied for the primary and secondary antibody that was combined with Rat Anti-SOM antibodies for double labeling experiments. The Rat Anti-SOM antibody was used together with Goat Anti-PV antibody and Rabbit Anti-VIP antibody.

Finally, all sections were mounted on 76*26 mm microscope slides with ProLong® Gold (antifade reagents, Invitrogen, Life Technologies, Carlsbad, California) and covered with cover glasses (24*60 mm). Results of immunostaining were compared to already published results using the same antibodies [85,93,97–99]. Four slices were mounted on each microscope slide, all labeled with

same combination of primary antibodies (applied combinations were: PV+SOM, PV+NPY, PV+VIP, VIP+SOM, VIP+CR, VIP+CB, CB+SOM, CB+NPY, CR+SOM, CR+NPY and CR+VIP). Between slices with same labeling combinations distance of 250-300 µm was respected which corresponds to thickness usually used for electrophysiological experiments. Furthermore, this approach reduced the probability of counting cells twice in the "z-axis" as same molecular markers were not used on adjacent slices. In order to quantify each molecular subpopulation of interneurons at similar dorso-ventral levels, maximal distance between sections labeled with different neurochemical markers was 250-300 µm.

2.3 Analysis and quantification of neuronal density

Numerical neuron density in the presubiculum was quantified by counting neuronal cell bodies in three different Gad67-GFP mice brains (named #13, #14, #16). For each brain, DAPI labeling and immunostaining with NeuN was realized on 4 slices, which results in a total of 12 DAPI+NeuN labeled slices. Unfortunately, slice 4 of brain #14 showed poor immunostaining quality and was therefore excluded from further analysis. The methodological approach is visualized in Figure 9.

Slices were systematically selected: every 4th cutting section of presubiculum from one randomly selected starting section was used for immunolabeling. After immunolabeling, layer (LI-LV/VI) were defined using the AMCA channel (visualizes DAPI staining) of an Olympus IX-81 inverted fluorescence microscope. A safety marge of several micrometers was respected between each layer to assure that every labeled cell could be unambiguously assigned to one layer. Volumes of manually defined layers were measured automatically using the implemented "cropped" function of the commonly used cellular imaging & analysis software, called "Volocity", which allows an acquisition of 3D structures with a three axes motor-driven specimen stage. Frames for counting and volume measurement of layers started at least 4µm at the lower and upper margins of the sections. NeuN positivity was detected within the three dimensional layer volume using the Cy3 channel. For cell counting, only the first edge-point of labeled particles that encountered the progressing plane of observation was considered[100,101]. Labeled cells were only considered for cell counting if the totality of the labeled cell body was located in the predefined volume of each layer. After identification of a NeuN+ particle, fluorescence was switched to the Fitc channel in order to evaluate if the counted cell also showed overlapping GFP expression.

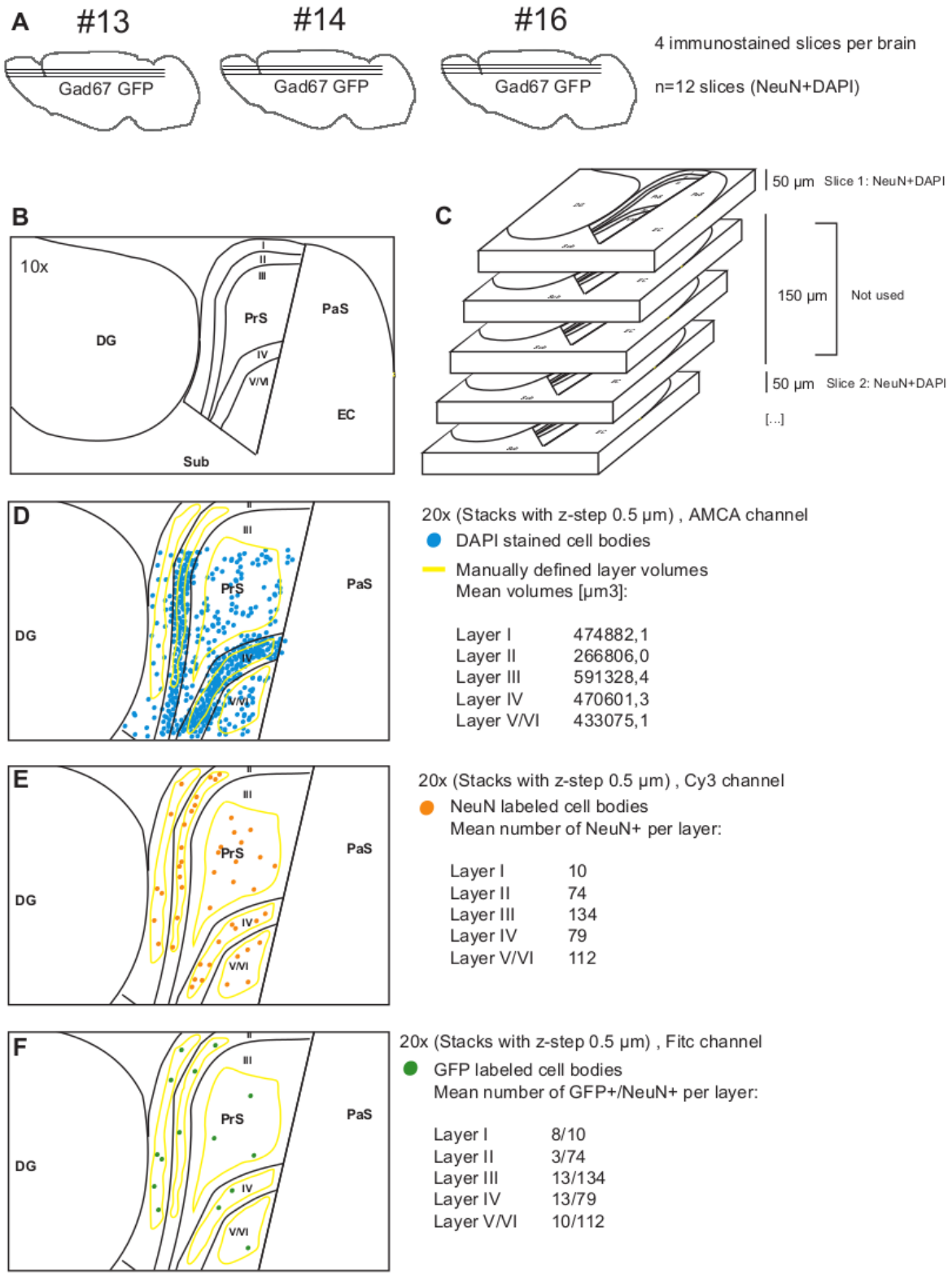

Figure 9: Quantification of neuronal density in presubiculum

A Schematic illustration of 3 Gad67 GFP knock in mice brains. 4 horizontal slices (50 µm) per brain were labeled with NeuN and DAPI. **B** All slices contained the sown structures. **C** Between slices that were used for immunolabeling lay 150 µm. **D** For each slice, first step consisted in layer definition (yellow), referring to DAPI staining, and layer specific volume measurement. **E** Then, NeuN+ cells (orange) were counted within these predefined layers. **F** Last step consisted in counting GFP+/NeuN+ cells.

Cells that showed NeuN positivity and GFP fluorescence were counted as GFP+/ NeuN+ cells. Each NeuN+ and NeuN+/GFP+ cell was assigned to a predefined layer. Number of counted cells (NeuN+ or NeuN+/GFP+) in each layer was divided by the predefined layer volume. For clarity and comparability of results, counted cellular density (/μm^3) was multiplied by factor 10^9 to extrapolate results to cell number per mm^3.

2.4 Analysis and quantification of labeled interneurons

After immunohistochemical experiments, slices were visualized with a QImaging Retiga EXI camera (Qimaging Surrey, BC, Canada) and scanned on an inverted Olympus IX81 microscope. An Optigrid II system (Thales Optem, Qioptik, Rochester, NY, USA) was used to acquire structured images. Overview images were acquired with a 4x objective of NA 0.16. Stacks of 75-250 images (z-step, 0.5µm) were acquired for each slice by using a high numerical aperture 20x NA 0.85 oil immersion objective. Subsequent visual analysis and measurements of defined volume for cell counting were realized with Volocity software (Improvision, Perkin-Elmer, Coventry, UK). No colour or contrast corrections were made on images prior to analysis but images shown in the figures were adjusted for contrast and brightness for the purpose of illustration.

Only slices with very low background fluorescence and optimal signal to noise ratio were included in the analysis. Fluorescent cells were identified visually while scanning through the optical sections of each brain slice and counted by hand. A cell was regarded as positive for an antibody or GFP if its somatic fluorescence was clearly distinct from background fluorescence.

First, overlap of GFP expression with molecular markers was quantified. For this purpose, cells immunoreactive for a molecular marker were identified in the Cy3/Cy5 channel and the location of their soma was tagged. Switching to the Fitc channel allowed checking overlap with GFP expression at same coordinates. Then, the ratio between the number of cells positive for a molecular marker and GFP and total number of cells positive for this molecular marker was calculated.

In a second step, layer specific quantification of molecular subpopulations within the general interneuron population was realized. For this purpose, layers and presubicular borders were identified by using distinctive cytoarchitectonic features visualized by DAPI staining. Delimitated layers were then cropped out of the section. Layer volume was a product of the layer area and the

number of optical sections in which cells were counted plus the spacing between acquired sections (z-step, 0.5µm). Cells divided by the predefined layers were not considered.

In each layer, GFP+ neurons were identified as explained above. After counting the GFP+ interneurons, color channel was switched to illustrate cells visible in the Cy3 and Cy5 channel and overlapping cells were counted. Double-labeled cells were detected the same way. This way, each presubicular interneuron could be assigned to one of four categories: positive for the marker in the Cy3 channel, positive for the other marker in the Cy5 channel, positive for both markers or negative for both. To determine numerical density, counted cell number was divided by measured layer volume. Results about layer specific distribution of interneuron subpopulations identified by marker expression were either given as numerical density or as portion of GFP+ cells counted in the same layer.

For each molecular subpopulation, striking morphological characteristics were described and mean soma diameter was indicated. Given soma diameter corresponds to longest diameter of labeled soma in the section where soma size was largest. At the conclusion of this analysis, the dataset comprised a list of 5068 GFP+ cells from 9 animals that were characterized by their laminar location, soma diameter and positivity for two antibodies.

2.5 Retrograde Tracing

For experiments, retrograde migrating fluorescent latex microspheres (Retrobeads®, Lumafluor) were applied. Retrobeads® are non-cytotoxic rhodamine-labeled fluorescent microspheres of 0.02-0.2 µl diameter. They are taken up by presynaptic terminals but also damaged axons and transported back to somata within 24-48 hours. Labeling persists unchanged in extent or quality for at least 10 weeks, allowing subsequent recordings from visually identified projection neurons in the slice preparation[102]. As these microspheres show little diffusion, a small injection volume between 100-200 nl was sufficient for our purpose.

Latex beads are very suitable for electrophysiological experiments as they are visible without further staining, can be combined with immunohistochemistry or intracellular injections and show no photodynamic damage after illumination. Their most outstanding property is however that viability of neurons is unaffected by transported microspheres.

2.6 Stereotactic surgery

Animals were anesthetized with a mixture of ketamine and xylazine (Sigma®) at a dose of 80–100 mg ketamine and 10 mg xylazine per kilogram body weight, applied intraperitoneally. Before starting the surgical procedure, a latency of 15-20 minutes was respected until no response to nociceptive stimuli was seen. The skull was shaved and the skin cleaned with 70% ethanol before making a midline incision with a surgical scalpel. The mouse head was then fixed and adjusted in a small animal stereotaxic apparatus (Kopf, model 963) by applying non-rupture ear bars and an incisor adapter.

The stereotaxic coordinates of the targeted brain regions (LMN and ADN) where taken of "The Mouse Brain in Stereotaxic Coordinates"[103] according to the antero-posterior (AP), medio-lateral (ML) and dorso-ventral (DV) axis to bregma. Holes were drilled unilaterally to perforate the skull. A 10µl needle (Hamilton® - 1701) filled with 100-200 nl of either red or green fluorescent retrobeads was adjusted to (AP / ML / DV) -0.82 / 0.75 / -2.85 for ADN and -2.80 / 0.75 / -5.35 for LMN with the aid of a dissecting microscope (Leica®). ADN lies at the border of the lateral ventricles. For injections into ADN, a small air bubble was taken up in the injection needle to separate both liquids in order to avoid losing too much tracer volume while crossing the ventricle. For all injections, the flow rate was fixed on an automatic pump to 10% of the total injection volume per minute. Before withdrawing the needle from the brain after the injection, the injector was left in place for 3 min in order to allow tracer diffusion and to avoid backflow into the puncture channel. After removing the injection needle, the skin was sutured with a non-absorbable 4/0 filament (Vicryl®) and the animal kept at 37°C on heated surface, until it fully recovered[104].

2.7 Verification of injection site

An adjustment of the injection site had to be realized before injecting retrograde tracer. The inactive tracer Fluoruby was therefore injected and animals sacrificed directly after surgery. Correctness of injection site was verified by comparing bright field images of 50 µm thick coronal slices comparing the targeted area with coronal plates from atlas "The Mouse Brain in Stereotaxic Coordinates". In a second time, Retrobeads were injected with the help of adjusted coordinates. Animals were sacrificed after 48 to 72 h. 5 animals were sacrificed without electrophysiological recordings, in order to verify the injection site, tracer diffusion which should not exceed the size of the targeted nuclei and expected retrograde labeling of presubicular neurons. Horizontal and coronal slices were made of these brains. That way, injection site, puncture channel and targeted

nuclei could be visualized in vertical slices, making comparison with the brain atlas easier. At the same time, horizontal sections of the PrS allowed better verification of the expected results. This way, comparison of results was easier, given that electrophysiological experiments were conducted on horizontal sections. For imaging and immunohistochemistry with Dapi, the same devices and protocols were used as described in the chapter about imaging of presubicular interneurons.

2.8 Electrophysiological recordings

After anaesthesia (see stereotaxic surgery) animals were perfused via the heart with a solution cooled to 2-6°C, containing (in mM): 110 choline Cl, 2.5 KCl, 25 $NaHCO_3$, 1.25 NaH_2PO_4, 7 D-glucose, 0.5 $CaCl_2$ and 7 $MgCl_2$, equilibrated with 5% CO_2 in O_2. Following the dissection of the forebrain, horizontal brain sections of 300µm thickness were put into the solution used for perfusion. Slices were cut in a 3.9–5.7 mm vertical range with respect to the ear bar horizontal plane. After being stored for at least 1 h at 22–25 ° C in ACSF (in mM: 124 NaCl, 2.5 KCl, 26 $NaHCO_3$, 1 NaH_2PO_4, 2 $CaCl_2$, 2 $MgCl_2$, and 11 D-glucose, all salts: Sigma, Lyon, France) and bubbled with 5% CO_2 in O_2 (pH 7.3, 305–315 mOsm/L), slices were transferred to a chamber (volume ~2 mL) and heated to 32 –34 °C on the stage of an Axioskop 2 FS plus microscope (Zeiss, France) for recordings. Slices were visualized using infrared-differential interference contrast optics. Fluorescently labeled retrobead positive neurons were visualized by LED illumination coupled to appropriate emission/excitation filters (OptoLED, Cairn Research, Faversham, UK). Recordings were then made with glass pipettes pulled with the help of a Brown– Flaming electrode puller (Sutter Instruments) from borosilicate glass. They had an external diameter of 1.5 mm and an internal diameter of 0.86 mm (Hilgenberg, Germany). The electrode was filled with a solution containing (in mM): 130 K-gluconate, 5 KCl, 10 HEPES, 10 ethylene glycol tetra-acetic acid, 2 $MgCl_2$, 4 MgATP, 0.4 Tris-GTP, 10 Na_2-phosphocreatine, adjusted to a pH of 7.3 with KOH and an osmolarity of 300 mOsm. After filling, electrode resistance was 3-6 MΩ. For further morphological reconstruction, 2.7 mM biocytin was added to the internal solution. Whole-cell current-clamp recordings were made using a MultiClamp 700B amplifier and pCLAMP software (Molecular Devices, Union City, CA). The signal was filtered at 6 kHz and digitized at 20 kHz. The estimated junction potential of ~15 mV, due to a contact between the chloride silver wire, the pipette solution and a 3 M KCl agar bridge, was not corrected.

2.9 Electrophysiological analysis

Recorded signals were analyzed with AxographX and routines written in MATLAB (The Mathwork). Cellular parameters were measured 3-5 min after break-in. Resting membrane potential (RMP) was defined as the mean potential over at least 10 seconds. Measurements of electrophysiological properties were generally done on responses to step current injections of 800 ms duration applied from a membrane potential maintained at -65 mV. Injected currents increased from first step at about -100 mV hyperpolarization to a depolarization resulting in maximum sustainable firing frequency. Maximum sustainable firing frequency was defined as maximum firing frequency before evident attenuation and broadening of action potentials (AP), indicating a progressive inactivation of voltage-gated Na^+-channels. Indeed, instantaneous frequency could increase or remain stable. Neuronal input resistance (Rin) was determined as the slope of the current-voltage (IV) relationship between -71 and -64 mV. Membrane time constant (τ) was estimated by fitting a double exponential to the negative deflection of membrane voltage (Levenberg-Marquardt algorithm)[105] observed after applying a 800 ms hyperpolarizing current injection that induced a voltage change not exceeding 15 mV. A "sag ratio", indicating Ih expression, was calculated as the ratio of the maximal negative potential (sag, typically between 0 and 200 ms), divided by the mean steady state voltage deflection (typically between 400 and 800 ms). Detection of APs was done from continuous periods of rising membrane potential with minimal amplitude of 30 mV. Rheobase (or threshold current for firing) was determined as the smallest current step of 800 ms eliciting at least one action potential.

Firing frequency (Hz) was either deduced by averaging all instantaneous frequencies of a given step (MeanInsF) or by dividing the number of APs over time (APs/sec). Input-output (I-O) curves were constructed by plotting firing frequency (either MeanInsF or APs/sec) as a function of the injected current. Their initial slopes (I-O gain) were obtained with linear fitting of the first 9 steps beyond rheobase. Coefficient of variation (CV) was a division of standard deviation and the mean of instantaneous frequencies when at least 3 APs were elicited. This gave an index of firing regularity; the higher the value, the more irregular the firing. First AP-Latency was calculated from first AP in spike trains following a two-fold rheobase current injection. Adaptation index (AI) was set as the ratio of the mean of the three last instantaneous frequencies divided by the first instantaneous frequency.

AP waveform features were obtained by averaging the measures from the first AP elicited from 3 consecutive depolarizing steps at a firing latency less than 100 ms. AP threshold corresponds to

the membrane potential at the point at which dV/dt > 30 mV/ms. AP peak was its maximum potential. The difference between the threshold and the AP peak voltage was called AP rising amplitude. The AP width was measured at the half-height of the AP rising phase. Maximal depolarization rate and maximal repolarization rate were designated as the maximum and minimum dV/dt, which occurred during rising phase and falling phase, respectively.

2.10 3D reconstruction of recorded neurons

After electrophysiological recordings, slices were first fixed at 4°C for 24 hours in 4% paraformaldehyde in 0.1 M phosphate buffer (PB) and then rinsed three times in PBS before being incubated in 30% sucrose solution at 4°C overnight. Three cycles of freezing and defrosting over dry ice followed by three rinses with PBS increased the permeability of membranes. Slices were then incubated in a blocking solution containing PBS (0.1M), milk 2% and 0.3% TritonX100 for 3h at room temperature. After this procedure the nuclear marker 4,6-diamidino-2-phenylindole (DAPI) (1:1000) and Streptavidin–Cy3 or Cy5 conjugate (1:500, Invitrogen, Eugene, OR, USA) were added for another 3 hours. After three rinsing cycles in PBS, slices were mounted on coverslips using anti-fade Prolong Gold medium. Stacks were collected with above named devices (see "Fluorescent imaging") and imported to the software Neurolucida (Microbrightfield, Williston, VT, USA).

To compare neurons of different slices, the somatic location of each recorded cell was projected onto a standardized map of the PrS that was situated between the subiculum on its left and the parasubiculum on its right side. One axis of this map followed the cortical surface from the border of the two adjacent brain regions and the other corresponded to the apical–basilar dendritic axis of pyramidal cells. This last axis mainly followed the orientation of the blood vessels that penetrate the PrS from the brain surface. That way, each recorded neuron was assigned on normalized x/y coordinates according to the location of its soma. To determine the layer-specific position of the neuron layers and boundaries of the PrS, Dapi staining was used. To describe dendritic arbors, wedge analysis was applied after creating 12 segments each occupying 30° of arc after setting the cortical surface as 0°C. It started with a 15° segment centered on the vertical from the soma of each cell and measuring the total dendritic length in each of these segments. The Neurolucida function 'layer length analysis' was used to determine dendritic length in each presubicular layer. No correction for tissue shrinkage was applied.

2.11 Statistics

Results are given as mean +/- SEM. Statistical analysis was performed with Prism (GraphPad Software, Inc.), Excel and MATLAB (The Mathwork).

3. RESULTS

3.1 Structures and boundaries of the presubiculum

In horizontal sections of the GAD67-GFP mouse brain, the PrS was localized in the hippocampal formation as shown in Fig. 9 A-C. The shape of the PrS changed from ventral to dorsal horizontal sections. On its ventral portion, it was small with a triangular shape, becoming broader toward its dorsal end (Fig. 9 B-C). Densities and distributions of presubicular GABAergic and non-GABAergic neurons presented in the following were analyzed at mid-dorsal level, where the PrS is shaped as shown in Fig. 9A. To properly distinguish the 6 cytoarchitectonic layers of presubicular cortex, DAPI staining was used. DAPI allowed a good visibility of the different layers. Layer I appeared as cell-poor, while layer II was densely packed. With its high cellular density, layer II served as a good landmark to delimitate the proximal border to subiculum and the distal transition to parasubiculum. Layer III appeared large at the distal and became narrower towards the proximal border. Layer IV, a thin layer of low cellular density, allowed layer III to be distinguished unambiguously from deep layers (Fig. 9A).

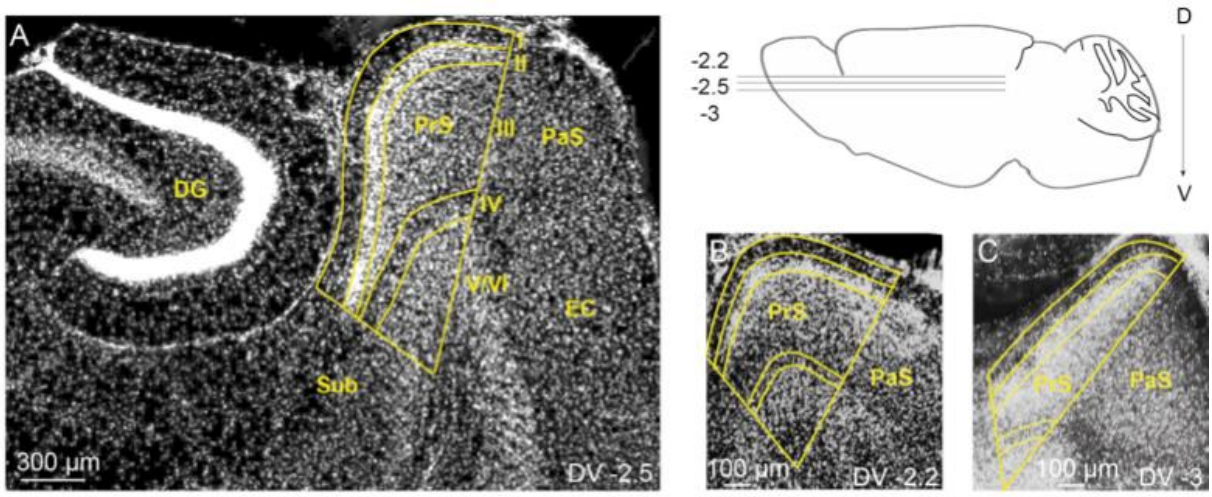

Figure 10 : Horizontal sections of the presubiculum as seen with DAPI staining

A Horizontal section. The presubiculum borders the subiculum (Sub), faces the dentate gyrus (DG), and is adjacent to parasubiculum (PaS) and entorhinal cortex (EC). Results presented in this study were obtained by analyzing sections showing presubiculum shaped at mid-dorsal level, respectively – 2.5 mm from Bregma at dorso-ventral (DV) axis. See at the top right the sagittal view of a schematic mouse brain. The disposition of presubiculum changes at DV level -2.2 **B** and DV level -3 **C**, as described in the text. Abbreviations: CR, Calretinin; DG, dentate gyrus; EC, entorhinal cortex; PaS, parasubiculum; PrS, presubiculum; Sub, subiculum

It was a new finding that the molecular marker Calretinin was shown to be a useful marker to define borders of the PrS (Fig. 10A, Fig. 10B). In the PrS, a bright background staining was seen along the whole dorso-ventral axis on 50µm thick sections of 3 different animals. CR labeling ended abruptly at borders with the neighboring subiculum, parasubiculum and entorhinal cortex. These areas lacked the specific presubicular immunoreactivity for CR. Within the presubicular cortex, bright CR staining was particularly pronounced in layer II/III and ended at transition between layer IV and deep layers. CR staining therefore specifically labeled layer I-IV and may be useful to distinguish deep layers V/VI from the more superficial ones. In addition to the PrS, Calretinin had a very specific staining pattern in the whole hippocampal-parahippocampal area. In line with previous studies, hilar mossy cells and a band in the supragranular layer of dentate gyrus of hippocampus were intensely stained[106]. Also, a large CR immunoreactive patch in deep layers of entorhinal cortex was seen in 3 different animals (Fig. 10A,C).

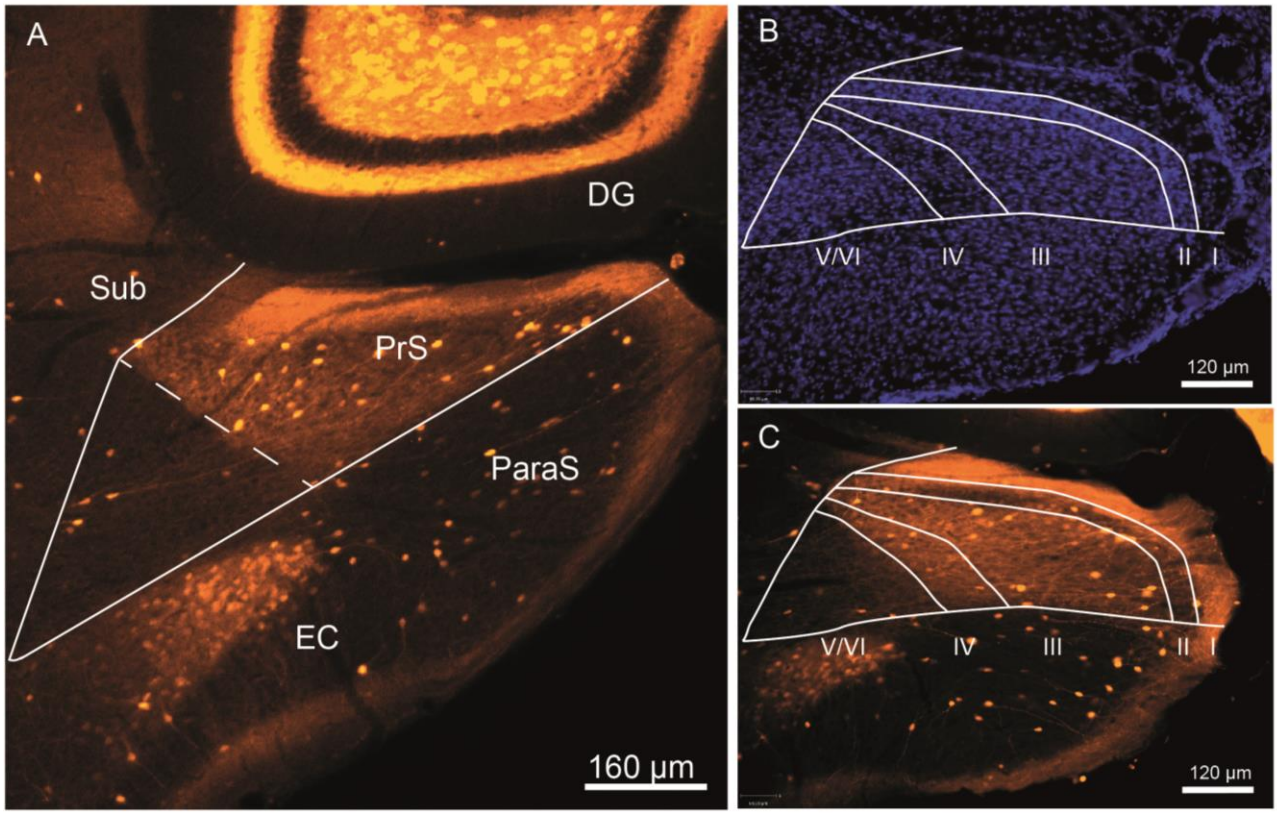

Figure 11 : Horizontal sections of the presubiculum as seen with Calretinin staining

Horizontal section of the presubiculum at mid-dorsal level stained with CR (A,C) and Dapi (B).**A** Presubicular layers I-IV show brighter background staining than deep layers. Note specific staining pattern in neighboring DG with intense staining of mossy cells and an intense band in supragranular layer. Also neighboring EC shows a bright CR+ patch in its deeper layers (**A**). For comparison, Dapi-staining (**B**) is compared with CR-staining (**C**) on the same section, highlighting the layer specific staining pattern of CR. Abbreviations: CR, Calretinin; DG, dentate gyrus; EC, entorhinal cortex; PaS, parasubiculum; PrS, presubiculum; Sub, subiculum

3.2 Interneurons of the presubiculum

3.2.1 Layer distribution of presubicular GABAergic and non-GABAergic neurons

Most presubicular neurons are glutamatergic while a much smaller portion is GABAergic. Densities and distributions of these GABAergic and non-GABAergic neurons were calculated by using GAD67-GFP knock-in mice and a NeuN immunostaining (Fig. 11A). The GAD67-GFP knock-in mouse is assumed to label all GABAergic neurons and thus allowed the quantification of this population. To calculate numerical densities, cell numbers were counted on 50 µm thick sections (n=75) of 9 different adult GAD67-GFP knock-in mice (Fig. 11B). Deep layers (layer V/VI) were largest with a mean volume of 840 000 μm^3, followed by layer III (830 000 μm^3) and layer I (765 000 μm^3). Layer IV (600 000 μm^3) and densely packed layer II (560 000 μm^3) were much smaller. On 3 animals, NeuN immunostainings were performed. NeuN labeled neurons (n=4495) were counted on 12 different sections from 3 animals (Fig. 11C). A sparsely populated layer I (22 000 cells/mm^3) contrasted with a high density of neurons in layer II (275 000 cells/mm^3) and layer III (227 000 cells/mm^3) that decreased in layer IV (170 000 cells/mm^3). As layers V and VI are not readily distinguished, we pooled cell counts for these layers together, and the neuronal density there was similar to that in layer III (Layers V and VI: 258 000 cells/mm^3). Numerical densities for GABAergic neurons were calculated from a total of 5068 GFP-positive cells from 9 adult GAD67-GFP knock-in animals. Layer I and layer II had a similar interneuron density (L1: 12 000 cells/mm^3, L2: 10 000 cells/mm^3). This contrasted with the general neuron distribution, where layer I is known to be sparsely populated while layer II is densely packed with neurons. Interneuron density increased in layer III (23 000 cells/mm^3) to reach its maximum in layer IV (31 000 cells/mm^3). Deep layer density of GABAergic neurons was moderate (L5/6: 19 0000 cells/mm^3) (Fig. 11C). The total share of presubicular GABAergic neurons (n=517/4495) from 3 animals was 11% of all NeuN immunoreactive neurons. The proportion of inhibitory cells varied across layers. While 80% of all neurons in layer I were inhibitory, their share decreased to only 4% in layer II. In layer III and deep layers, interneurons accounted for 9% of all neurons. In layer IV 16% of all counted cells were interneurons (Fig. 11D). Detailed counting results are presented in Tables 1-4.

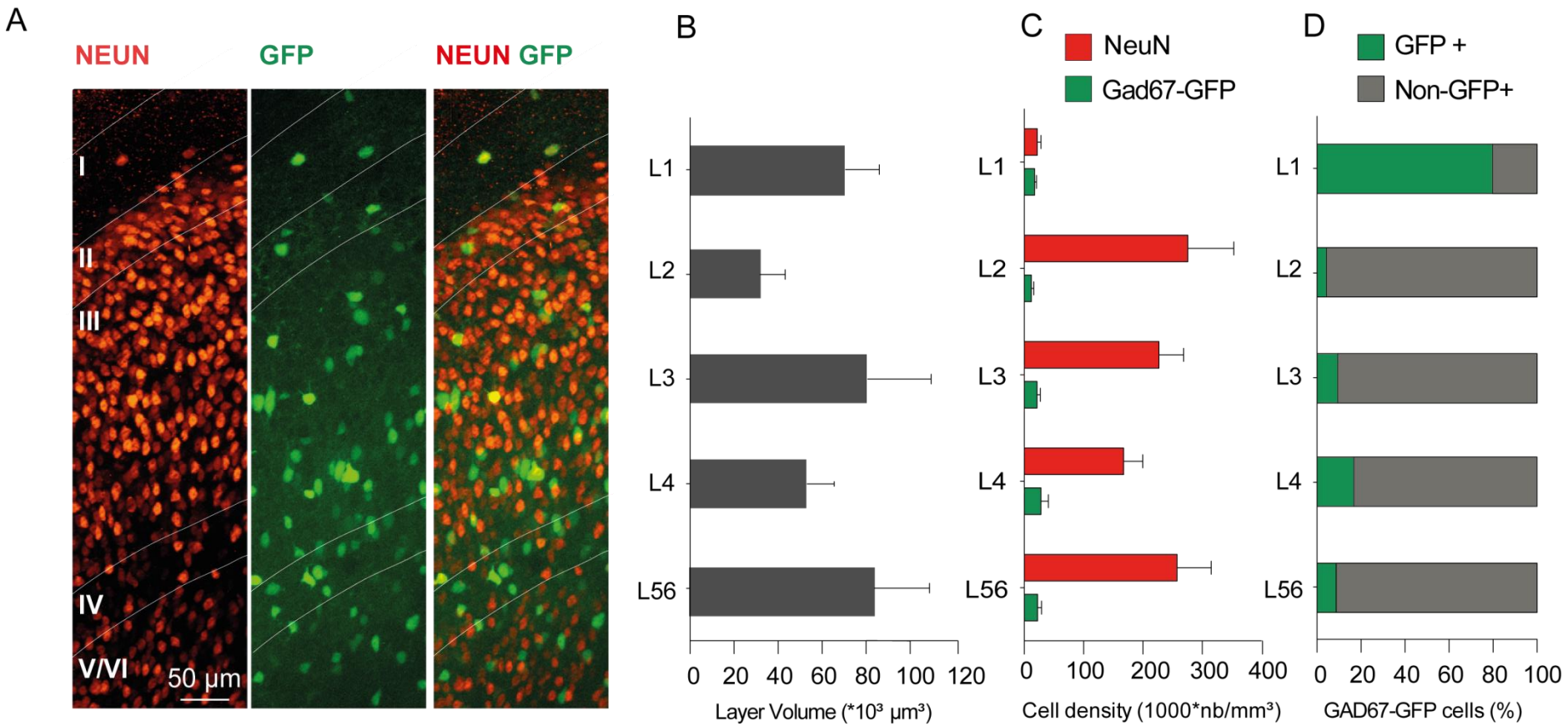

Figure 12: Distribution of GABAergic and Non-GABAergic cells in the presubiculum

A All layers of presubiculum as seen with NeuN staining (left), GFP fluorescence (middle), and an overlay (right) in a section from a GAD67-GFP mouse. **B** Mean layer volumes as measured for calculation of numerical cell density. **C** Mean density of NeuN stained neurons (red) and GFP+ neurons (green) for each layer. Mean and standard error of neuronal density were measured from 12 horizontal sections of 3 GAD67-GFP mice. (D) Layer specific portion of GAD67-GFP+ neurons (NeuN+/GFP+, green) and non-GABAergic neurons (NeuN+/GFP-, grey).

Table 1-3: Results of layer specific neuron count and neuron density for each counted slice

		NeuN+	GFP+	Vol [µm3]	DensNeuN+ [No/mm3]	Dens GFP+ [No/mm3]
		#13				
Slice #1	Layer I	5	5	480401	10408	10408
	Layer II	74	2	195596	378330	10225
	Layer III	146	16	654563	223050	24444
	Layer IV	74	11	533224	138779	20629
	Layer V/VI	134	8	697367	192151	11472
Slice #2	Layer I	4	2	233525	17129	8564
	Layer II	91	3	173359	524923	17305
	Layer III	143	4	396932	360263	10077
	Layer IV	37	13	136610	270843	95161
	Layer V/VI	75	7	144991	517274	48279
Slice #3	Layer I	6	5	206657	29034	24195
	Layer II	67	4	139856	479065	28601
	Layer III	100	9	270938	369088	33218
	Layer IV	75	17	448609	167183	37895
	Layer V/VI	201	16	600565	334685	26642
Slice #3	Layer I	17	8	396909	42831	20156
	Layer II	90	4	221007	407227	18099
	Layer III	85	13	352238	241314	36907
	Layer IV	86	7	308591	278686	22684
	Layer V/VI	55	3	175514	313365	17093
		#14				
Slice #1	Layer I	18	18	970839	18541	18541
	Layer II	64	4	537901	118981	7436
	Layer III	193	28	1470704	131230	19038
	Layer IV	63	14	461768	136432	30318
	Layer V/VI	134	17	548486	244309	30994
Slice #2	Layer I	8	6	398172	20092	15069
	Layer II	44	3	317779	138461	9441
	Layer III	159	10	647290	245639	15449
	Layer IV	114	18	629291	181156	28604
	Layer V/VI	83	5	292479	283781	17095
Slice #3	Layer I	12	12	474867	25270	25270
	Layer II	44	3	200350	219615	14974
	Layer III	137	5	456733	299956	10947
	Layer IV	117	18	793181	147507	22693
	Layer V/VI	89	4	439693	202414	9097

		#16				
Slice #1	**Layer I**	11	6	254741	43181	23553
	Layer II	119	6	317698	374570	18886
	Layer III	168	20	571174	294131	35016
	Layer IV	58	5	235839	245930	21201
	Layer V/VI	81	10	283645	285568	35255
Slice #2	**Layer I**	8	8	479212	16694	16694
	Layer II	63	1	233936	269304	4275
	Layer III	137	12	638735	214487	18787
	Layer IV	61	12	301373	202407	39818
	Layer V/VI	111	6	292360	379669	20523
Slice #3	**Layer I**	16	12	654909	24431	18323
	Layer II	54	1	264493	204164	3781
	Layer III	112	8	568501	197009	14072
	Layer IV	84	16	615012	136583	26016
	Layer V/VI	171	15	751276	227613	19966
Slice #3	**Layer I**	9	9	673470	13364	13364
	Layer II	99	4	332891	297395	12016
	Layer III	97	14	476805	203437	29362
	Layer IV	98	14	713117	137425	19632
	Layer V/VI	94	16	537449	174900	29770

Table 4: Mean values of neuron count and neuron density for each layer

	Mean (+/-STD)of 11 slices				
Layer	**NeuN+**	**GFP+**	**Vol [µm3]**	**DensNeuN+ [No/mm3]**	**Dens GFP+ [No/mm3]**
Layer I	10 (5)	8 (4)	474882,1	21823,6	17420,6
Layer II	74 (24)	3 (1)	266806,0	275651,4	11925,6
Layer III	134 (33)	13 (7)	591328,4	227069,6	21369,5
Layer IV	79 (24)	14 (4)	470601,3	167484,0	28010,6
Layer V/VI	112 (44)	10 (5)	433075,1	257776,0	22460,9

3.2.2 Labeling of GABAergic neurons in the presubiculum using molecular markers

Some of the most commonly used molecular makers for subpopulations of interneurons are Parvalbumin (PV), Vasointestinal Peptide (VIP), Calretinin (CR), Calbindin (CB), Somatostatin (SOM) and Neuropeptide Y (NPY). However, some exceptions have been described where these markers are present in excitatory neurons, too. Therefore, I first examined whether in the PrS antibodies against these proteins or peptides specifically labeled interneurons of the GAD67-GFP mouse and to what extent they colocalized with GFP expression. Immunostainings using antibodies against Calcium-binding proteins PV, CB and CR and neuropeptides SOM, VIP and NPY were performed on 63 sections of 6 different adult GAD67-GFP knock-in animals (Fig. 12; Fig. 13). The neurochemical markers with the highest specificity for interneurons in the PrS were PV and VIP. 96% of PV immunoreactive cells (n=658/688) and 94% of VIP+ neurons (n=237/252) also expressed GFP. The SOM antibody also labeled mostly GABAergic cells, as 90% of all SOM+ cells showed green fluorescence (n=319/356). Specificity slightly decreased for CR, about 88% of all CR+ cells (n=162/182) being interneurons. Although SOM+ and CR+ cells tended to have less specificity for GFP+ neurons, a great majority of them could be clearly identified as GABAergic. CB was the only marker protein that labeled mostly presubicular principal neurons. In the PrS, only 36% of CB labeled cells showed GFP positivity (n=181/495). Interestingly, the relative distribution of CB+/GFP+ cells differed strongly between layers. CB+ cells densely populated layer II. However, only 5% of these cells were GABAergic (n=15/276). In contrast, the portion of CB+ interneurons was much higher in layers III-VI, accounting for 85-93% of all cells labeled by CB (n=248/283). Therefore, except for layer II, interneuron specificity of CB was similar to that of CR or SOM but less specific than PV or VIP. As for NPY, this antibody labeled only 12 presubicular cells. 3 of the 12 NPY+ cells colocalized with GFP expression (25%).

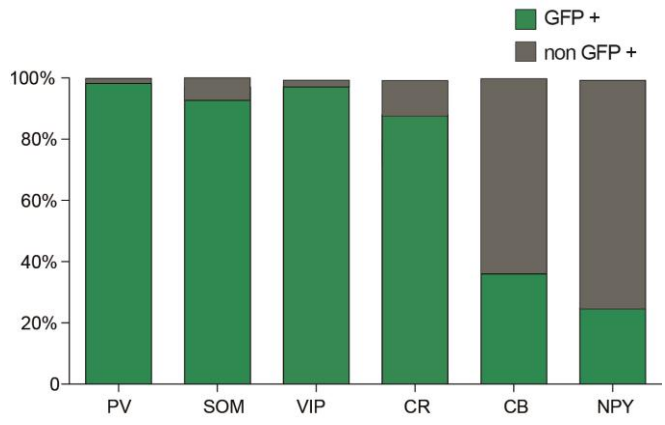

Figure 13 : Co-expression of GFP and molecular markers

Portion of GABAergic (GFP+, green) and non-GABAergic (grey) cells labeled by each molecular marker. More than 90% of PV, SOM and VIP positive cells were GABAergic while CB and NPY labeled mainly non-GABAergic cells.

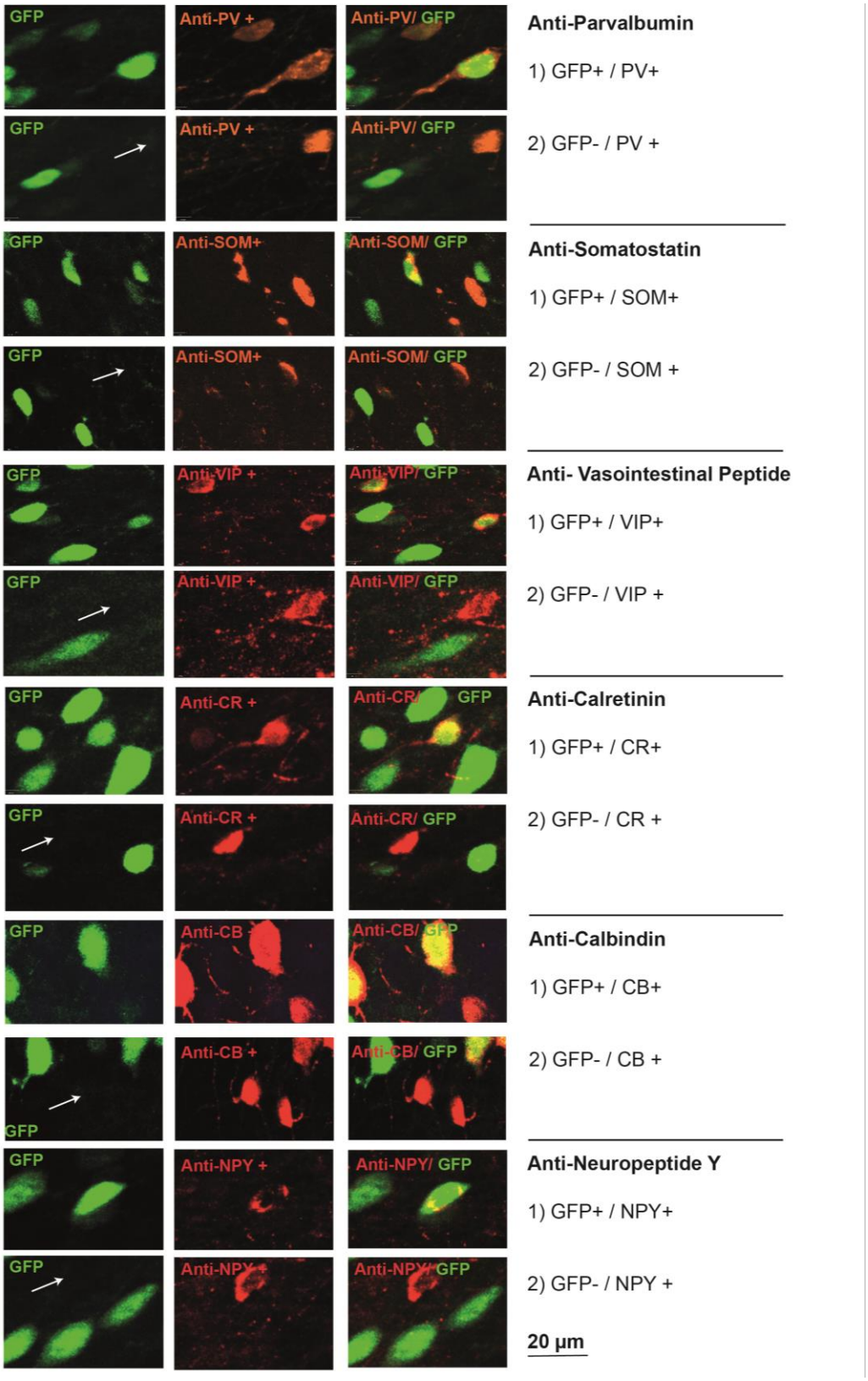

Figure 14 : Examples of GABAergic and non-GABAergic cells

For each panel, GFP + neurons are on the left (green), immunostaining for a specific marker in the middle (red) and merged image on the right (green, red). For each marker, the first row shows an example of a labeled cell with immunoreactivity for GFP (GFP+ cell) and the second for a cell positive for the neurochemical marker but negative for GFP (GFP-).

3.2.3 GABAergic neurons of the presubiculum express different molecular markers

To quantify different interneuron subtypes, I examined the neurochemical marker expression of presubicular GABAergic neurons. In the PrS, the portion of interneurons identified by the marker proteins applied showed great laminar differences (Fig. 13F). In layer I, major parts of interneurons remained to unidentified (>95%), whereas in layers II/III over 90% interneurons showed immunoreactivity for at least one molecular marker. In deeper layers, especially in layer IV, labeling even exceeded 100%. This was most likely due to co-expression of two or more markers per interneuron.

PV immunoreactive cells constituted the major interneuron population, as they accounted for 36% of all GFP+ neurons (n=644/1807). Second were CR immunoreactive cells; this protein was expressed in 18% of all presubicular interneurons (n=131/718). CB (n=102/651) and SOM (n=319/2025) positive interneurons formed the third largest fraction; both were expressed in 16% of all GABAergic cells in the PrS. VIP (n=200/2192) was expressed to a lesser extend (9%). NPY labeling was seen in a very small subpopulation of 0.3% (n=2/545) interneurons.

Next, the laminar distribution and some morphologic characteristics of each molecular subpopulation were examined. The absolute numbers and percentage of each molecular subtype are indicated in Table 5. For examples and laminar distribution for all molecular markers, see Fig.14.

	PV			SOM			VIP			CR			CB			NPY		
	IN	PV	%	IN	SOM	%	IN	VIP	%	IN	CR	%	IN	CB	%	IN	NPY	%
L1	211	0	0	241	0	0	276	0	0	94	2	2,13	87	0	0	50	0	0
L2	144	22	15,28	151	12	7,95	189	55	29,1	50	18	36	56	3	5,36	44	0	0
L3	516	230	44,57	623	75	12,04	673	84	12,48	191	41	21,47	180	25	13,89	142	0	0
L4	501	212	42,32	543	103	18,97	536	35	6,53	223	44	19,73	163	45	27,61	164	1	0,61
L5/6	433	180	41,57	467	129	27,62	518	26	5,02	160	26	16,25	165	29	17,58	145	1	0,69
Total	**1807**	**644**	**35,63**	**2025**	**319**	**15,75**	**2192**	**200**	**9,12**	**718**	**131**	**18,25**	**651**	**102**	**15,67**	**545**	**2**	**0,37**

Table 5: Laminar distribution of interneuron subtypes in absolute numbers

The total number of interneureons (IN) is given for each layer and the total number of cells labeled by the marker indicated on top of the row. Every molecular subtype is also expressed as percentage of interneurons in layers I-VI. Totals are given at the bottom.

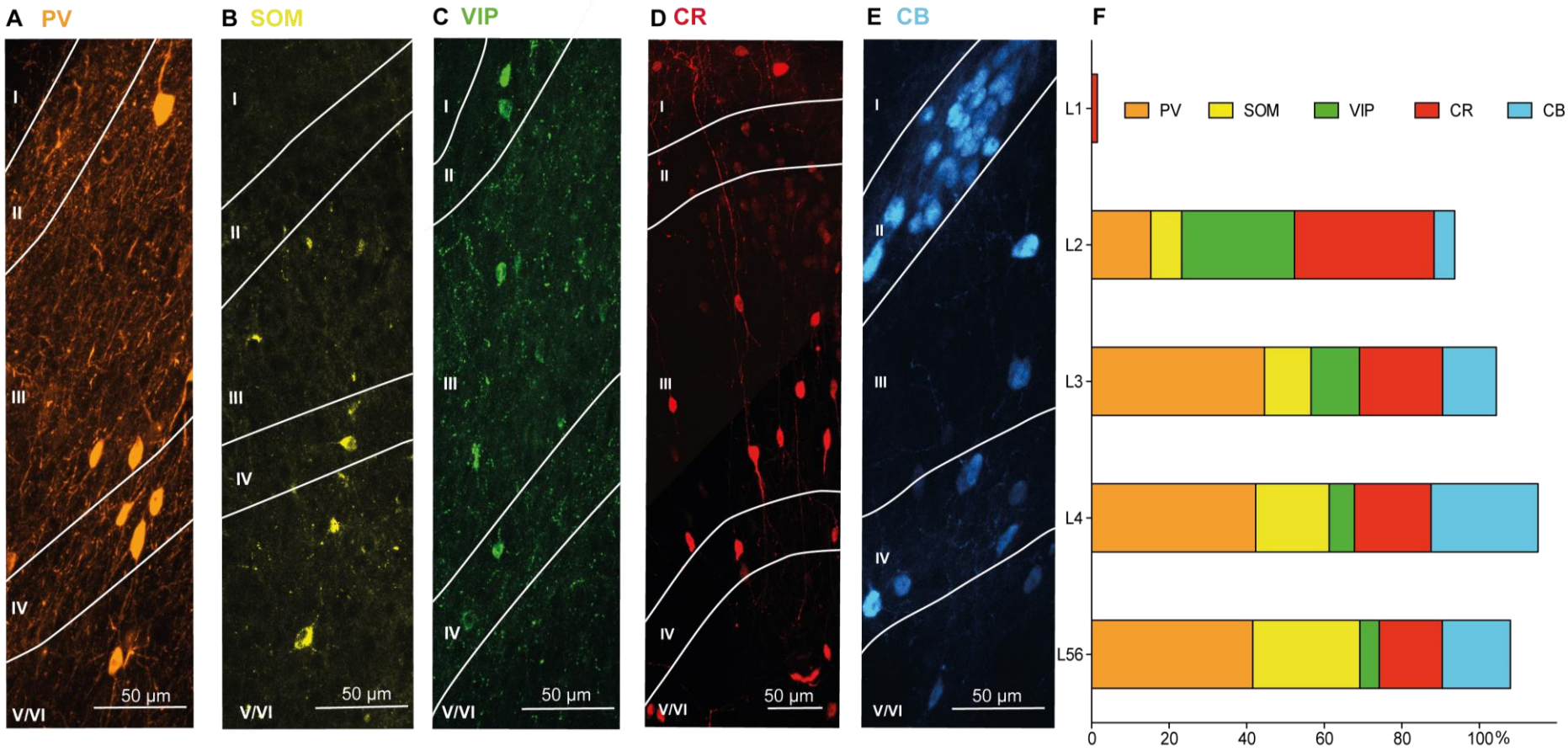

Figure 15: Layer specific distribution of molecular subtypes

A-E Horizontal sections of presubiculum, with fluorescently labeled neurons immunoreactive for PV (A), SOM (B), VIP (C), CR (D) and CB (E). Layers are indicated and the scale bar is 50µm. **F** Layer specific contribution of each molecular subpopulation to the general interneuron population. Percentages do not necessarily sum to 100% in each layer due to double-labeled cells and cells that do not express any label.

PV+ neurons

A total of 646 PV immunoreactive cells were counted on 24 sections of 6 animals. With 36 % of all GFP-positive neurons, PV expressing interneurons constituted the major subpopulation of interneurons in the PrS. There was an absence of PV-labeled neurons in layer I. A low portion (15%) of PV+ cells in layer II (n=22/144) contrasted with layer III where PV+ cells accounted for 44% of all GFP+ cells (n=230/516). From layer IV (n=212/501) to deep layers (n=180/433), PV expressing neurons were evenly distributed, generally labeling about 42% of all GABAergic cells. Therefore, over 80% of all PV+ cells were located in either layer III or deep layers (V/VI), see Table 5.

Morphologically, PV positive cells had rather big cell bodies with triangular or ovoid shape. Soma size was measured in horizontal sections at its largest diameter (n=123). It had a mean value of 14 ± 4 µm (ranging between 10-30 µm). PV+ cells were therefore larger than the average interneuron population (9±2 µm, ranging between 6-30 µm). Orientation of somata was mainly parallel to the course of blood vessels towards the pial surface. A very dense, probably dendritic, arborization was seen in layers II-IV and PV positive axons seemed to form baskets around non-GFP+ cells (Fig. 15).

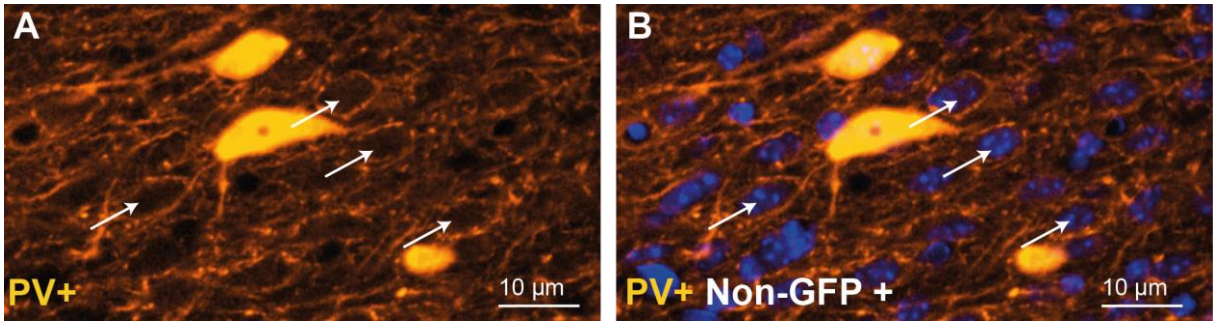

Figure 16: Evidence for perisomatic inhibition mediated by PV+ cells

A PV+ cells and fibres in layer IV. White arrows indicate non-labeled areas by PV. **B** Merged image with PV+ cells (orange) and Dapi-stained nuclei (blue) of non-PV expressing cells as seen in **A**. This is an example of PV+ perisomatic boutons around non-GABAergic cell bodies in layer IV. Most likely they correspond to axons of PV+ interneurons forming baskets around principal cell somata as they did not show GFP. Evidence for this connectivity pattern was seen in layers II-VII of all animals.

SOM+ neurons

A total of 319 SOM immunoreactive cells were counted on 27 sections of 6 animals. SOM labeled 16% of all interneurons (n=319/2025). The density of SOM-expressing interneurons increased continuously from upper layers (L1 0%- L2 8% - L3 12%) to deeper layers (L4 19%- L5/6 27%). Morphology was difficult to evaluate, as labeling showed mainly speckled soma. Soma shape seemed round and soma size appeared rather small. Measured SOM+ cell somata (n=105) were similar to the general average with a mean diameter of 10 ± 3 µm (ranging between 5-15 µm). The applied antibodies labeled neither axons nor dendrites clearly, although some spots, probably dendritic, were visible.

VIP+ neurons

A total of 200 VIP immunoreactive cells were counted on 27 sections of 6 animals. VIP labeled only 9 % of all counted interneurons (n=200/2192). In superficial layers of the PrS, VIP expressing interneurons were relatively common. In layer II, VIP-labeling was seen in 29% of GABAergic cells in this layer (n=55/189). In layer III their portion was smaller and only 12% interneurons showed immunoreactivity for VIP (n=84/673). The fraction of VIP+ cells further decreased to 6% in layer IV (n=35/536) and 5% in deep layers (n=26/518). Thus, VIP+ interneurons were located for most parts in upper layers (layers II/III). Morphologically, VIP immunoreactive interneuron somata appeared rather small and ovoid. In 81 measured cells their mean soma diameter was 10±2 µm (range, 5-17 µm), similar to that of SOM+ interneurons. As for SOM, dendritic and axonal processes were difficult to evaluate because labeling was irregularly scattered through the cellular compartments.

CR+ neurons

A total of 131 CR immunoreactive cells were counted on 10 sections of 3 animals. CR expressing neurons constituted with 19% the second largest group of interneurons (n=131/718). Although to a small amount of 2% (n=2/94), CR was the only molecular marker used in this study that labeled Layer I - interneurons. The portion of CR labeled neurons was highest in layer II where 36% of all GFP+ cells showed immunoreactivity for CR (n=18/50). It decreased continuously towards deeper layers, accounting for 21% in layer III (n=41/191), 20% in layer IV (n=44/223) and 16% in deep layers (n=26/160). Shape of somata was mainly fusiform and for 65 measured somata, the mean diameter was 14 ± 2 µm (ranging between 8-20 µm). CR positive cells were mainly bipolar cells with radially orientated processes towards the pial surface, extending up to layer I (Fig. 16).

CR+ interneurons of layer I differed from the general CR+ cell population in that they had rounder somata and lacked any well labeled, long processes.

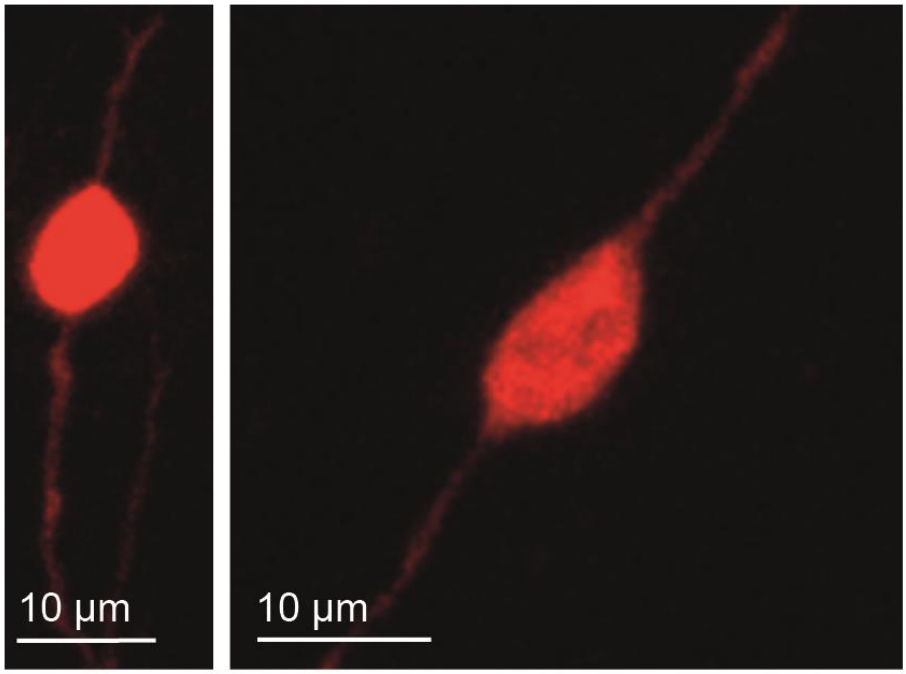

Figure 17 : **Morphology of CR+interneurons**

Examples of bipolar appearance of CR+ interneurons of two different brains. Shown examples were located in layers III and V/VI (from left to right).

CB+ neurons

A total of 102 CB immunoreactive cells were counted on 10 sections of 3 animals. CB positive neurons formed with 16% (n=102/651) the third largest group of presubicular interneurons. CB+ cells were absent in layer I and interneuron density was lowest in layer II, accounting only for 5% of the whole GABAergic cell population in this layer (n=3/56) and highest in layer IV where 28% of interneurons were labeled by this marker (n=45/163). In layer III, CB+ interneurons provided for 14% of all inhibitory neurons. In deep layers about 17% GFP+ cells were immunoreactive for CB. Taken together, the great majority of CB+ interneurons (70%) was scattered through layers IV and V/VI. Morphologically, CB+ somata showed great variability: fusiform, triangular, round or other shapes were seen. CB+ cell bodies had a mean size of 15 ± 4 µm with a large range (8 to 30 µm). Unfortunately, stained axons and dendrites could not clearly be assigned to CB+ interneurons, as this molecular marker also labeled many non-GABAergic cells.

NPY+ neurons

The subpopulation of presubicular interneurons that expressed NPY was very small (n=3). The quality of labeling did not allow precise measurements of soma size or description of axons or dendrites.

3.2.4 Double-labeling of GABAergic neurons

In order to reveal more specific subpopulations of interneurons in the PrS, double labeling experiments were realized for a subset of the possible combinations of PV, SOM, VIP, CR, CB and NPY. The combination of PV, SOM, CR and VIP was of particular interest as these antibodies have previously been described the large majority of interneurons in the neocortex[85,87,107] and the different markers are often connected to distinct electrophysiological and morphological properties as well as to typical connectivity patterns[77]. Therefore, most combinations of these molecular markers (PV+SOM, PV+VIP, SOM+VIP, SOM+CR and VIP+CR) plus additional combinations (PV+NPY, SOM+CB and VIP+CB) were applied on 6 adult GAD67-GFP knock-in mice (Fig. 17).

PV + cells

There was no colocalization between PV-immunopositive cells and cells immunopositive for VIP (n=0/666) across all presubicular layers. In two animals, rare co-localization with SOM was seen. PV+/SOM+ population accounted for 2% of all interneurons in the PrS (n=13/642). Expressed as a portion of PV+ and SOM+ cells, about 5% of all PV+ cells (n=13/279) and 20% of all SOM+ cells (n=13/61) showed immunoreactivity for both proteins. In further double-labeling experiments with PV and NPY (n=0/146), absence of co-localization was revealed. Therefore, PV+ interneurons could generally be considered as non-overlapping subpopulation of interneurons in the PrS, except for their occasional co-expression of SOM+.

SOM + cells

In addition to the SOM/PV co-expression pattern, an extensive co localization of SOM with CB was revealed in a population of 357 interneurons. Double labeling experiments with CB and SOM showed 23% (n=10/43) of the SOM expressing interneurons in the PrS to be CB+ and 16% (n=10/61) of the CB expressing interneurons to be SOM+. The SOM+/CB+ neurons were evenly distributed in all layers except for upper layers I/II where they were absent. Double labeled

SOM+/CB+ cells accounted for 3% of all presubicular interneurons (n=10/357). No double labeled cells were seen in combination with VIP (n=728).

VIP + cells

Neither VIP nor CR showed an overlap with PV and SOM expressing interneurons in the PrS. In contrast, co-expression of VIP and CR was a frequent pattern in the PrS, accounting for 9% of all GABAergic cells in a population of 304 interneurons (n=29/304). This portion is likely to be slightly overestimated given that in a sample of 2192 interneurons the total population of VIP+ cells also accounted for 9% (n=200/2192). Portion of the double labeled cells was highest in layers II/III where these cells account for 15% (L2: n=3/19–L3: n=13/81) and decreased to 7-9% in deeper layers (L4 9% - Deep Layers 7%). Expressed as a portion of both subpopulations, 78% VIP+ (n=29/37) and 54% CR+ cells (n=29/66) showed double labeling.

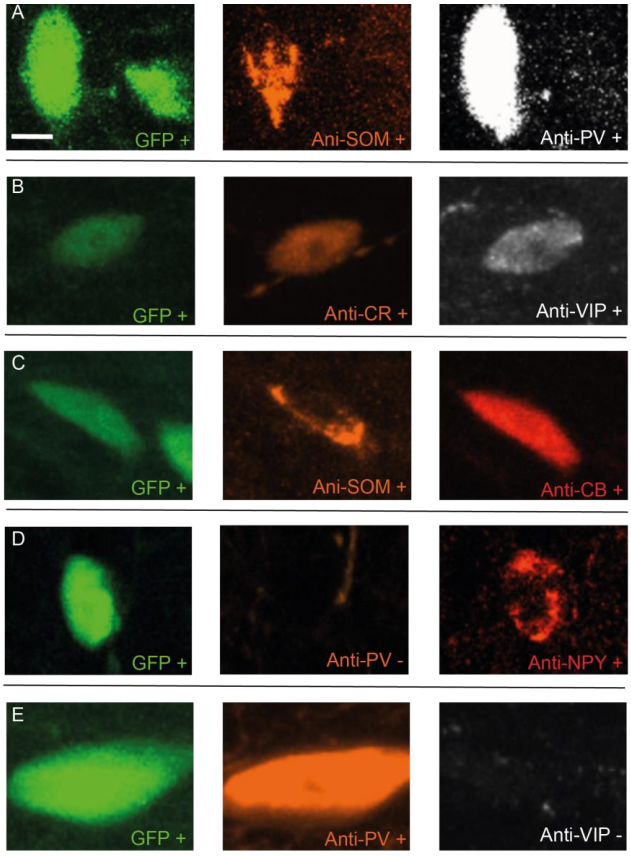

Figure 18 : Co-expression of molecular markers in double labeling experiments

Horizontal sections of the PrS in GAD67-GFP mice. See different combinations of double labeling. For each panel fluorescently labeled GFP+ interneurons are on the left, immunostaining for one molecular marker in the middle and for the other on the right. Co-expression was seen for SOM+PV (A), CR+VIP (B) and SOM+CB (C). No co-expression was seen for PV+NPY (D), PV+VIP (E). The scale bar is 5 µm.

3.3 Projection specific neuronal subpopulations in the presubiculum

3.3.1 Animals

Electrophysiological recordings were realized on 17 LMN-injected and 9 ADN-injected animals. Some of these recordings were done in mice of the GAD67-GFP line where no colocalization of green fluorescent interneurons and red microspheres was seen after injection of retrogradely migrating tracer, indicating an absence of GABAergic long range projection neurons to LMN or ADN.

3.3.2 Laminar distribution of LMN and ADN projecting neurons

Retrobeads appeared as small fluorescent spheres in the somata of labeled cells. Histological analysis revealed accuracy of injection sites by comparing coronal slices of injected areas with those of "The Mouse Brain Atlas" (Paxinos and Franklin, Second Edition, 2001). On the same brains (n=3), horizontal slices were realized to confirm that a correct injection site matched with the expected projection pattern in the PrS. Labeled cells were found in layer IV when LMN was aimed as injection site and in deep layers when ADN was the injection target (Fig. 18). This topographical distribution of ADN and LMN projecting neurons matched with previously described projection specificity by Yoder and Taube (2011). While Yoder and Taube described labeling only in the dorsal portion of the PrS (addressed as postsubiculum in their study), results of the present study revealed labeling at more ventral levels, too. The dorsal portion of the PrS is rather broad while its more ventral part has a triangular shape in horizontal slices. Our recordings and immunohistochemical experiments were done on a relatively ventral to mid-dorsal level, which corresponded to the area generally referred to as the PrS.

After injection in LMN many stained neurons were seen in nearby subiculum as well (Fig. 18 B3). As ventral subiculum is known to project to the lateral[108] and medial mammillary bodies[23], this result was expected. The latter is an area very close to LMN and difficult to avoid completely when targeting the LMN. For electrophysiological recordings, animals were excluded if the distribution pattern of projecting neurons of the prepared slice did not match the expected pattern.

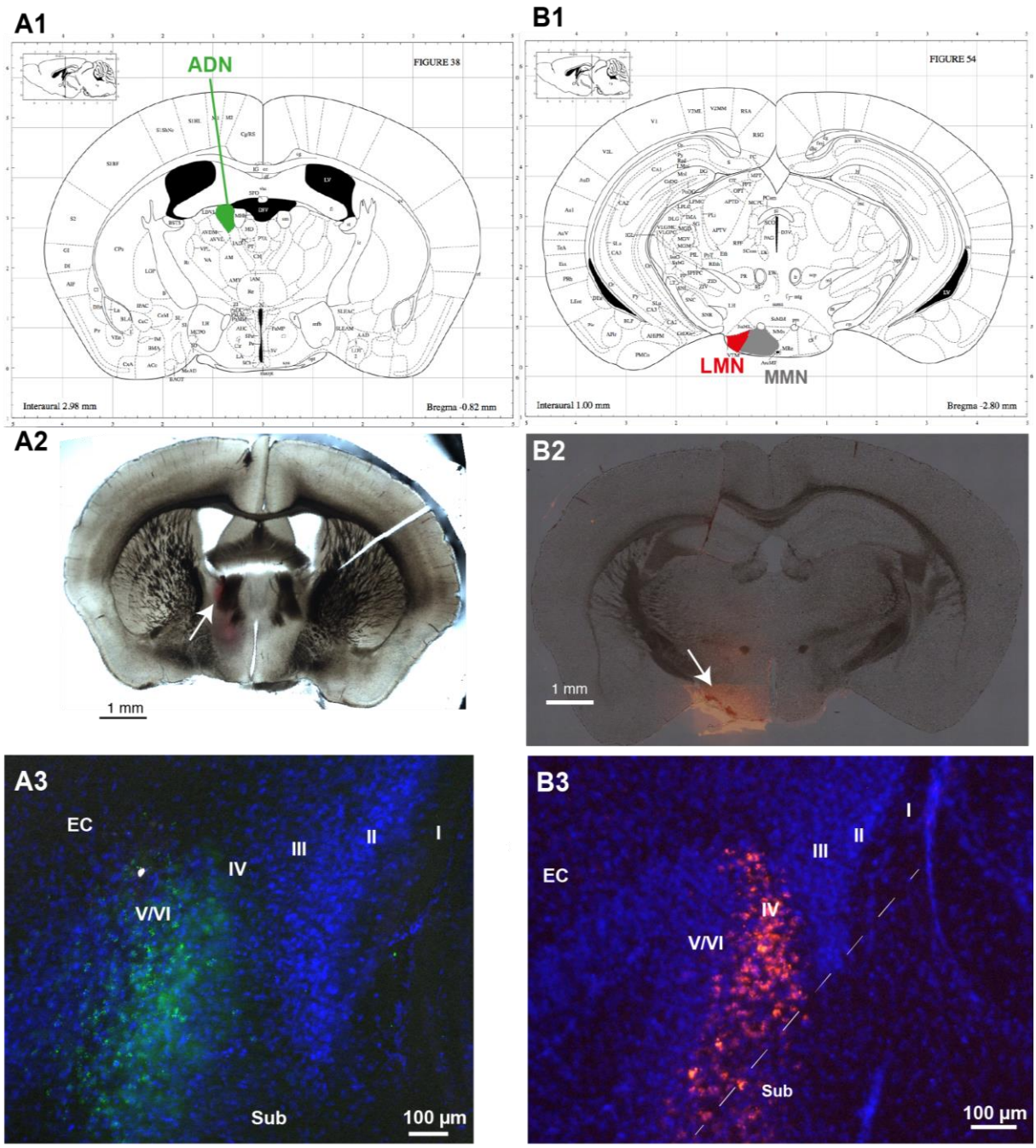

Figure 19 : Retrograde labeling of projection specific neurons in layers IV and V/VI

Coronal plates from Brain Atlas (Franklin, 2001) showing the antero-posterior level for stereotaxic injections in ADN (**A1- A3**) and LMN (**B1-B3**). Note in **B1** that MMN is located close to LMN, both receiving projections from subiculum. **A2** and **B2** show coronal sections after injection in the adjusted coordinates for ADN (**A2**, Fluoruby) and LMN (**B2**, red retrobeads, superimposed with bright field image). **A3** and **B3** show retrogradely labeled somata of projecting neurons in the PrS after injection of Retrobeads in ADN (**A3**, green) and LMN (**B3**, red). ADN projecting neurons were localized exclusively in deep layers V-VI of the PrS. LMN projection neurons were seen in layer IV, but also in nearby subiculum, given that it projects to medial mammillary nucleus (MMN) and LMN (see on **B**).

3.3.3 LMN projecting neurons

A total of 16 LMN projecting neurons identified by fluorescent labeling after retrobead injection in LMN were recorded. Morphology and results of electrophysiological recordings are visualized in Fig. 19. You will find the synopsis of passive and active intrinsic physiological parameters in Table 6.

All recorded neurons were filled with biocytin to reveal their anatomy post-hoc. Axonal and dendritic morphologies of one well-filled cell were completely reconstructed with Neurolucida. Dendrites had a length of 2657 µm and the length of reconstructed axons was 2232 µm. All recorded cells were visualized in Volocity. Their somata were always localized in layer IV of the PrS and appeared as pyramidal cells, extending their apical dendritic tree to ramify in layer I. Their basal dendrites mainly covered layer IV, with some extension in layer III and deep layers.

All cells showed an initial single spike or burst followed by irregular spiking. Both intrinsic burst and single spike firing cells, had an extremely short firing latency (54 ± 4.3 ms, mean ± SEM) which was promoted by a fast membrane time constant (tau=12.9 ± 1.3 ms) and the presence of a depolarizing current at the onset of a depolarization. After the initial discharge, cells showed regular sparse firing. When neurons did not fire in bursts, a depolarizing envelope always underlay the single spike, and the afterhyperpolarization amplitude was low (-13 ± 3 mV, compared to -17 ± 0.9 mV for ADN projecting neurons). These characteristics provided evidence for the ability to fire bursts[12,60].

Regarding their passive membrane properties, mean resting membrane potential was -65.9 ± 2 mV with a neuronal input resistance (R_{in}) at 198 ± 20 MΩ. Hyperpolarizing current injections induced a marked voltage sag (sag ratio 1.1 ± 0.02). In one recorded cell, no sag was measured, as hyperpolarization of -100 mV could not be reached. Injected currents initiated action potentials easily, with a mean rheobase of 74 ± 6 pA. The firing frequency was 38 ± 20 Hz with 13 ± 3 spikes per second at double rheobase and a mean instantaneous frequency of 50 ± 12 Hz. The action potential threshold was -35.5 ± 1.1 mV. Action potential peak value was at 38 ± 2 mV with a rise time of 0.3 ± 0.01 ms. The maximum action potential depolarization and repolarization rates were 465 ± 47.6 and -151 ± 7 $V.s^{-1}$, respectively, with half width duration of 0.5 ± 0.02 ms. Spike after-hyperpolarization reached -49 ± 1.3 mV with a latency of 19 ± 4 ms. Coefficient of variation at twice rheobase was 1 ± 0.2.

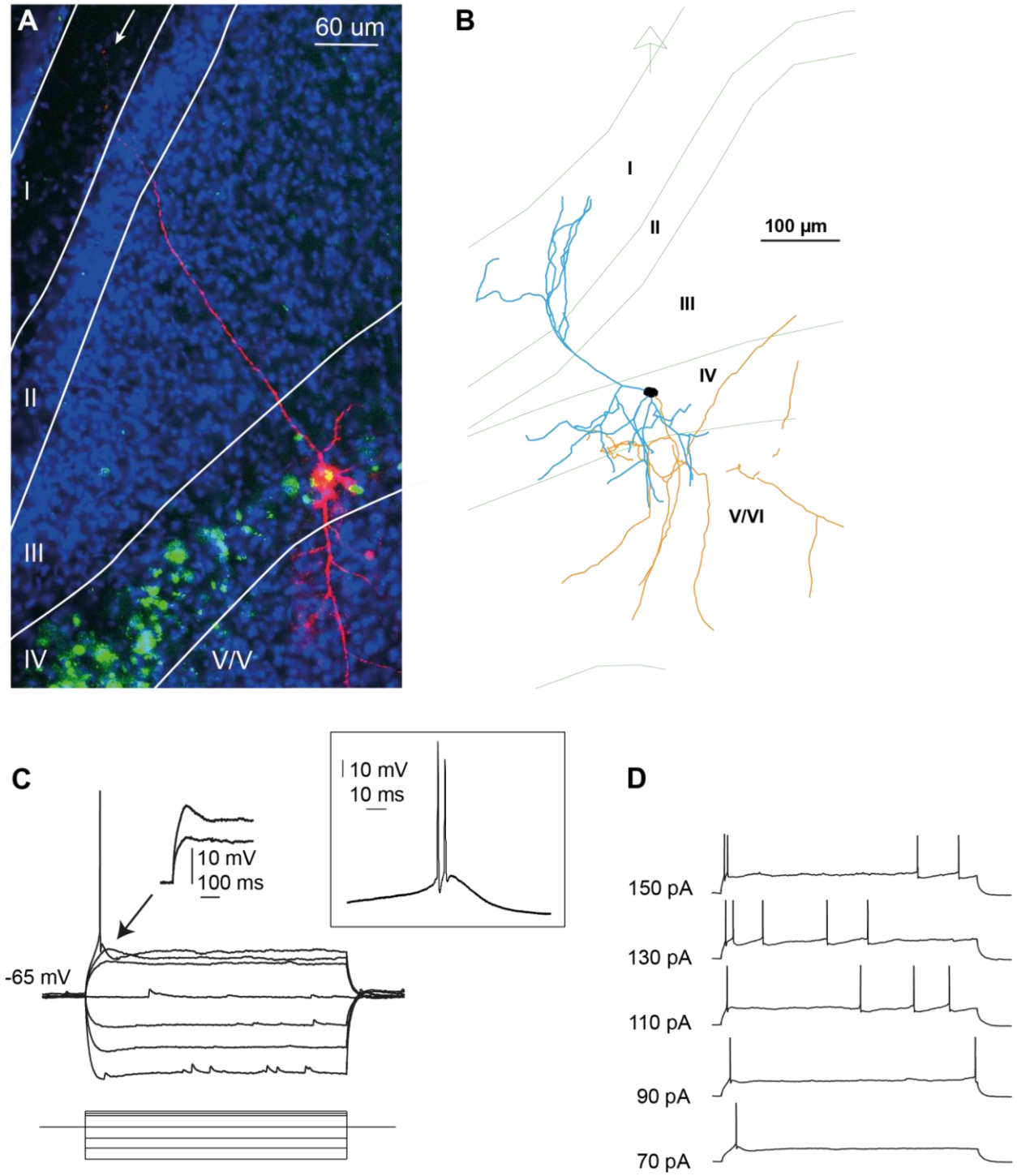

Figure 20 : Morphological and electrophysiological properties of LMN projecting cells

A Horizontal section of the presubiculum with Dapi staining showing a LMN projecting neuron after Biocytin filling. Soma is filled with green retrobeads (RB). Other RB-filled cells (green) are distributed through layer IV. Note the labeled dendrite, extending up to layer I (white arrow). **B** Reconstruction of another recorded LMN projecting neuron. Dendrites in light blue, axon in orange and layer limits in green. The arrow indicates the radial axis (as defined in Simonnet et al., 2013). The reconstructed neuron resembles a star pyramidal cell. **C** Membrane response to negative and positive current steps (starting at –100 mV, then Δ 25 pA) of 800 ms up to rheobase. Note the magnification of the depolarizing onset that causes discharge with short latency. Inset: Intrinsic bursting behavior of another LMN projecting neuron. **D** Evolution of discharge from rheobase, for the neuron in (B).

3.3.4 ADN projecting neurons

Only a small number of ADN-projecting cells (n=9) have been recorded and revealed to date. As it seemed to be a very heterogeneous cell population, it was difficult to deduce regularity yet. Fig. 20 A-D describes the passive, firing and action potential properties of the neuronal population of ADN-projecting neurons and electrophysiological parameters are summarized in Table 6.

After Biocytin filling and Dapi staining all recorded cells could clearly be localized in deep layers. Dendritic arborization extended across all layers of the presubiculum. One reconstructed neuron revealed a dendritic length of 1482 μm and an axonal length of 1065 μm.

ADN projecting cells were regularly spiking principal cells (Fig. 20 D) able to sustain high firing frequency (33 spikes per second at two times the rheobase). Their resting membrane potential was -69.4 ± 2.9 mV, slightly more negative than for LMN projecting neurons, with a neuronal input resistance of 419.69 ± 28.3 MΩ and a time constant of 36 ± 6 ms, almost three times lower than for LMN projecting neurons. Hyperpolarizing current injections induced a pronounced voltage sag (sag ratio of 1.1 ± 0.02). Rheobase was 71 ± 15 pA and a mean instantaneous frequency of 42 ± 6 Hz with an adaptation index of 0.6 ± 0.01 at double rheobase (not shown in Table 6). Firing latency at twice rheobase was 328 ± 105 ms, much longer than in LMN projecting neurons. The input-output curves rose steeply, with an I-O gain of 526 ± 58 $Hz.nA^{-1}$ and a coefficient of variation at twice the rheobase of 0.3 ± 0.05. For action potentials, threshold was -31.4 ± 1.2 mV, peak amplitude 41.8 ± 1.6 mV, maximum rise rate 384 ± 16 V/s, half-width duration 0.57 ± 0.05 ms and afterhyperpolarization amplitude -17.8 ± 0.9 mV. Differences in firing patterns between LMN and ADN projecting neurons can be seen in two representative examples in Fig. 21.

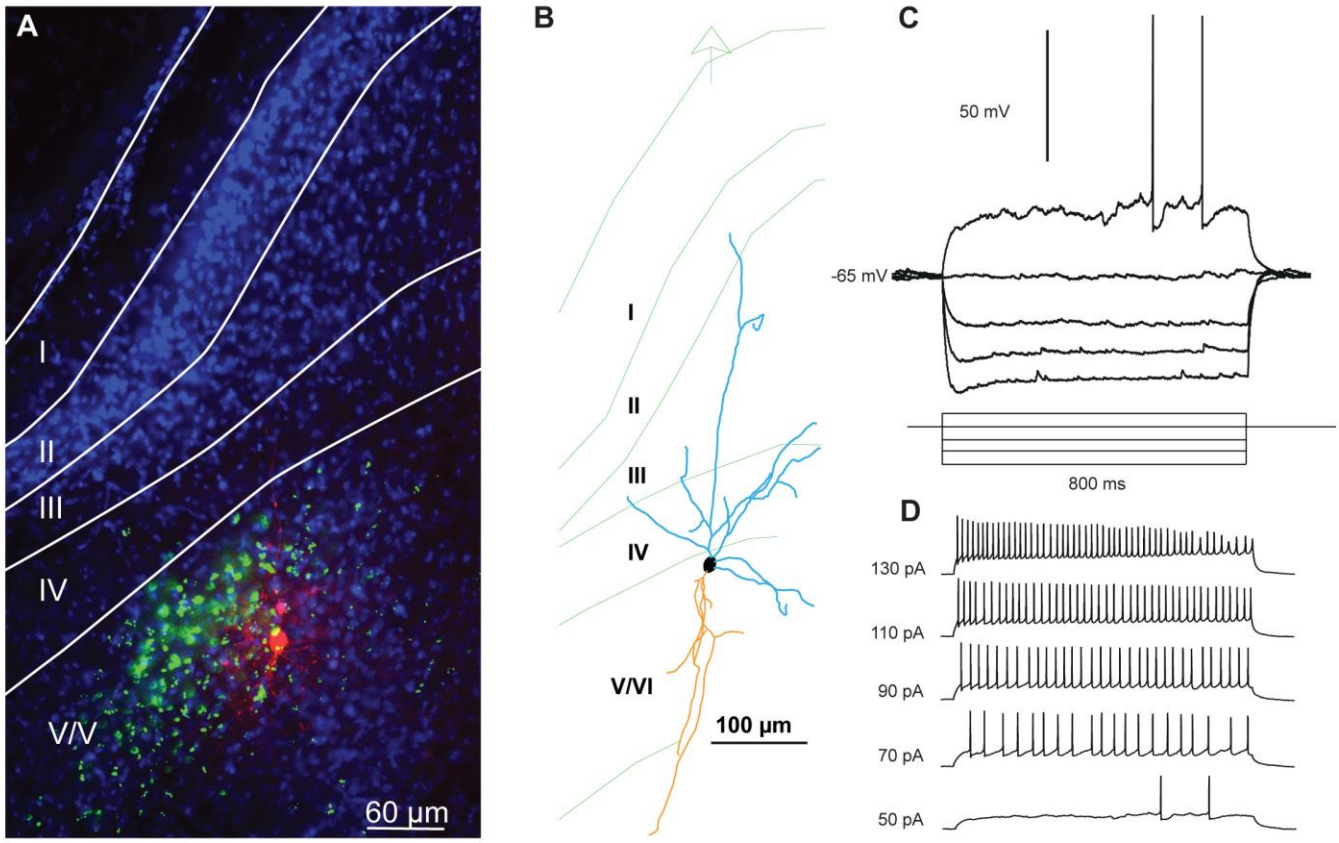

Figure 21 : Morphological and electrophysiological properties of ADN projecting cells

A Horizontal section of presubiculum with Dapi staining showing an ADN projecting neuron after Biocytin filling. Soma is filled with green retrobeads. Other RB-filled cells (green) are distributed through deep layers. Note the labeled dendrite, also extending to upper layers. **B** Reconstruction of another recorded ADN projecting neuron. Color mapping as in Figure 19. **C** Membrane response to negative and positive DC steps of 800 ms up to rheobase (starting at -100 mV) and **D** the evolution of discharge from rheobase, for the neuron in (B).

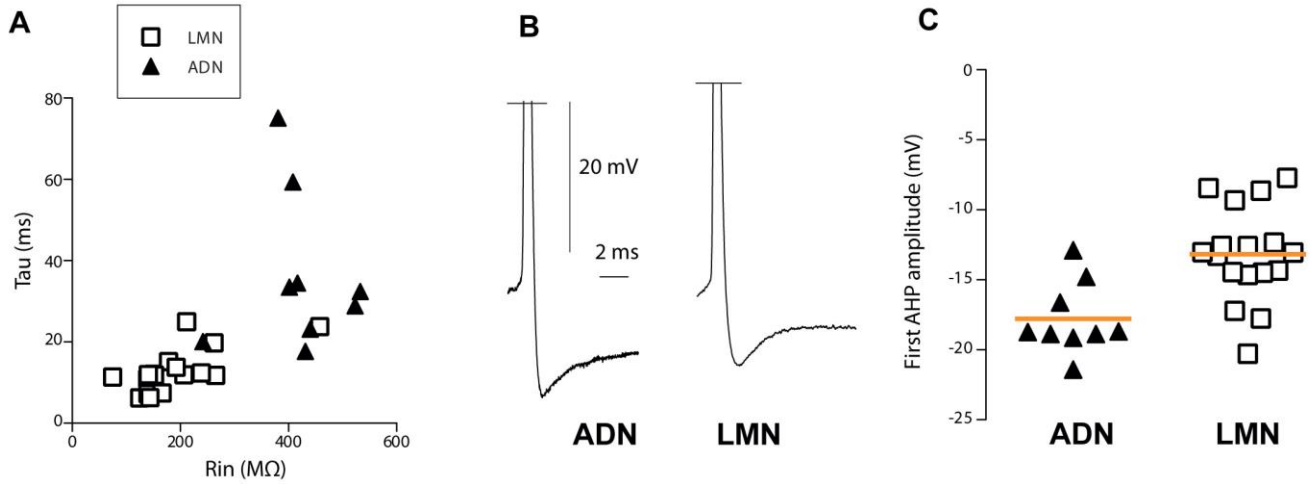

Figure 21 : Differences between intrinsic properties of ADN and LMN projecting cells

A Although some overlap exists, membrane time constant (Tau) as a function of input resistance (Rin) suggests two populations with distinct properties. **B, C** Action potential afterhyperpolarization was deeper in ADN compared to LMN projecting neurons. This was most likely due to the underlying depolarization that favors emergence of bursts in LMN projecting neurons. Black filled triangles correspond to results of recordings in ADN projecting cells, blank rectangles to those of LMN projecting neurons.

	LMN projecting cells			ADN projecting cells		
	Mean	SEM	n	Mean	SEM	n
RMP (mV)	-65.9	1.6	16	-69.4	2.9	9
R_{in} (MΩ)	198	20	16	419	28.3	9
Tau (ms)	12.9	1.3	16	36	6.3	9
Sag Ratio	1.1	0.02	15	1.14	0.02	9
Rheobase (pA)	74	6.2	16	71	15	9
AP Threshold (mV)	-35.5	1.1	16	-31.4	1.2	9
AP Peak amplitude (mV)	38	2.4	16	41.8	1.6	9
AP Rise time (ms)	0.3	0.01	16	0.34	0.01	9
AP Rise amplitude (mV)	73.6	3	16	73.1	2	9
AP Width (ms)	0.51	0.02	16	0.57	0.05	9
AP Max depolarization rate (V/s)	465	47.6	16	384	15.8	9
AP Max replorization rate (V/s)	-151	7.3	16	-136	14.5	9
AP Latency (ms)**	54	4.9	16	328	105	9
AP Number**	13	3.4	16	33	6	9
AP Frequency (Hz)	38	20	16	2.8	0.9	9
AP Mean inst frequency **	50	12	16	42	6.2	9
I-O gain (Hz/nA) (APs/sec) **	13.3	3	16	526	58	9
Coefficient of variation **	1	0.18	16	0.27	0.05	9
AHP (mV)	-49	1.3	16	-49.2	1.2	9
AHP Amplitude (mV)	-13	3	16	-17	0.9	9
AHP Latency (ms)	18.9	3.9	16	2.5	0.6	9

Table 6: Intrinsic electrophysiological properties of LMN and ADN projecting neurons

AHP: Afterhyperpolarization; AP: Action potential; I-O gain: Input-Output slope; Mean inst frequency: Mean instantaneous frequency; RMP: Resting membrane potential; Rin: Neuronal Input Resistance; Tau: Membrane time constant; ** Value was measured at two times rheobase (if not specified, measurements were done at rheobase).

4. DISCUSSION

In this thesis, I examined molecular, morphological an electrophysiological features of inhibitory and excitatory neurons of the mouse PrS. In the first part of my work, I showed the distribution and molecular identity of presubicular GABAergic neurons by using an immunohistochemical approach on an interneuron specific transgenic mouse model. In the second part, I investigated the morphological and electrophysiological properties of projection specific neurons in the PrS. I concentrated on two efferent projection targets of the PrS: LMN and ADN. My work generated previously unknown information about the identity of excitatory and inhibitory neurons of the PrS as well as its connectivity with other brain areas. In the following chapter, I will discuss summarized results of my work, in order to evaluate their functional relevance and suggest perspectives for future investigations.

4.1 Interneurons of the presubiculum

The present study provides the first comprehensive categorization of interneurons in the mouse PrS and reveals new aspects of its neuronal organization. I quantified the total population of inhibitory neurons in the presubicular cortex and further examined presubicular interneurons by using a neurochemical approach commonly used in various brain areas[67,109]. Indeed, interneuron subpopulations can be distinguished on the basis of their contents of the calcium binding proteins PV, CR and CB and the neuropeptides SOM, VIP and Neuropeptide Y. I performed double immunolabeling with several combinations of these marker proteins because some interneurons co-express different molecular markers. Inhibitory activity is thought to pattern cortical activity by modulating excitability and by synchronizing cortical networks. In the hippocampus and entorhinal cortex, inhibitory cells seem to structure the operation of microcircuits in spatial signaling[110]. GABAergic activity also contributes to the direction selectivity of principal cells in cat visual cortex[111]. In the PrS, local interneurons may therefore be involved in temporal and spatial processing of the head directional signal. While extensive studies of presubicular excitatory neurons have been published recently[12,57], very little information is available about inhibitory cells in this region. Some previous studies evaluated staining intensity for calcium binding proteins and for acetylcholinesterase [112–114]. However, experiments of my work go considerably further in that they quantify the laminar distribution and the overall proportions of neurochemically defined subsets of interneurons. Part of this work has been published in an article that identified morphological and electrophysiological properties of PV+ and SOM+ interneurons in the PrS[115].

4.1.1 Evaluation of chosen methods – Cell counting

While the word "counting" emanates apparent simplicity, neuronal cell counting is no unambiguous or unbiased issue. There are various counting methods which comprise different error sources and assumptions. Each approach may or may not be adapted for the question that is asked. Therefore, the applied method has to be described extensively to allow the reader an informed interpretation of the results.

Recently, a new counting method named the automatic isotropic fractionation [116] has been established that allows fast and reliable estimations of absolute cell numbers in different brain regions. This technique is without question the most accurate available tool for cell counting so far but is no suitable approach if the experiment requires extensive histology, the examined structure needs to remain identifiable or the investigator is interested in more precise spatial information, such as layer-specific affiliation of each counted cell body[117]. Moreover, specific equipment and expertise is needed, which is not available in every routine histology lab. In these cases, alternatives consist either in so called two dimensional profile-based or three dimensional stereological methods. In the overwhelming majority of quantitative studies conventional, profile-based (2D) or model-based methods are used [118]. Typically, particle profiles are counted in very thin paraffin sections and corrected afterwards for the overcount due to split particles visible in multiple sections[119]. While high availability of equipment and the simple concept are the advantages of this approach, disadvantages consist in the uncertainty about the extent of bias due to assumptions about anatomical characteristics (i.e. size, form and orientation) of counted particles which need to be made when applying a correction factor. To cope with this problem, a design-based approach for cell counting called "stereology" has been developed. In stereology, counting is realized in a three dimensional probe, the optical disector (thick slice, ~50 µm). The investigator selects a random sample of sections containing the structure of interest (optical disector) by starting at a randomly chosen starting position and selecting every following nth section containing the structure of interest. Within each optical disector, cells are counted in a counting grid which is composed of counting frames that are built of an inclusion and an exclusion line (particles divided by the inclusion line are counted while those divided by the exclusion line are not). In the z-axis, the counting frames start and end several micrometers before the upper and lower section edges, which avoids counting lost caps of cut particles. Results are then extrapolated to the entire volume of the structure.

In the present study, we chose to combine profile-based with design-based counting methods. As stereological methods are time-consuming and dependent of investigators expertise and a specific set-up, we chose to rely on established methods of the lab and reduce error sources by utilizing the available stereological tools. Instead of counting cells in thin sections and apply a correction factor, each slice was 50µm thick in order to create a three dimensional counting probe (optical disector) for subsequent cell counting. Slices were chosen as every n^{th} section starting from a random starting point thereby meeting the criteria for systematic random sampling as recommended for a design-based stereological counting approach[120,121]. Counting frames for each layer started several micrometers at the lower and upper margins of the sections to avoid bias associated with cutting artifacts such as uneven surfaces leading to wrong volume estimations or cells cut into pieces during histologic sectioning that would lead to an overestimation of cellular density[118]. For cell counting, only the first edge-point of labeled particles that encountered the progressing plane of observation was considered[100,101]. As a point has no shape and orientation which influences the probability of being sampled, the "equal opportunity rule" as a basic requirement for random sampling was hence fulfilled[122].

Yet, it is important to ask oneself which aspects of this methodological setting could have led to a wrong estimation of neuron density. Volume measurement is a limitation that affects all stereological and profile based methods. Measurement of the z-axis within a slice can be influenced by tissue-shrinkage or irregularity in surface (disadvantage of vibratome cut slices) but also variables related to the optics (eg thickness of coverslips and type of lens). In order to limit this bias all slices were histologically processed in the same session and counted after 2 days of drying. This way, tissue shrinkage would at least apply in similar proportion to all sections. Regarding the detection of particles, high contrast settings were applied in order to rend all immunostained cellbodies visible. Still, the observer's eye is always an undeniable limitation of manual cell counting. However, a recent review showed that the manual approach still generates the most reliable results regarding quantitative investigations in biological tissues compared to the performance of automated cell detection alogorithms[123]. In addition, inter-rater reliability was tested within our lab. Sample wise comparisons of cell count results from two independent investigators using the same methods were conducted to facilitate the objectivity of the reported findings. No striking discrepancy was revealed in any of the tested samples.

4.1.2 Neuronal density in the presubiculum

In the present work, one sub question referred to the neuronal density of the mouse presubiculum that has never been reported before. In the presubiculum, the overall neuronal density is 180.000 neurons per mm^3 with striking layer-specific differences in cellular density (ranging 22 to 280 $x10^3$ cells per mm^3). Indeed, the cellular density of the presubicular cortex as reported in this manuscript and published in Nassar et al. (2015)[115] seems high compared to numerical neuronal densities that have been reported previously in other cortical areas of rat, lying layer-dependently between 14 and 170.000 $x10^3$ cells per mm^3 [124–126]. Yet, those studies all focused on neocortical areas unlike the present work that quantifies the neuronal population of the presubiculum, which is part of phylogenetically older Periallocortex. A recent study that quantified various functional areas of mice cerebral cortex revealed quantitatively different cortical zones[127]. As Periallocortex shows different characteristics in cytoarchitecture than neocortex, high cellular density may be one of them. In addition to limitations of comparisons between brain areas, comparisons of neuronal densities between species proves to be even more difficult, as total neuron numbers seem to vary little with brain size indicating a higher neuronal density in animals with smaller brain volume[128,129]. To the best of knowledge, a quantification of cellular density in the presubiculum has never been done before and we therefore have no region specific reference of any similar species to verify our published results. Indeed, compared to neighboring areas rodent presubiculum has been described as a densely packed region in the literature, which further supports our results:

- "Cell bodies in superficial layers of presubiculum were smaller and more compact than in MEC and parasubiculum."[8]
- "In mouse, PrS can be distinguished by its higher cell packing than in CA1 and Subiculum."[54]
- "One surprising finding in the present study is the large numbers of neurons in the layers of the pre- and parasubiculum […]" [130]

Recently, it has been reported that in mice, nearby entorhinal cortex has a mean neuronal density of 100 $x10^3$ neurons per mm^3 which is already quite high compared to neocortical areas such as frontal cortex (66 $x10^3$ neurons per mm^3) or motor cortex (74 $x10^3$ neurons per mm^3)[127]. Given that presubicular cortex has been characterized various times by its high cellular density compared to neighboring regions such as entorhinal cortex, a mean neuronal density of 180 $x10^3$ neurons per mm^3 seems a likely estimation.

Another aspect in favor of the presented results is the fact that GABAergic cells/Principal cells ratio is comparable to other brain areas (11% overall, with layer specific variability, such as the common finding that in layer I over 80% are interneurons). As expression of GFP was independent from immunohistochemistry, overlap of both methods support the viability of our findings. For future studies it would be interesting to elucidate the neuronal distribution within the presubiculum as the variance of cellular density between the sections suggests a gradient in the dorso-ventral axis. However, the sample size of this study was too small to pursue this observation.

4.1.3 Specific distribution of interneurons in the presubiculum

The overall distribution of GABAergic neurons of the PrS was examined in the GAD67-GFP transgenic mouse model in combination with an Anti-NeuN immunostaining. The general neuron density was highest in layer II and lowest in layer I. In contrast to principal cells, the density of GFP+ cells was lowest in layers I/II and highest in layer IV. Interneurons were present in all layers of mouse PrS and accounted for 11% of all presubicular neurons. Generally, reported proportions of inhibitory cells remain ambiguous across previous publications and are likely to differ between sampled areas and species. In rodent neocortical areas, older reviews estimated 20-30% of all neurons to be interneurons[67,96,131] while recent studies emphasize that their portion may have previously been overestimated, suggesting 11-13% to be a more realistic approximation[125,126,132]. Indeed, this figure lies closer to what has been shown for hippocampus proper[81] or entorhinal cortex[133] where interneurons are thought to provide for 7-10% of all neurons. The proportion of interneurons in the PrS in the present study is therefore similar to previous reports from other areas of the hippocampal- parahippocampal region as well as recent estimations for neocortical areas.

In the PrS, the fraction of interneurons within the general neuronal population varies strongly between layers, ranging from 80% in layer I to 4% in layer II. This pattern seems to be specific for the presubicular cortex. In entorhinal cortex for instance, interneurons are more evenly distributed, accounting for about 20% of neurons[133]. Therefore, although the general portion of interneurons in the PrS is similar to other parahippocampal structures, their laminar distribution revealed important differences. Most likely, the distinct organization of the inhibitory microcircuit in the PrS is linked to specific functional requirements such as the non-adapting HD-signal. In order to reveal more details about subtypes of inhibitory neurons in the presubicular microcircuit, I applied several double-immunostaining combinations of six commonly used molecular markers for interneurons (PV, CR, CB, SOM, VIP, NPY).

These marker proteins are regularly used to selectively target specific interneuron populations either by genetic labeling (transgenic mouse models such as PvalbCre or SstCre) or by immunohistochemistry[77,85–87,97]. Because combinations and distribution of chemical markers in GABAergic neurons are species- and region-specific[134] and vary according to the functional specialization of the brain structures[135], regions of interest have to be examined separately. This is particularly valid for the PrS, considering its unique transitional position between neocortical areas and archicortical hippocampus.

4.1.4 Colocalization of GABA and marker proteins in the presubiculum

Previous studies have shown that GABA expression co-localizes with a subset of molecules[85,87,97]. However, there are few studies examining in detail the extent of this colocalization. Indeed, in some species or brain areas, commonly used interneuron markers are present in excitatory neurons, too[8]. For instance, CB and VIP have been seen in principal cells of the hippocampus[81,136]. As neurochemical markers for interneurons have rarely been used in the PrS[113,114], their validity to identify GABAergic neurons in the PrS had first to be confirmed. The present study revealed that most molecular markers were relatively specific (>90%) for interneurons in the mouse PrS, however, none of the applied markers colocalized 100% with GFP+ cells in the PrS.

Of all CBPs used in the present study, highest interneuron specificity was seen for PV (96%), which is similar to mouse visual cortex[87]. In mouse somatosensory cortex, non- GABAergic PV+ cells have been identified as a distinct subpopulation of cortico-striatal projection neurons[137]. Further investigations on non-GABAergic PV+ neurons in the PrS should shed light on the question of whether they also constitute a distinctive long-range projecting cell population.

CR is also a quite specific CBP for GABAergic cells as 88% of all CR+ cells were GFP+. This is consistent with previously published data from mouse neocortex[87,96] but differs from results in entorhinal cortex of rat, where CR sparsely co-located with GABA[138]. This study showed that CR immunoreactive fibres delimit layers I to IV of the presubiculum. These may either originate from local CR+ interneurons or from CR+ neurons located in other brain areas. The assumption of interlaminar projections of presubicular CR+ interneurons is supported by the bipolar morphology of those cells that is supposed to be accompanied by vertical translaminar axonal arborization[139]. Yet, in a recent tracing study an overlap of thalamic fibres and CR staining has been observed (Mathon and Fricker, unpublished) which suggests that CR+ fibres in the presubiculum may derive from CR+ neurons located in the thalamic nuclei.

The only CBP that is mostly expressed by presubicular principal neurons is CB. It has already been reported that in mice as well as in primates (human/non-human) CB is expressed in GFP+ and GFP- cells while it seems to be restricted to GFP+ cells in human tissue[114]. In mouse PrS, CB+ excitatory cells are densely packed in layer II where they serve as a distinguishing landmark[4,13] and are suggested to account for a specific subpopulation of projection neurons[112]. This assumption is supported by the finding that non- GABAergic CB+ cells seem to be restricted to layer II. Indeed, CB expression is highly specific (>90%) in the other presubicular layers. Therefore, CB can be considered as a reliable interneuron marker for all layers in mouse PrS, except for layer II. Among neuropeptides, VIP had the highest specificity for presubicular interneurons (94%). However, VIP is less specific for interneurons in the PrS than in the visual cortex, where total overlap with GABA was reported[77,85,87]. In contrast, hippocampal VIP+ neurons seem to include GABAergic and a small number of non-GABAergic cells[140]. These findings may reflect a common origin of presubicular and hippocampal VIP+ cells. SOM is a quite specific neuropeptide for GFP+ cells in presubiculum as well. Still, about 10% of all presubicular SOM+ cells are non-GABAergic. A similar portion of non-GABAergic SOM+ cells in the PrS was observed in a transgenic Cre mouse that is supposed to selectively express a fluorescent reporter in SOM+ cells[115]. In the neocortex, the overlap of SOM labeling with the local interneuron population ranges between 94 and 98%, contrasting with entorhinal cortex where SOM is mainly expressed in principal cells[133].

Although minor populations of labeled non-GABAergic cells are not a concern in the present study, as quantification considered only GFP+ cells, variability between brain areas of the same species emphasizes the need for an extensive characterization of marker expression for each region. Labeling of non-GABAergic neurons by commonly used marker proteins raises the question as to which neurotransmitter these cells contain. Future work will also have to examine laminar distribution and connectivity of those neurons in order to reveal their neuronal identity and their potentially distinctive roles within the presubicular microcircuit.

4.1.5 Molecular subtypes of presubicular interneurons

PV+ interneurons in the PrS

With 36%, PV+ interneurons constituted the major subpopulation of GABAergic cells in the PrS. Similar percentages have been reported for several cortical areas such as visual, somatosensory, motor and piriform cortex of rodents[85,87,96,141]. In the hippocampus, the percentage of PV+

interneurons is known to be smaller, varying between 15-25%[81,142]. Expressed as a portion of all interneurons, PV+ interneurons of the PrS were absent from layer I, accounted for a small population in layer II (15%) and contributed evenly to the interneuron population of layers III-VI (about 40%). These results are similar to quantifications obtained in other cortical areas, including neighboring entorhinal cortex of humans and rodents[77,87,112,141,143,144]. The numerical density of PV+ cells per volume was slightly lower in layers II/III than in deeper layers IV-VI, mainly because of high cellular density in layer IV. Similar results had been previously reported in a qualitative description of PV+ cells in the PrS[112].

Nassar et al. (2015) quantified laminar densities of presubicular PV+ interneurons in a transgenic mouse line that selectively expresses fluorescent labeling in PV immunoreactive neurons (PvalbCre::tdTomato). In this work, the density of superficial layers (II/III) PvalbCre tomato+ cells was compared to that in deep layers (IV-VI), and the density appeared a little higher in superficial layers. While absolute values were similar in Nassars work on PvalbCre tomato cells and my own work on GAD67-GFP mice for superficial layers, density of deeper layers IV to VI was higher in mine. The slightly differing results may reflect differences between the PvalbCre and the GAD67-GFP mouse line or indicate that not all PV+ cells are labeled in PvalbCre mice. Indeed, Nassar et al. (2015) showed that Cre was transmitted by maternal inheritance and immunostaining experiments showed a lack of complete labeling in the PvalbCre::tdTomato mouse line.

A recent work of Boccara et al. (2015) that described intensity of PV labeling in the hippocampal-parahippocampal formation obtained additional information by looking at different intensities of neuropil staining. Authors observed stronger immunoreactivity in superficial than in deep layers of the PrS separated by a thin stripe which could correspond to layer IV[13]. The contrast between cellular density of PV+ neurons and neuropil staining in layer IV may reflect a distinct connectivity pattern of layer IV PV+ interneurons.

SOM+ interneurons in the PrS

SOM positivity accounts for 16% of the general interneuron population of the PrS. In the hippocampus, the proportion of SOM+ interneurons is similar to that in the PrS[81]. In contrast, SOM expression is much higher in most neocortical areas, varying between 25 and 30%[87,96,143], except for neighboring entorhinal cortex that comprises a very small SOM+ subpopulation, contributing only to 8% to the total number of GABAergic cells[133]. The laminar distribution of

presubicular SOM+ interneurons however showed a typical neocortical pattern. Just as in somatosensory, frontal or visual cortex[87,96], density of SOM+ interneurons in the PrS increased continuously towards deeper layers, from 8% in layer II up to 27% in layer V/VI. These findings have been confirmed in the Sst-Cre tomato transgenic mouse[115].

VIP+ interneurons in the PrS

VIP expression was observed in 9% of all GABAergic neurons in the PrS, representing a rather small subpopulation. Comparison with other regions is difficult as numbers vary between sources and species. In mouse visual cortex, authors reported portions ranging from 6 to 17%, [77,85,87] while in cat visual cortex, only 1-2% of all interneurons expressed VIP[145]. The great majority of presubicular VIP+ cells was located in superficial layers (II/III), which is consistent with previous studies reporting the same distribution pattern in different areas and species[141,145–147]. Unfortunately, VIP labeling was not evenly distributed through the cellular compartments, making morphological properties difficult to evaluate. In cat visual cortex, VIP+ neurons have been described as mainly vertically orientated, with a bipolar or bitufted shape and few fibres[145]. Rarely, morphology of small basket cells with axonal arborization ”en arcade” was observed in rat frontal cortex[98].

CR+ interneurons in the PrS

CR expressing neurons accounted for 18% of all presubicular interneurons, representing the second-largest subpopulation of presubicular interneurons. The proportion of CR+ interneurons is relatively uniform between cortical brain areas and species, always accounting for 17-25% of interneurons[85–87,147]. In the neighboring entorhinal cortex or hippocampus, 9-13% of GABAergic neurons are immunoreactive for CR, [138,142] which makes them slightly less numerous than in the PrS. Distribution pattern of presubicular CR+ neurons in mouse was, however, similar to that observed in parahippocampal areas of other species, [114,138,148] where CR+ interneurons are evenly distributed through all layers. A somewhat unique feature of CR is its labeling of layer I neurons which has also been described in other brain areas although to different extent. In visual cortex[87,139], about 40% of layer I interneurons were immunoreactive for CR, thus much more than in the PrS (2%). Morphologically, bipolar appearances of CR+ interneurons dominated in the PrS which is in line with what has been reported in other cortical areas[87,114,138,148]. CR+ interneurons of presubicular layer I, however, displayed a different morphology with a rather small, round soma and lacking the bipolar appearance of deep layer CR+ cells.

CB+ interneurons in the PrS

Like SOM, CB was expressed by 16% of all GABAergic cells in the PrS. In frontal cortex[97], CB+ interneurons accounted for more than 40%, while this percentage is much lower in visual cortex, where only 20% of GABAergic cells showed immunoreactivity for CB[86]. In dentate gyrus, CB had recently been revealed in 24% of hippocampal interneurons[142]. Therefore, although the number of CB+ interneurons varies strongly between areas, it is still rather low in the PrS which contrasts with the high density of non-GABAergic CB+ cells in presubicular cortex. Non-GABAergic CB+ neurons densely populated layer II, whereas CB+ interneurons were rare in this layer but tended to accumulate in layer IV. CB labeling revealed very small to very large cell bodies with various shapes, indicating a heterogeneous population of CB+ neurons, which is in agreement with previous studies[139].

4.1.6 Double labeling reveals additional subtypes

In order to reveal additional neurochemical distinctions and overlapping or non-overlapping subpopulations of interneurons, some double labeling combinations were realized. In mouse neocortex, the molecular markers PV, SOM and VIP are thought to label distinct interneuron populations[77,85,87,96]. Similar subpopulations were expressed in the PrS as PV, SOM and VIP mainly did not show any overlap.

While no VIP expression has been observed in either PV+ or SOM+ interneurons, a striking difference between the PrS and neocortex consists in a small subpopulation of interneurons that co-express PV and SOM. This pattern is typical for the hippocampus, where 10-20% of all interneurons co-express PV and SOM but has not been observed in other cortical regions yet[81,85,87,134,149,150]. Note that the hippocampal PV+/SOM+ neuronal population exists in a complementary way rather than forming a homogenous subpopulation. In CA1, there seem to be strong SOM+ and weakly PV+ OLM- interneurons while bistratisfied cells show an intense PV positivity and a less pronounced SOM staining. As this co-localization exists in a subtle way, it may have been overlooked in other brain areas. In the PrS, the great majority of PV+ interneurons showed no overlap with SOM or any other molecular marker and presubicular PV+ interneurons can practically be considered as a distinct subpopulation.

In line with co-expression patterns of neocortex, presubicular SOM+ interneurons were often CB positive and large parts of VIP+ interneurons of the PrS immunoreactive for CR, too. In contrast to neocortical areas of mice, CR and SOM seemed not to co-localize in the PrS[151]. The high

proportion of CR-expressing VIP+ cells suggests that the VIP+/CR+ interneuron population rather forms a subgroup of CR+ cells and that CR+ interneurons probably form a non-overlapping subpopulation of interneurons in the PrS. Summing up, it seems as PV, SOM and CR-expressing interneurons form mainly non-overlapping, distinct subpopulations in the PrS.

In the present study, not all possible combinations of the six molecular markers were realized. Quantifications of PV+CR, PV+CB and CR+CB are still missing. Also, the combination of SOM and CR was realized only on few sections and a bigger sample size is needed in order to exclude any co-localization of both GABAergic populations in the PrS. Furthermore, poor staining quality of NPY did not allow a reliable quantification of its co-expression patterns. Therefore, results of the present study should be considered partial and should be completed in the future. Although not an extensive description of all possible combinations, my results suggest that interneuron subpopulations of the PrS are similar to those of neocortex but also show characteristics of hippocampal interneurons, like the PV+/SOM+ subpopulation.

4.1.7 Functional relevance of the findings

In the present work, I examined the density, laminar distribution and content of molecular markers of interneurons in the PrS. Immunohistochemical experiments are commonly used as convenient labels for interneuron subtypes and do not give a direct functional insight. However, results of the present study allow some assumptions on the functional aspects of the inhibitory microcircuit of the PrS and give a basis for future detailed analysis of the GABAergic population in this region. Indeed, marker expression shows a remarkable degree of specificity both for the localization of synapses on the targeted cell and the afferent and efferent connectivity (interneuron or principal cell, local or distant neurons)[63,65,77]. This validates the molecular approach not only as a categorization tool for interneuron types but also as a predictor of their functional role within a microcircuit network [63].

As interneurons are thought to shape input and output locally, soma location often indicates the site of action. Therefore, the general distribution of interneurons may reflect the functional requirements of a specific brain area and indicate inhibitory connectivity patterns. An interneuron may target dendrites, soma or axons of principal cells. One would expect location of soma-targeting interneurons close to principal cell bodies and dendrite-targeting interneurons close to the dendritic arborization of its targeted principal neuron. It should be noted that this assumption is limited as illustrated for instance by the SOM+ Martinotti cell, located in deeper layers but

targeting dendrites in more superficial layers and particularly in layer I[93]. Inhibitory synapses on dendrites select input signals while somatic or axonal localization is believed to have more effect on the action potential output[66].

Most principal cells of the PrS extend their dendrites to layer I which receives many afferent projections[12]. Recently, SOM+ interneurons with a Martinotti-like anatomy and adapting firing behavior have been revealed in layer III of the PrS[115]. They would be well suited to control specific inputs from afferent projections of thalamus and retrosplenial cortex, known to target the apical dendrites of principal cells in layers I and III[16,152].

In neocortical areas, SOM+ interneurons strongly inhibit other molecular interneuron subpopulations such as PV+, VIP+ but also layer I interneurons, leading to a shift of inhibition along the somatodendritic axis[77]. Such a connectivity pattern remains to be validated for the PrS. Preliminary data (Simonnet et al., in preparation) suggest that presubicular SOM+ interneurons of superficial layers are not contacted directly by afferent inputs and rather provide feedback inhibition, similar to what has been shown in neocortical brain areas[63,64].

Unlike dendrite-targeting interneurons, soma-targeting GABAergic cells would be expected close to the cell bodies of principal neurons. Interestingly, the layer with the highest interneuron density, layer IV, contains a subpopulation of principal neurons that are known to target the lateral mammillary nucleus. This projection is believed to play a critical role for the visual update of the head direction signal within the HD generative circuit[153]. High density of GABAergic cell bodies in this layer may translate strong perisomatic inhibition onto the LMN- projecting neurons. This could lead to rebound excitation and synchronization in these cells as perisomatic inhibition is known to enforce precisely spike timing through fast, phasic inhibition in hippocampus or somatosensory cortex[66,154–156]. Perisomatic inhibition further correlates with PV-expression[67,77], fast firing behavior and basket cell like morphology[68,157]. While those electrophysiological and morphological properties of PV+ cells have recently been shown to apply to the PrS[115], my work provides evidence for their connectivity pattern: PV+ stained fibres which outline PV negative somata indicate axon terminals targeting perisomatic areas of non-GABAergic cells. Therefore, the finding that PV+ interneurons densely populate layer IV further supports the hypothesis that strong perisomatic inhibition acts on layer IV principal cells, as mentioned above. In layer IV of rat barrel cortex, soma-targeting PV+ basket cells were shown to be the target of thalamic afferences[154]. This raises the question whether PV+ cells of presubicular layer IV may also be

targeted by specific afferences. In other brain regions, PV+ interneurons are directly recruited by long-range projections indicating a feed forward inhibitory circuit[63,64]. For presubicular layer III, preliminary data obtained with optogenetic stimulation of afferences suggests that PV+ interneurons are indeed specifically targeted by thalamic afferences (Nasser et al, in preparation). They may also be systematically recruited by visual input, as seen for PV+ interneurons in layer II/III of neocortex[65]. Interestingly, visual input is believed to enter the HD circuit via the LMN projecting neurons of presubicular layer IV.

In general, less is known about other subpopulations than the well studied PV+ basket cells or the SOM+ Martinotti cells. Investigations on electrophysiological or morphological properties of CB+ interneurons are particularly rare, given that CB is not exclusively expressed in interneurons. In rodents, CB+ interneurons were described to display an intrinsic bursting behavior[158] and to give rise to perisomatic boutons[159,160]. In neocortical areas, CB+ interneurons seem to be entirely contacted by VIP+ interneurons and project themselves onto pyramidal cells[161]. As the distribution pattern of GABAergic and non-GABAergic CB+ cells is rather specific for the PrS, further investigations should be performed on this widely unexplored cell population.

A quite large subpopulation of presubicular interneurons is immunoreactive to the calcium binding protein CR, regularly co-expressed with VIP. CR+ interneurons have been reported to be accommodating or irregular spiking cells[67] while VIP expression is present in irregular- and regular-spiking bipolar or small basket cells[77,162]. CR+VIP co-expression is associated with bipolar, bitufted, or double-bouquet morphologies[163]. This is consistent with the staining pattern of CR+ interneurons observed in the PrS while the quality of VIP immunostaining did not allow evaluation of morphology. The bipolar morphology of CR+ interneurons is assumed to be accompanied by a vertical, translaminar axonal arborization[164].

Interestingly, it has been shown for neocortical as well as hippocampal VIP+ and CR+/VIP+ cells that they preferentially target other GABAergic cells, many of them containing either CR or SOM [63,77,88,139,161,165]. This connectivity is particularly present in superficial layers probably because of the high concentration of CR neurons in superficial layers[77]. Conversely, bipolar CR+/VIP+ interneurons also seem often to be inhibited by SOM+ interneurons[139]. In the PrS, these interneurons may therefore be recruited to limit the presumed feedback inhibitory circuit of Martinotti cells. Within the population of presubicular CR+ interneurons, those located in layer I did not display the typical bipolar morphology seen in the other layers. Their multipolar

appearance is assumed to be accompanied by horizontal transcolumnar ramification[164]. It is thus possible, that the small subpopulation of CR+ interneurons in presubicular layer I targets other, so far molecularly unidentified interneurons of this layer, which may in turn target dendrites of pyramidal cells. In mouse visual cortex, CR+ interneurons of layer I receive feedback inhibition from cortical afferents[65]. Further studies should reveal if presubicular CR+ cells of layer I are also activated by specific long-range inputs from cortical or subcortical sources instead of only integrating only excitatory and inhibitory inputs from local origin.

Summing up, the present study revealed a unique distribution pattern of interneurons and their molecular subtypes in presubicular cortex. Aspects that clearly distinguish presubicular cortex from its neighboring cortices are the distribution of non-GABAergic CB+ neurons and the delimitating CR-staining. The PrS resembles neocortical areas with regard for instance to portion and laminar distribution of the PV+ subpopulation or some co-expression patterns such as the colocalization of VIP+/CR+ and SOM+/CB+. Lying at the junction between hippocampus and neocortex[12,15], the PrS also shows hippocampal elements within its inhibitory microcircuit, like the number of interneurons within the general neuronal population, the low number of SOM-expressing interneurons or the SOM+/PV+ interneuron subpopulation. The PrS seems therefore to comprise a heterogeneous and atypical interneuron population, which could have emerged due to the transitional location of this cortical region.

4.1.8 Prospects

Findings of this study provide a basis for further classification and understanding of presubicular interneurons. As some presubicular interneurons remain unidentified, particularly in layer I, the molecular characterization has to be completed“Layer I interneurons may be immunoreactive to Actinin 2, a presumed marker of neurogliaform cells that labels 60% of layer I interneurons in rat frontal cortex[166]. In order to establish connectivity motifs of interneuron subpopulations in the PrS, future investigations may require pair recordings of interneurons and principal cells. In addition, optogenetics could reveal if presubicular afferences specifically target distinct interneuron populations. Desdemona Fricker’s group currently pursues *in vitro* recordings of genetically targeted molecular subpopulations of interneurons after injection of viral vectors into afferent regions of the PrS. Preliminary results, obtained with optogenetic stimulation of afferences, suggest for example that PV+ interneurons but not SOM+ interneurons of superficial layers are directly recruited by thalamic input. Direct recruitment of PV+ cells may indicate a feedforward inhibitory circuit, while SOM+ interneurons may exert feedback inhibition[63,64]. Finally, it will be

important to explore whether the identified interneuron subtypes affect differently the tuning properties of HD-cells. The functional implication of different interneuron subpopulations in processing the head direction signal could be addressed in vivo, using specific inactivation with halorhodopsin[167] or optical activation of optogenetically identified interneuron populations.

4.2 Projection- specific neuronal subpopulations in the presubiculum

In the second part of my work I identified two projection specific neuronal subpopulations by studying the relationship between the target of presubicular principal cells and their firing properties.

I used *in vivo* injections of retrogradely transported fluorescent beads into the lateral mammillary nucleus (LMN) and the anterodorsal nucleus (ADN). While LMN projecting neurons were exclusively seen in presubicular layer IV, principal cells targeting ADN were restricted to deep layers V/VI. For both LMN and ADN projecting neurons, labeling could be found in dorsal and ventral parts of the PrS. This complemented previous findings of Yoder et al. (2011), who described this specific laminar distribution only in dorsal portion of the PrS (referred to as postsubiculum in their study), and suggests that directional information is processed by dorsal and ventral parts of the PrS. Recordings of LMN projecting neurons indicate a relatively homogenous neuronal population displaying either single spike or intrinsic bursting behavior. Recordings of ADN projecting neurons revealed regular spiking neurons with heterogeneous intrinsic properties. Morphologically, both populations extended their dendrites up to superficial layers. In the following chapter I will evaluate the chosen methods, discuss functional relevance of the results and propose future experimental approaches.

4.2.1 Evaluation of chosen methods

Accuracy of injection site

An accurate injection site is critical for the validity of tracing results. LMN is a quite small region and located deep in the brain, which requires an injection needle with small diameter and a bevelled edge. Blunt injection needles caused higher compression induced tissue damage compared to sharp cut needles. Due to small size of LMN, tracer diffusion to the nearby medial mammillary nucleus (MMN) could not be avoided. This diffusion was tolerated, as MMN is not a target of presubicular efferences. Indeed, both MMN and LMN receive projections from subiculum[23,168], which explains why this neighboring region also contained labeled cell bodies

after injection. Injection into ADN was complicated by its position at the border of the lateral cerebral ventricle. Besides ADN, other adjacent thalamic nuclei, AVN and LDN also receive dense projections from the PrS[45]. Although a large majority of tracer material was confined to ADN, some tracer uptake by nearby nuclei could not be entirely excluded. This may have contributed to the heterogeneity of labeled cells projecting to the thalamus.

Retrograde tracing with Retrobeads

The purpose of the present study was to chart connections between the PrS and its efferent projections and to identify the electrophysiological and morphological properties of projecting neurons. Such an experimental protocol requires a non-cytotoxic retrogradely migrating tracer. Furthermore, the injected tracer had to produce sharply defined injection sites, given the size and location of targeted nuclei. Retrobeads exhibit this set of attributes[102]. Labeling with Retrobeads is typically confined to the cytoplasm and accumulates in the soma. It has a granular fluorescence, most likely due to a vesicular transport. This makes morphological aspects difficult to evaluate. During whole-cell recordings, neurons were therefore filled with biocytin which allowed a post-hoc morphological visualization. It should be noted that tracing results could have been biased by retrograde labeling from regions that are crossed by the injection needle and that may be "contaminated" by backflow of the beads. This was of minor concern regarding ADN projecting neurons, as in this case the needle track does not cross other efferent targets of the PrS. In contrast, it may have been relevant for stereotactical injections into LMN, where retrosplenial cortex, a major efferent target of the PrS[16], had to be traversed. Although we can't rule out that some labeled presubicular cells may be actually projecting to RSP instead of LMN, typical localization in layer IV of labeled cells, their homogenous intrinsic properties and the fact that RSP projecting neurons originate exclusively in layer V[16] emphasizes the reliability of our results.

4.2.2 Functional role of presubicular projections to subcortical nuclei

The HD circuit is an ascending pathway, which conveys information about head direction. It also comprises a descending pathway which feeds back visual information to the HD generator[153]. Indeed, visual landmark information already gains control over the HD signal in its early stages through the PrS → LMN pathway which originates in layer IV of the PrS[2,153].

In the present study, we revealed that LMN projecting neurons of layer IV constitute a homogenous cell population with resemblance to IB neurons previously described by Simonnet et al. (2013) in the rat PrS. Functionally, intrinsic properties of LMN projecting neurons correspond

well with their assumed function of operating visual control. The visual update was shown to be effective within very short latency (80ms) in thalamus[169], suggesting an extremely rapid integration within the pathway. Fast integrative properties and the intrinsic burst firing behavior of LMN projecting neurons are hypothesized to favor such fast transfer of information. Another characteristic of subcortical head direction cells is their anticipation of future head direction[38,44]. To avoid disruption of the anticipatory time interval, visual update was suggested to be delivered at low frequencies (<1 Hz)[170]. Intrinsically bursting neurons of layer IV may provide the necessary sparse coding as they do not sustain high frequency firing[12].

Another downstream projection of the PrS targets ADN, an important relay station within the head direction circuit, given complete disruption of the HD-signal after ADN lesion[38]. This projection originates in deep layers of the PrS and some authors postulated that the ADN → PrS → ADN excitatory loop may correspond to the internally organized mechanism which is thought to drive HD cell activity[5]. Our study revealed a rather heterogeneous population of ADN-projecting cells that share regular spiking behavior but differ in several other electrophysiological characteristics. Morphologically, ADN projecting neurons, just as LMN projecting cells, showed dendritic arborization extending up to superficial layers. We thus suggest that deep layer cells projecting to ADN may be directly targeted by visual input and exert visual control as well (Visual cortex → PrS → ADN). In addition to the direct pathway, layer IV principal cells might also recruit ADN projecting neurons in deep layers. In the rat PrS, layer IV IB neurons send axons to deep layers. LMN projecting neurons in layer IV might therefore participate in a second, indirect pathway via recurrent excitation (Visual cortex → PrS: Layer IV → PrS: Deep layers → ADN). The intrinsic properties of layer IV neurons may favor fast information transfer in both pathways, direct and indirect, by rapidly sending efficient excitatory drive in parallel to the LMN and to ADN projecting neurons in deep layers.

4.2.3 Prospects

The integrative properties suggest how neurons may convert input into output. This study provides the first evidence about intrinsic properties of two projection-specific presubicular cell populations. ADN projecting neurons were generally regular spiking but showed diverse intrinsic properties. The integrative properties of this heterogeneous cell population will have to be studied more extensively in the future. To predict how visual control is operated within the PrS, for example via recurrent excitation of layer IV onto ADN projecting neurons, additional knowledge about information flow and information processing is needed. For this purpose, neuronal

populations that are recruited by visual afferences should be identified. Visual projections either directly target LMN and/or ADN projecting neurons but could also activate neither of them directly. Visual information could be processed within presubicular microcircuit first, before being transmitted to LMN projecting neurons. Therefore, other principal cells of the PrS, such as layer III neurons, or interneurons could be recruited by visual afferences.

To elucidate this question, a combination of the retrograde tracing technique and stimulation of visual afferences by using optogenetics seems promising. Retrograde tracer can be injected in LMN and/or ADN and viral constructions expressing channelrhodopsin[171] in visual cortex at the same time. The first will label a projection specific neuronal population, whereas the latter will let us stimulate corresponding afferent fibers in acute brain slices[172]. That way, specific targets of visual cortex in the PrS could be revealed and the hypothesis about the central role of layer IV IB neurons as the relay of visual information from visual cortex to subcortical areas confirmed or refuted. Of course, the same technique could be extended to other afferences of the PrS (thalamus, retrosplenial cortex, etc.) that may target specifically distinct cell populations. Furthermore, possible intralaminar connections between layer IV and deep layer neurons leading to recurrent excitation should be examined, for example by stimulating LMN projecting neurons while simultaneously recording ADN projecting neurons. For this purpose, a retrograde tracer of differing fluorescence (red and green are available) would have to be injected in LMN and ADN of the same animal, allowing the identification of both populations in acute brain slices. Double recordings would show if both populations are linked and if so, to what extent. Information processing at the microcircuit level includes excitatory and inhibitory activity. If we assume that LMN projecting neurons in layer IV are contacted by visual afferences, it is most likely that this excitatory loop is patterned by inhibitory activity.

In the first part of my work I described high density of PV+ interneurons in layer IV contacting the perisomatic region of principal cells. In layers II/III of visual cortex, PV+ interneurons have been shown to be the main target of long range visual input[65]. In the PrS, a similar feed-forward inhibitory pathway may operate visual information processing and limit output of LMN-projecting neurons. After injection of an optogenetic tracer in visual cortex, visual afferences could be selectively activated. In vitro paired recordings of retrogradely labeled LMN projecting neurons and genetically targeted PV+ interneurons could then reveal a feedback inhibition pathway.

REFERENCES

1. Brodman, K. *Vergleichende Lokalisationslehre der Großhirnrinde : in ihren Prinzipien dargestellt auf Grund des Zellenbaues*. (Barth, 1909).
2. Yoder, R. M. & Taube, J. S. Projections to the anterodorsal thalamus and lateral mammillary nuclei arise from different cell populations within the postsubiculum: implications for the control of head direction cells. *Hippocampus* **21,** 1062–73 (2011).
3. Taube, J. S., Muller, R. U. & Ranck, J. B. Head-direction cells recorded from the postsubiculum in freely moving rats. I. Description and quantitative analysis. *J. Neurosci.* **10,** 420–35 (1990).
4. Ding, S.-L. Comparative anatomy of the prosubiculum, subiculum, presubiculum, postsubiculum, and parasubiculum in human, monkey, and rodent. *J. Comp. Neurol.* **521,** 4145–62 (2013).
5. Peyrache, A., Lacroix, M. M., Petersen, P. C. & Buzsáki, G. Internally organized mechanisms of the head direction sense. *Nat. Neurosci.* **18,** 569–575 (2015).
6. Amaral, D. G. & Witter, M. P. The three-dimensional organization of the hippocampal formation: A review of anatomical data. *Neuroscience* **31,** 571–591 (1989).
7. Caballero-Bleda, M. & Witter, M. P. Regional and laminar organization of projections from the presubiculum and parasubiculum to the entorhinal cortex: an anterograde tracing study in the rat. *J. Comp. Neurol.* **328,** 115–29 (1993).
8. Boccara, C. N. *et al.* Grid cells in pre- and parasubiculum. *Nat. Neurosci.* **13,** 987–94 (2010).
9. Slomianka, L. & Geneser, F. A. Distribution of Acetylcholinesterase in the Hippocampal Region of the Mouse : I. Entorhinal Area, Parasubiculum, Retrosplenial Area, and Presubiculum. *J. Comp. Neurol.* **354,** 339–354 (1991).
10. Funahashi, M. & Stewart, M. Presubicular and parasubicular cortical neurons of the rat: functional separation of deep and superficial neurons in vitro. *J. Physiol.* **501,** 387–403 (1997).
11. Honda, Y. & Ishizuka, N. Organization of connectivity of the rat presubiculum: I. Efferent projections to the medial entorhinal cortex. *J. Comp. Neurol.* **473,** 463–84 (2004).
12. Simonnet, J., Eugène, E., Cohen, I., Miles, R. & Fricker, D. Cellular neuroanatomy of rat presubiculum. *Eur. J. Neurosci.* **37,** 583–97 (2013).
13. Boccara, C. N. *et al.* A Three-Plane Architectonic Atlas of the Rat Hippocampal Region. *Hippocampus* **20,** 1–20 (2015).
14. van Strien, N. M., Cappaert, N. L. M. & Witter, M. P. The anatomy of memory: an interactive overview of the parahippocampal-hippocampal network. *Nat. Rev. Neurosci.* **10,** 272–82 (2009).
15. O'Mara, S. M., Commins, S., Anderson, M. & Gigg, J. The subiculum: a review of form, physiology and function. *Prog. Neurobiol.* **64,** 129–155 (2001).
16. van Groen, T. & Wyss, J. M. The connections of presubiculum and parasubiculum in the rat. *Brain Res.* **518,** 227–43 (1990).
17. Jones, B. F. & Witter, M. P. Cingulate cortex projections to the parahippocampal region and hippocampal formation in the rat. *Hippocampus* **17,** 957–76 (2007).
18. Honda, Y., Umitsu, Y. & Ishizuka, N. Organization of Connectivity of the Rat

Presubiculum : II . Associational and Commissural Connections. *J. Comp. Neurol.* **658,** 640–658 (2008).

19. Kim, Y. & Spruston, N. Target-specific output patterns are predicted by the distribution of regular-spiking and bursting pyramidal neurons in the subiculum. *Hippocampus* **22,** 693–706 (2012).
20. Vogt, B. A. & Miller, M. W. Cortical connections between rat cingulate cortex and visual, motor, and postsubicular cortices. *J. Comp. Neurol.* **216,** 192–210 (1983).
21. Canto, C. B., Koganezawa, N., Beed, P., Moser, E. I. & Witter, M. P. All layers of medial entorhinal cortex receive presubicular and parasubicular inputs. *J. Neurosci.* **32,** 17620–31 (2012).
22. Yoder, R. M. *et al.* Both visual and idiothetic cues contribute to head direction cell stability during navigation along complex routes. *J. Neurophysiol.* **105,** 2989–3001 (2011).
23. Ishizuka, N. Laminar organization of the pyramidal cell layer of the subiculum in the rat. *J. Comp. Neurol.* **435,** 89–110 (2001).
24. Taube, J. S., Muller, R. U. & Ranck, J. B. Head-direction cells recorded from the postsubiculum in freely moving rats. II. Effects of environmental manipulations. *J. Neurosci.* **10,** 436–47 (1990).
25. Taube, J. S. The head direction signal: origins and sensory-motor integration. *Annu. Rev. Neurosci.* **30,** 181–207 (2007).
26. Yoder, R. M., Clark, B. J. & Taube, J. S. Origins of landmark encoding in the brain. *Trends Neurosci.* **34,** 561–71 (2011).
27. Bartesaghi, R., Maio, V. D. I. & Gessi, T. Topographic Activation of the Medial Entorhinal Cortex by Presubicular Commissural Projections. *J. Comp. Neurol.* **299,** 283–299 (2005).
28. Tolner, E. A. *et al.* Presubiculum Stimulation In Vivo Evokes Distinct Oscillations in Superficial and Deep Entorhinal Cortex Layers in Chronic Epileptic Rats. *J. Neurosci.* **25,** 8755–8765 (2005).
29. Eid, T., Jorritsma-Byham, B., Schwarcz, R. & Witter, M. P. Afferents to the seizure-sensitive neurons in layer III of the medial entorhinal area: a tracing study in the rat. *Exp. Brain Res.* **109,** 209–218 (1996).
30. Du, F. *et al.* Preferential neuronal loss in layer III of the entorhinal cortex in patients with temporal lobe epilepsy. *Epilepsy Res.* **16,** 223–233 (1993).
31. O'Keefe. The hippocampus as a spatial map . Preliminary evidence from unit activity in the freely-moving rat. *Brain Res.* **34,** 171–175 (1971).
32. Muir, G. M. *et al.* Disruption of the head direction cell signal after occlusion of the semicircular canals in the freely moving chinchilla. *J. Neurosci.* **29,** 14521–33 (2009).
33. Goodridge, J. P., Dudchenko, P. A., Worboys, K. A., Golob, E. J. & Taube, J. S. Cue Control and Head Direction Cells. *Behav. Neurosci.* **112,** 749–761 (1998).
34. Hafting, T., Fyhn, M., Molden, S., Moser, M.-B. & Moser, E. I. Microstructure of a spatial map in the entorhinal cortex. *Nature* **436,** 801–806 (2005).
35. Solstad, T., Boccara, C. N., Kropff, E., Moser, M.-B. & Moser, E. I. Representation of Geometric Borders in the Entorhinal Cortex. *Science (80-.).* **322,** 1865–1868 (2008).
36. Sargolini, F. *et al.* Conjunctive Representation of Position, Direction and Velocity in Entorhinal Cortex. *Science (80-.).* **312,** 4015–4028 (2006).

37. Lever, C., Burton, S., Jeewajee, A., O'Keefe, J. & Burgess, N. Boundary vector cells in the subiculum of the hippocampal formation. *J. Neurosci.* **29,** 9771–9777 (2009).

38. Goodridge, J. P. & Taube, J. S. Interaction between the postsubiculum and anterior thalamus in the generation of head direction cell activity. *J. Neurosci.* **17,** 9315–30 (1997).

39. Blair, H. T. & Sharp, P. E. Anticipatory head direction signals in anterior thalamus: evidence for a thalamocortical circuit that integrates angular head motion to compute head direction. *J. Neurosci.* **15,** 6260–70 (1995).

40. Fricker, D., Dinocourt, C., Eugène, E., Wood, J. N. & Miles, R. Pyramidal cells of rodent presubiculum express a tetrodotoxin-insensitive Na+ current. *J. Physiol.* **587,** 4249–4264 (2009).

41. Sharp, P. E., Blair, H. T. & Cho, J. The anatomical and computational basis of the rat head-direction cell signal. *Trends Neurosci.* **24,** 289–294 (2001).

42. Taube, J. S. Head Direction Cells Recorded in the Anterior Thalamic Nuclei of Freely Moving Rats. *J. Neurosci.* **15,** 70–86 (1995).

43. Mizumori, S. J. Y. & Williams, J. D. Directionally Selective Mnemonic Properties of Neurons in the Lateral Dorsal Nucleus of the Thalamus of Rats. *J. Neurosci.* **13,** 4015–4028 (1993).

44. Stackman, R. W. & Taube, J. S. Firing properties of rat lateral mammillary single units: head direction, head pitch, and angular head velocity. *J. Neurosci.* **18,** 9020–37 (1998).

45. Clark, B. J. & Taube, J. S. Vestibular and attractor network basis of the head direction cell signal in subcortical circuits. *Front. Neural Circuits* **6,** 1–12 (2012).

46. Bassett, J. P., Tullman, M. L. & Taube, J. S. Lesions of the tegmentomammillary circuit in the head direction system disrupt the head direction signal in the anterior thalamus. *J. Neurosci.* **27,** 7564–77 (2007).

47. Winter, S. S., Clark, B. J. & Taube, J. S. Disruption of the head direction cell network impairs the parahippocampal grid cell signal. *Science (80-.).* 1–8 (2015).

48. Clark, B. J. & Taube, J. S. Intact landmark control and angular path integration by head direction cells in the anterodorsal thalamus after lesions of the medial entorhinal cortex. *Hippocampus* **21,** 767–782 (2011).

49. van Groen, T. & Wyss, J. M. The postsubicular cortex in the rat: characterization of the fourth region of the subicular cortex and its connections. *Brain Res.* **529,** 165–77 (1990).

50. van Groen, T. & Wyss, J. M. Projections from the laterodorsal nucleus of the thalamus to the limbic and visual cortices in the rat. *J. Comp. Neurol.* **324,** 427–48 (1992).

51. Knierim, J. J. & Zhang, K. Attractor Dynamics of Spatially Correlated Neural Activity in the Limbic System. *Annu. Rev. Neurosci.* **35,** 267–285 (2012).

52. Zhang, K. Representation of spatial orientation by the intrinsic dynamics of the head-direction cell ensemble: a theory. *J. Neurosci.* **16,** 2112–2126 (1996).

53. Altwegg-Boussac, T., Chavez, M., Mahon, S. & Charpier, S. Excitability and responsiveness of rat barrel cortex neurons in the presence and absence of spontaneous synaptic activity in vivo. *J. Physiol.* **592,** 3577–3595 (2014).

54. Ding, S.-L. Comparative Anatomy of the Prosubiculum, Subiculum, Presubiculum, Postsubiculum and Parasubiculum in Human, Monkey and Rodent. *J. Comp. Neurol.* (2013). doi:10.1002/cne.

55. Jarsky, T., Mady, R., Kennedy, B. & Spruston, N. Distribution of Bursting Neurons in the

CA1 Region and the Subiculum of the Rat Hippocampus. *J. Comp. Neurol.* **547,** 535–547 (2008).

56. Mountcastle, V. The columnar organization of the neocortex. *Brain* **120,** 701–722 (1997).
57. Abbasi, S. & Kumar, S. S. Electrophysiological and morphological characterization of cells in superficial layers of rat presubiculum. *J. Comp. Neurol.* **521,** 3116–32 (2013).
58. Contreras, D. Electrophysiological classes of neocortical neurons. *Neural Networks* **17,** 633–646 (2004).
59. Spruston, N. Pyramidal neurons: dendritic structure and synaptic integration. *Nat. Rev. Neurosci.* **9,** 206–221 (2008).
60. Connors, B. W. & Gutnick, M. J. Intrinsic firing patterns of diverse neocortical neurons. *Trends Neurosci.* **13,** 99–104 (1990).
61. Agmon, A. & Connors, B. W. Correlation between Intrinsic Firing Patterns and Thalamocortical Synaptic Responses of Neurons in Mouse Barrel Cortex. *J. Neurosci.* **12,** 319–329 (1992).
62. Chagnac-Amitai, Y. & Connors, B. W. Synchronized excitation and inhibition driven by intrinsically bursting neurons in neocortex. *J Neurophysiol* **62,** 1149–1162 (1989).
63. Lee, S., Kruglikov, I., Huang, Z. J., Fishell, G. & Rudy, B. A disinhibitory circuit mediates motor integration in the somatosensory cortex. *Nat. Neurosci.* **16,** 1662–70 (2013).
64. Cruikshank, S. J., Urabe, H., Nurmikko, A. V. & Connors, B. W. Pathway-Specific Feedforward Circuits between Thalamus and Neocortex Revealed by Selective Optical Stimulation of Axons. *Neuron* **65,** 230–245 (2010).
65. Gonchar, Y. & Burkhalter, A. Distinct GABAergic targets of feedforward and feedback connections between lower and higher areas of rat visual cortex. *J. Neurosci.* **23,** 10904–10912 (2003).
66. Isaacson, J. S. & Scanziani, M. How inhibition shapes cortical activity. *Neuron* **72,** 231–43 (2011).
67. Markram, H. *et al.* Interneurons of the neocortical inhibitory system. *Nat. Rev. Neurosci.* **5,** 793–807 (2004).
68. Ascoli, G. a *et al.* Petilla terminology: nomenclature of features of GABAergic interneurons of the cerebral cortex. *Nat. Rev. Neurosci.* **9,** 557–68 (2008).
69. Ramon y Cajal, S. *Textura del sistema nervioso del hombre y de los vertebrados.* (Oxford Univ Press., 1899).
70. Freund, T. F., Ylinen, A., Pitkanen, A. & Riekkinens, P. J. Pattern of Neuronal Death in the Rat Hippocampus After Status Epilepticus . Relationship to Calcium Binding Protein Content and Ischemic Vulnerability. *Brain Res.* **28,** 27–38 (1991).
71. Cossart, R. *et al.* Dendritic but not somatic GABAergic inhibition is decreased in experimental epilepsy. *Nature* **4,** 52–62 (2001).
72. Sloviter, R. S. *et al.* 'Dormant basket cell' hypothesis revisited: relative vulnerabilities of dentate gyrus mossy cells and inhibitory interneurons after hippocampal status epilepticus in the rat. *J. Comp. Neurol.* **459,** 44–76 (2003).
73. Burkhalter, A. Many specialists for suppressing cortical excitation. *Front. Neurosci.* **2,** 155–67 (2008).
74. Karube, F., Kubota, Y. & Kawaguchi, Y. Axon Branching and Synaptic Bouton Phenotypes

in GABAergic Nonpyramidal Cell Subtypes. *J. Neurosci.* **24,** 2853–2865 (2004).

75. Somogyi, P. A specific axo-axonal interneuron in the visual cortex of the rat. *Brain Res.* **136,** 345–350 (1977).
76. Kawaguchi, Y., Wilson, C. J., Augood, S. J. & Emson, P. C. Striatal interneurones : chemical, physiological and morphological characterization. *Trends Neurosci.* **3,** 527–535 (1995).
77. Pfeffer, C. K., Xue, M., He, M., Huang, Z. J. & Scanziani, M. Inhibition of inhibition in visual cortex: the logic of connections between molecularly distinct interneurons. *Nat. Neurosci.* **16,** 1068–76 (2013).
78. Naegele, J. R. & Barnstable, C. J. Molecular determinants of GABAergic local-circuit neurons in the visual cortex. *Trends Neurosci.* **12,** 28–34 (1989).
79. Schwaller, B. Cytosolic Ca2+ Buffers. *Cold Spring Harb. Perspect. Biol.* **2,** 1–20 (2010).
80. Vreugdenhil, M. *et al.* Parvalbumin-Deficiency Facilitates Repetitive IPSCs and Gamma Oscillations in the Hippocampus. *J Neurophysiol* **89,** 1414–1422 (2003).
81. Freund, T. F. & Buzsáki, G. Interneurons of the Hippocampus. *Hippocampus* **470,** 347–470 (1996).
82. Baraban, S. C. & Tallent, M. K. Interneuron Diversity series: Interneuronal neuropeptides-endogenous regulators of neuronal excitability. *Trends Neurosci.* **27,** 135–42 (2004).
83. Cauli, B. *et al.* Cortical GABA interneurons in neurovascular coupling: relays for subcortical vasoactive pathways. *J. Neurosci.* **24,** 8940–9 (2004).
84. Wang, Y., Gupta, A., Toledo-Rodriguez, M., Wu, C. Z. & Markram, H. Anatomical, physiological, molecular and circuit properties of nest basket cells in the developing somatosensory cortex. *Cereb. Cortex* **12,** 395–410 (2002).
85. Gonchar, Y., Wang, Q. & Burkhalter, A. Multiple distinct subtypes of GABAergic neurons in mouse visual cortex identified by triple immunostaining. *Front. Neuroanat.* **1,** 1–11 (2007).
86. Gonchar, Y. & Burkhalter, A. Three Distinct Families of GABAergic Neurons in Rat Visual Cortex. *Cereb. cortex* **7,** 347–58 (1997).
87. Xu, X., Roby, K. D. & Callaway, E. M. Immunochemical Characterization of Inhibitory Mouse Cortical Neurons: Three Chemically Distinct Classes of Inhibitory Cells. *J. Comp. Neurol.* **518,** 389–404 (2010).
88. Kepecs, A. & Fishell, G. Interneuron cell types are fit to function. *Nature* **505,** 318–26 (2014).
89. Defelipe, J. *et al.* New insights into the classification and nomenclature of cortical GABAergic interneurons. *Nat. Rev. Neurosci.* **14,** 202–216 (2014).
90. Butt, S. J. B. *et al.* The temporal and spatial origins of cortical interneurons predict their physiological subtype. *Neuron* **48,** 591–604 (2005).
91. Miyoshi, G. *et al.* Genetic fate mapping reveals that the caudal ganglionic eminence produces a large and diverse population of superficial cortical interneurons. *J. Neurosci.* **30,** 1582–94 (2010).
92. Hu, H., Gan, J. & Jonas, P. Fast-spiking, parvalbumin GABAergic interneurons: From cellular design to microcircuit function. *Science (80-.).* **345,** 529–542 (2014).
93. Wang, Y. *et al.* Anatomical, physiological and molecular properties of Martinotti cells in

the somatosensory cortex of the juvenile rat. *J. Physiol.* **561,** 65–90 (2004).

94. Gentet, L. J. Functional diversity of supragranular GABAergic neurons in the barrel cortex. *Front. Neural Circuits* **6,** 52 (2012).

95. Battaglia, D., Karagiannis, A., Gallopin, T., Gutch, H. W. & Cauli, B. Beyond the frontiers of neuronal types. *Front. Neural Circuits* **7,** 13 (2013).

96. Tamamaki, N. *et al.* Green Fluorescent Protein Expression and Colocalization with Calretinin, Parvalbumin, and Somatostatin in the GAD67-GFP Knock-In Mouse. *J. Comp. Neurol.* **467,** 60–79 (2003).

97. Kubota, Y., Hattori, R. & Yui, Y. Three distinct subpopulations of GABAergic neurons in rat frontal agranular cortex. *Brain Res.* **649,** 159–173 (1994).

98. Kawaguchi, Y. & Kubota, Y. Physiological and morphological identification of somatostatin- or vasoactive intestinal polypeptide-containing cells among GABAergic cell subtypes in rat frontal cortex. *J. Neurosci.* **16,** 2701–15 (1996).

99. Oliva Jr, A. A., Jiang, M., Lam, T., Smith, K. L. & Swann, J. W. Novel Hippocampal Interneuronal Subtypes Identified Using Transgenic Mice That Express Green Fluorescent Protein in GABAergic Interneurons. *J. Neurosci.* **20,** 3354–3368 (2000).

100. Coggeshall, R. E. A consideration of neural counting methods. *Trends Neurosci.* **15,** 9–13 (1992).

101. Geuna, S. The revolution of counting 'tops': two decades of the disector principle in morphological research. *Microsc. Res. Tech.* **66,** 270–4 (2005).

102. Katz, L. C., Burkhalter, A. & Dreyer, W. J. Fluorescent latex microspheres as a retrograde neuronal marker for in vivo and in vitro studies of visual cortex. *Nature* **310,** 498–500 (1984).

103. Paxinos, G. & Franklin, K. *Paxinos and Franklin's the Mouse Brain in Stereotaxic Coordinates*. (Academic Press, 2012).

104. Cetin, A., Komai, S., Eliava, M., Seeburg, P. H. & Osten, P. Stereotaxic gene delivery in the rodent brain. *Nat. Protoc.* **1,** 3166–73 (2006).

105. Golowasch, J. *et al.* Membrane capacitance measurements revisited: dependence of capacitance value on measurement method in nonisopotential neurons. *J. Neurophysiol.* **102,** 2161–2175 (2009).

106. Liu, Y., Fujise, N. & Kosaka, T. Distribution of calretinin immunoreactivity in the mouse dentate gyrus. I. General description. *Exp. Brain Res.* **108,** 389–403 (1996).

107. Rudy, B., Fishell, G., Lee, S. & Hjerling-Leffler, J. Three groups of interneurons account for nearly 100% of neocortical GABAergic neurons. *Dev. Neurobiol.* **71,** 45–61 (2011).

108. Shibata, H. Descending projections to the mammillary nuclei in the rat, as studied by retrograde and anterograde transport of wheat germ agglutinin-horseradish peroxidase. *J. Comp. Neurol.* **285,** 436–52 (1989).

109. McBain, C. J. & Fisahn, A. Interneurons unbound. *Nat. Rev. Neurosci.* **2,** 11–23 (2001).

110. Chrobak, J. & Buzsáki, G. High-Frequency Oscillations in the Output Networks of the Hippocampal-Entorhinal Axis of the Freely Behaving Rat. *J. Neurosci.* **76,** 3056–3066 (1996).

111. Katzner, S., Busse, L. & Carandini, M. GABA A Inhibition Controls Response Gain in Visual Cortex. *J. Neurosci.* **31,** 5931–5941 (2011).

112. Fujise, N., Hunziker, W., Heizmann, C. W. & Kosaka, T. Distribution of the calcium binding proteins, calbindin D-28K and parvalbumin, in the subicular complex of the adult mouse. *Neurosci. Res.* **22,** 89–107 (1995).

113. Bakst, I. & Amaral, D. G. The distribution of acetylcholinesterase in the hippocampal formation of the monkey. *J. Comp. Neurol.* **225,** 344–371 (1984).

114. Seress, L. *et al.* Distribution, Morphological Features, and Synaptic Connections of Parvalbumin- and Calbindin D28k-Immunoreactive Neurons in the Human Hippocampal Formation. *J. Comp. Neurol.* **337,** 208–230 (1993).

115. Nassar, M. *et al.* Diversity and overlap of parvalbumin and somatostatin expressing interneurons in mouse presubiculum. *Front. Neural Circuits* **9,** 1–19 (2015).

116. Azevedo, F. A. C. *et al.* Automatic isotropic fractionation for large-scale quantitative cell analysis of nervous tissue. *J. Neurosci. Methods* **212,** 72–78 (2013).

117. Herculano-Houzel, S., von Bartheld, C. S., Miller, D. J. & Kaas, J. H. How to count cells: the advantages and disadvantages of the isotropic fractionator compared with stereology. *Cell Tissue Res.* 29–42 (2015). doi:10.1007/s00441-015-2127-6

118. Von Bartheld, C. S. Counting particles in tissue sections: Choices of methods and importance of calibration to minimize biases. *Histol. Histopathol.* **17,** 639–648 (2002).

119. Abercrombie, M. Estimation of nuclear population from microtome sections. *Anat. Rec.* **94,** 239–247 (1946).

120. West, M. J., Slomianka, L. & Gundersen, H. J. G. Unbiased Stereological Estimation of the Total Number of Neurons in the Subdivisions of the Rat Hippocampus Using the Optical Fractionator. *Anat. Rec.* **231,** 482–497 (1991).

121. West, M. J. & Gundersen, H. J. Unbiased stereological estimation of the number of neurons in the human hippocampus. *J. Comp. Neurol.* **296,** 1–22 (1990).

122. Geuna, S. Appreciating the difference between design-based and model-based sampling strategies in quantitative morphology of the nervous system. *J. Comp. Neurol.* **427,** 333–9 (2000).

123. Schmitz, C. *et al.* Current automated 3D cell detection methods are not a suitable replacement for manual stereologic cell counting. *Front. Neuroanat.* **8,** 27 (2014).

124. Meyer, H. S. *et al.* Number and Laminar Distribution of Neurons in a Thalamocortical Projection Column of Rat Vibrissal Cortex. 2277–2286 (2010). doi:10.1093/cercor/bhq067

125. Meyer, H. S. *et al.* Inhibitory interneurons in a cortical column form hot zones of inhibition in layers 2 and 5A. **108,** 16807–16812 (2011).

126. Markram, H. *et al.* Reconstruction and Simulation of Neocortical Microcircuitry. *Cell* **163,** 456–492 (2015).

127. Herculano-Houzel, S., Watson, C. & Paxinos, G. Distribution of neurons in functional areas of the mouse cerebral cortex reveals quantitatively different cortical zones. *Front. Neuroanat.* **7,** 35 (2013).

128. Herculano-Houzel, S., Mota, B. & Lent, R. How to build a bigger brain: Cellular scaling rules for rodent brains. *Evol. Nerv. Syst.* **3,** 155–166 (2010).

129. Buzsáki, G. *et al.* Hippocampal network patterns of activity in the mouse. *Neuroscience* **116,** 201–211 (2003).

130. Mulders, W. H. A. M., West, M. J. & Slomianka, L. Neuron numbers in the presubiculum, parasubiculum, and entorhinal area of the rat. *J. Comp. Neurol.* **385,** 83–94 (1997).

131. Ren, J. Q., Aika, Y., Heizmann, C. W. & Kosaka, T. Quantitative analysis of neurons and glial cells in the rat somatosensory cortex, with special reference to GABAergic neurons and parvalbumin-containing neurons. *Exp. Brain Res.* **92,** 1–14 (1992).

132. Meyer, H. S. *et al.* Cellular organization of cortical barrel columns is whisker-specific. *Proc. Natl. Acad. Sci. U. S. A.* **110,** 19113–8 (2013).

133. Wouterlood, F. G. & Pothuizen, H. Sparse colocalization of somatostatin- and GABA-immunoreactivity in the entorhinal cortex of the rat. *Hippocampus* **10,** 77–86 (2000).

134. Jinno, S. & Kosaka, T. Colocalization of parvalbumin and somatostatin-like immunoreactivity in the mouse hippocampus: quantitative analysis with optical dissector. *J. Comp. Neurol.* **428,** 377–88 (2000).

135. Silberberg, G., Gupta, A. & Markram, H. Stereotypy in neocortical microcircuits. *Trends Neurosci.* **25,** 227–230 (2002).

136. Kosaka, T. *et al.* GABAergic Neurons Containing CCK-8-Like and/or VIP-Like Immunoreactivities in the Rat Hippocampus and Dentate Gyrus. *J. Comp. Neurol.* **239,** 420–430 (1985).

137. Jinno, S. & Kosaka, T. Parvalbumin Is Expressed in Glutamatergic and GABAergic Corticostriatal Pathway in Mice. *J. Comp. Neurol.* **201,** 188–201 (2004).

138. Wouterlood, F. G., van Denderen, J. C., van Haeften, T. & Witter, M. P. Calretinin in the entorhinal cortex of the rat: distribution, morphology, ultrastructure of neurons, and co-localization with gamma-aminobutyric acid and parvalbumin. *J. Comp. Neurol.* **425,** 177–192 (2000).

139. Cauli, B. & Staiger, J. F. Revisiting enigmatic cortical calretinin-expressing interneurons. *Front. Neuroanat.* **8,** 1–18 (2014).

140. Hajos, N., Acsady, L. & Freund, T. F. Target Selectivity and Neurochemical Characteristics of VIP-immunoreactive lnterneurons in the Rat Dentate Gyrus. *Eur. J. Neurosci.* **8,** 1415–1431 (1992).

141. Suzuki, N. & Bekkers, J. M. Inhibitory neurons in the anterior piriform cortex of the mouse: classification using molecular markers. *J. Comp. Neurol.* **518,** 1670–87 (2010).

142. Hosp, J. A. *et al.* Morpho-physiological criteria divide dentate gyrus interneurons into classes. *Hippocampus* (2014). doi:10.1002/hipo.22214

143. Kubota, Y. *et al.* Selective Coexpression of Multiple Chemical Markers Defines Discrete Populations of Neocortical GABAergic Neurons. *Cereb. cortex* **21,** 1803–17 (2011).

144. Tunon, T., Insausti, R., Ferrer, I., Sobreviela, T. & Soriano, E. Parvalbumin and calbindin D-28K in the human entorhinal cortex. An immunohistochemical study. *Brain Res.* **12,** 24–39 (1992).

145. Demeulemeester, H., Vandesande, F., Orban, G. A., Brandon, C. & Vanderhaeghen, J. J. Heterogeneity of GABAergic Cells in Cat Visual Cortex. *J. Neurosci.* **8,** 988–1000 (1988).

146. Köhler, C. & Chan-Palay, V. Somatostatin and vasoactive intestinal polypeptide-like immunoreactive cells and terminals in the retrohippocampal region of the rat brain. *Anat. Embryol. (Berl).* **167,** 151–172 (1983).

147. Cauli, B. *et al.* Molecular and Physiological Diversity of Cortical Nonpyramidal Cells. *J. Neurosci.* **17,** 3894–3906 (1997).

148. Wolansky, T., Pagliardini, S., Greer, J. J. & Dickson, C. T. Immunohistochemical Characterization of Substance P Receptor (NK1R)- Expressing Interneurons in the

Entorhinal Cortex. *J. Comp. Neurol.* **441,** 427–441 (2007).

149. Klausberger, T. *et al.* Brain-state- and cell-type-specific firing of hippocampal interneurons in vivo. *Nature* **421,** 844–848 (2003).

150. Katona, L. *et al.* Sleep and movement differentiates actions of two types of somatostatin-expressing GABAergic interneuron in rat hippocampus. *Neuron* **82,** 872–86 (2014).

151. Xu, X., Roby, K. D. & Callaway, E. M. Mouse cortical inhibitory neuron type that coexpresses somatostatin and calretinin. *J. Comp. Neurol.* **499,** 144–60 (2006).

152. Kononenko, N. L. & Witter, M. P. Presubiculum Layer III Conveys Retrosplenial Input to the Medial Entorhinal Cortex. *Hippocampus* **895,** 881–895 (2012).

153. Yoder, R. M., Peck, J. R. & Taube, J. S. Visual Landmark Information Gains Control of the Head Direction Signal at the Lateral Mammillary Nuclei. *J. Neurosci.* **35,** 1354–1367 (2015).

154. Gabernet, L., Jadhav, S. P., Feldman, D. E., Carandini, M. & Scanziani, M. Somatosensory integration controlled by dynamic thalamocortical feed-forward inhibition. *Neuron* **48,** 315–27 (2005).

155. Fricker, D., Verheugen, J. A. H. & Miles, R. Cell-attached measurements of the firing threshold of rat hippocampal neurones. *J. Physiol.* **517,** 791–804 (1999).

156. Freund, F. Interneuron Diversity series : Rhythm and mood in perisomatic inhibition. *Trends Neurosci.* **26,** 489–495 (2003).

157. Klausberger, T. *et al.* Complementary roles of cholecystokinin- and parvalbumin-expressing GABAergic neurons in hippocampal network oscillations. *J. Neurosci.* **25,** 9782–93 (2005).

158. Toledo-Rodriguez, M. *et al.* Correlation maps allow neuronal electrical properties to be predicted from single-cell gene expression profiles in rat neocortex. *Cereb. Cortex* **14,** 1310–27 (2004).

159. Kubota, Y. & Jones, E. G. Co-localization of two calcium binding proteins in GABA cells of rat piriform cortex. *Brain Res.* **600,** 339–44 (1993).

160. Ekstrand, J. J., Domroese, M. E., Feig, S. L., Illig, K. R. & Haberly, L. B. Immunocytochemical Analysis of Basket Cells in Rat Piriform Cortex. *J. Comp. Neurol.* **328,** 308–328 (2001).

161. Staiger, J. F., Masanneck, C., Schleicher, A. & Zuschratter, W. Calbindin-Containing Interneurons Are a Target for VIP-Immunoreactive Synapses in Rat Primary Somatosensory Cortex. *J. Comp. Neurol.* **468,** 179–189 (2004).

162. Kawaguchi, Y. & Kubota, Y. GABAergic cell subtypes and their synaptic connections in rat frontal cortex. *Cereb. Cortex* **7,** 476–86 (1997).

163. Miyoshi, G., Butt, S. J. B., Takebayashi, H. & Fishell, G. Physiologically distinct temporal cohorts of cortical interneurons arise from telencephalic Olig2-expressing precursors. *J. Neurosci.* **27,** 7786–98 (2007).

164. Caputi, A., Rozov, A., Blatow, M. & Monyer, H. Two calretinin-positive gabaergic cell types in layer 2/3 of the mouse neocortex provide different forms of inhibition. *Cereb. Cortex* **19,** 1345–1359 (2009).

165. Klausberger, T. & Somogyi, P. Neuronal diversity and temporal dynamics: the unity of hippocampal circuit operations. *Science (80-.).* **321,** 53–57 (2008).

166. Uematsu, M. *et al.* Quantitative chemical composition of cortical GABAergic neurons

revealed in transgenic venus-expressing rats. *Cereb. Cortex* **18,** 315–330 (2008).

167. Zhang, F., Aravanis, A. M., Adamantidis, A., de Lecea, L. & Deisseroth, K. Circuit-breakers: optical technologies for probing neural signals and systems. *Nat. Rev. Neurosci.* **8,** 577–581 (2007).

168. Shibata, H. Descending projections to the mammillary nuclei in the rat, as studied by retrograde and anterograde transport of wheat germ agglutinin-horseradish peroxidase. *J. Comp. Neurol.* **285,** 436–52 (1989).

169. Zugaro, M. B., Arleo, A., Berthoz, A. & Wiener, S. I. Rapid spatial reorientation and head direction cells. *J. Neurosci.* **23,** 3478–3482 (2003).

170. van der Meer, M. A. A., Knierim, J. J., Yoganarasimha, D., Wood, E. R. & van Rossum, M. C. W. Anticipation in the rodent head direction system can be explained by an interaction of head movements and vestibular firing properties. *J. Neurophysiol.* **98,** 1883–1897 (2007).

171. Nagel, G. *et al.* Channelrhodopsin-2, a directly light-gated cation-selective membrane channel. *Proc. Natl. Acad. Sci. U. S. A.* **100,** 13940–13945 (2003).

172. Petreanu, L., Huber, D., Sobczyk, A. & Svoboda, K. Channelrhodopsin-2-assisted circuit mapping of long-range callosal projections. *Nat. Neurosci.* **10,** 663–668 (2007).

EIDESSTATTLICHE VERSICHERUNG

„Ich, Roxanne Lofredi, versichere an Eides statt durch meine eigenhändige Unterschrift, dass ich die vorgelegte Dissertation mit dem Thema: „Characterization of inhibitory and projection specific neurons of the presubiculum“ selbstständig und ohne nicht offengelegte Hilfe Dritter verfasst und keine anderen als die angegebenen Quellen und Hilfsmittel genutzt habe.
Alle Stellen, die wörtlich oder dem Sinne nach auf Publikationen oder Vorträgen anderer Autoren beruhen, sind als solche in korrekter Zitierung (siehe „Uniform Requirements for Manuscripts (URM)“ des ICMJE -*www.**icmje**.org*) kenntlich gemacht. Die Abschnitte zu Methodik (insbesondere praktische Arbeiten, Laborbestimmungen, statistische Aufarbeitung) und Resultaten (insbesondere Abbildungen, Graphiken und Tabellen) entsprechen den URM (s.o) und werden von mir verantwortet.
Meine Anteile an etwaigen Publikationen zu dieser Dissertation entsprechen denen, die in der untenstehenden gemeinsamen Erklärung mit dem/der Betreuer/in, angegeben sind. Sämtliche Publikationen, die aus dieser Dissertation hervorgegangen sind und bei denen ich Autor bin, entsprechen den URM (s.o) und werden von mir verantwortet.

Die Bedeutung dieser eidesstattlichen Versicherung und die strafrechtlichen Folgen einer unwahren eidesstattlichen Versicherung (§156,161 des Strafgesetzbuches) sind mir bekannt und bewusst.“

Datum 05.10.2015 Unterschrift

<u>Anteilserklärung an etwaigen erfolgten Publikationen</u>

Roxanne Lofredi hatte folgenden Anteil an den folgenden Publikationen:

Publikation 1: Nassar, M., Simonnet, J**., Lofredi, R**., Cohen, I., Savary, E., Yanagawa, Y., Miles, R. & Fricker, D. , Diversity and overlap of parvalbumin and somatostatin expressing interneurons in mouse presubiculum. Frontiers of Neural Circuits (2015)

Beitrag im Einzelnen (bitte kurz ausführen):

Roxanne Lofredi führte die immunhistochemischen Experimente mit Anti- NeuN, Anti-SOM und Anti-PV Antikörpern bei der transgenetischen Mauslinie Gad67 GFP durch und quantifizierte die Ergebnisse.
So konnten die in der Publikation veröffentlichten Ergebnisse bezüglich Interneuron- Dichte und Layer spezifischer Verteilung der allgemeinen Interneuron - Population sowie der PV+ und SOM+ Interneurone im Präsubikulum ermittelt werden.

Unterschrift, Datum und Stempel des betreuenden Hochschullehrers/der betreuenden Hochschullehrerin

Unterschrift des Doktoranden/der Doktorandin

PUBLIKATIONSLISTE

Nassar, M., Simonnet, J., **Lofredi, R.,** Cohen, I., Savary, E., Yanagawa, Y., Miles, R. & Fricker, D. **Diversity and overlap of parvalbumin and somatostatin expressing interneurons in mouse presubiculum.** *Frontiers of Neural Circuits (2015)*

Lofredi, R., Simonnet, J., Eugène, E., Miles, R. & Fricker, D. **Functional characterization of projection-specific output neurons of presubiculum.** *Poster-Präsentation anlässlich des 11. Kolloquiums der Französischen Sozietät für Neurowissenschaften, Lyon, Frankreich (2013)*

LEBENSLAUF

Mein Lebenslauf wird aus datenschutzrechtlichen Gründen in der elektronischen Version meiner Arbeit nicht veröffentlicht.

DANKSAGUNG

Ich möchte zunächst den Gutachtern meiner Promotion dafür danken, sich bereit erklärt zu haben, diese Arbeit zu lesen und mit ihrer qualifizierten Meinung zu bewerten.

Mein Dank gilt weiterhin PD Dr. Desdemona Fricker, die diese Arbeit betreut und durch ihre anhaltende Unterstützung ermöglicht hat. Ich möchte Ihr dafür danken, jederzeit für Fragen und Diskussionen verfügbar gewesen zu sein, die Entwicklung dieser Arbeit immer mit Interesse und Engagement verfolgt und durch ihr Wissen bereichert zu haben.

Ich möchte außerordentlich Prof. Imre Vida danken, der als Doktorvater immer zu meiner Disposition stand. Besonders betonen möchte ich hierbei, dass meine Arbeit außerhalb des von Prof. Vida geleiteten Instituts für Integrative Neuroanatomie realisiert wurde und seine Unterstützung daher von großer Selbstlosigkeit und Freundlichkeit gezeugt hat.

Weiter möchte ich Prof. Richard Miles danken, der mich in seiner Arbeitsgruppe aufgenommen und mit seinem freundlichen Wesen und seinen qualifizierten und wertvollen wissenschaftlichen Ratschlägen auch aus Entfernung immer unterstützt hat. Mein Dank gilt weiterhin und ganz besonders Dr. Jean Simonnet, der mir mit großem Engagement einen Großteil der angewandten Techniken beigebracht und mich bei meiner Arbeit täglich unterstützt hat sowie bei jeder Frage zur Stelle war. Vielen Dank für die wertvollen Ideen und Gedanken, die Ratschläge und die fruchtbare Zusammenarbeit, ohne die die Umsetzung dieser Arbeit nicht möglich gewesen wäre.. Natürlich gilt mein Dank ganz besonders Constanze Mauthe, mit der ich meine Arbeit im Labor begonnen habe und mich eine sehr enge Freundschaft verbindet. Danke, dass wir all die Zweifel und schwierigen Momente zusammen durch gestanden und das Labor zum Hotspot gemacht haben. Danke an Etienne, Caroline, Katia, Mérie, Maria, Juliane, Vincent, Vera und Sean für die gute Stimmung, die das Arbeiten so viel leichter gemacht hat.

Danke auch an die, die nicht direkt an dieser Arbeit beteiligt waren aber durch ihre Freundschaft und Unterstützung trotzdem zu ihrer Umsetzung beigetragen haben. Danke Felix, Lea, Sophie, Max, Daniel, Eva und all die tollen Freunde, die einem helfen die Person zu sein, die man sein möchte.

Ganz besonders gilt mein Dank meinen Eltern, die mich immer und fortwährend bei allem unterstützen, dass ich tue. Die an mich glauben und immer für mich da sind. Und ein großes Danke an meinen kleinen Bruder Victor, der mich mit seinem Computer- Know How vor dem einen oder anderen Nervenzusammenbruch bewahrt hat.

Natürlich gilt der allergrößte Dank dieser Doktorarbeit selbst, weil ich durch sie Tristan kennengelernt habe, der mich seitdem begleitet und unterstützt.